Western Graduate&PostdoctoralStudies

Western University
Scholarship@Western

Electronic Thesis and Dissertation Repository

8-1-2023 2:00 PM

Nonlinear Adaptive Control of Drilling Processes

Maksim Faronov, *Western University*

Supervisor: Polushin, Ilia, *The University of Western Ontario*

A thesis submitted in partial fulfillment of the requirements for the Doctor of Philosophy degree in Electrical and Computer Engineering

© Maksim Faronov 2023

Follow this and additional works at: https://ir.lib.uwo.ca/etd

Part of the Controls and Control Theory Commons

Recommended Citation

Faronov, Maksim, "Nonlinear Adaptive Control of Drilling Processes" (2023). *Electronic Thesis and Dissertation Repository*. 9474.
https://ir.lib.uwo.ca/etd/9474

This Dissertation/Thesis is brought to you for free and open access by Scholarship@Western. It has been accepted for inclusion in Electronic Thesis and Dissertation Repository by an authorized administrator of Scholarship@Western. For more information, please contact wlswadmin@uwo.ca.

Abstract

This work deals with the modeling and control of automated drilling operations. Advances in drilling automation are of substantial importance because improvements in drilling control algorithms will result in more efficient drilling, which is beneficial from both economic and environmental points of view. While the primary application of the results is extraction of natural resources, potentially there exists a wide range of applications, including offshore exploration, archaeological research, and automated extraterrestrial mining, where implementation of new methods and control algorithms for drilling processes can bring substantial benefits.

The main contribution of the thesis is development of new methods and algorithms for control of drilling processes in industrial drilling systems, ensuring stability and high performance characteristics. The problems of regulation of vertical penetration rate and drilling power in rotary drilling systems are solved; as a result, stability and vibration mitigation is ensured. A number of challenges is addressed, such as complexity and nonlinearity of the drilling model, lack of information about environment and parameters of the drilling system itself, and poor communication between downhole sensors and ground-level equipment. Several cases are considered, depending on the amount of information that is available in advance or in real time. Two mathematical models of the drilling system are investigated: one is finite-dimensional, and another is a distributed parameter model. Several solutions are proposed for both of them, using methods of adaptive, robust, and sliding mode control, and comparisons are made. Feasibility and efficiency of the proposed control algorithms are confirmed by simulations in MATLAB/Simulink.

Keywords: Drilling automation, Rotary drilling systems, Process control, Adaptive control, Robust control, Sliding mode control, Nonlinear systems.

Summary for Lay Audience

Nowadays, extraction of natural resources is essential for generation of energy and raw materials. Drilling is an important part of this process, because these resources often lie deep underground. Automation of drilling processes (*i.e.*, making a drilling system work with minimum human supervision and intervention) makes a positive impact from economic and environmental points of view, because it may improve safety of operations, reduce the number of breaks, failures, and wearouts, as well as make operators' work easier and more effective.

In this thesis, we propose new methods for automatic control of drilling processes, assuming that our knowledge about characteristics of the material that we are drilling is extremely limited, and measurements from the bottom end are often unavailable. Utilizing a number of mathematical models that describe a conventional drilling system with acceptable precision, we design several control algorithms that generate control signal (in our case, electrical voltage) in real time. This control signal, when applied to the motor on the ground level, successfully brings the whole system into a certain desired stable mode of operation.

Results presented in this thesis correspond to gradual relaxation of simplifying assumptions, and complexity of control schemes described in different chapters depends on how much we know about the drilling system and environment where it is operating. Effectiveness and feasibility of the results are confirmed by simulation using the software package MATLAB.

Co-Authorship Statement

The thesis presented here has been written by Maksim Faronov under supervision of Dr. Ilia Polushin. It is based on the following papers that were published during work on this project, being written by Maksim Faronov and supervised/edited by Dr. Ilia Polushin:

Journal Articles:

1. Maksim V. Faronov and Ilia G. Polushin. Observer-based control of vertical penetration rate in rotary drilling systems. Journal of Process Control, Volume 106, pp. 29–43, 2021.

Peer-reviewed Conference Proceedings:

2. Maksim V. Faronov and Ilia G. Polushin. Algorithm for power stabilization in rotary drilling systems. In 2019 *IEEE 15th International Conference on Automation Science and Engineering (CASE)*, pp. 867–872, Vancouver, Canada, August 2019.

3. Maksim V. Faronov and Ilia G. Polushin. Regulation of penetration rate and drilling power in rotary drilling systems. In *IEEE 16th International Workshop on Advanced Motion Control (AMC 2020)*, pp. 97–104, Kristiansand, Norway, September 2020.

4. Maksim V. Faronov and Ilia G. Polushin. Observer-based control of drilling mode in rotary drilling systems. In *2021 American Control Conference*, pp. 97–104, New Orleans, USA, May 2021.

5. Maksim V. Faronov and Ilia G. Polushin. Control of penetration rate in distributed parameter rotary drilling systems. In *2021 IEEE Conference on Control Technology and Applications (CCTA)*, pp. 1095–1102, San Diego, USA, August 2021.

6. Maksim V. Faronov and Ilia G. Polushin. Control of rotary drilling systems with uncertain parameters. In *2023 IEEE Conference on Control Technology and Applications (CCTA)*, Bridgetown, Barbados, August 2023 (accepted).

Acknowledgments

I would like to express my deep gratitude to my supervisor Dr. Ilia Polushin, who helped and supported me at all stages of my PhD studies. His help and encouragement over the years were invaluable.

I would like to thank Fabiana Tepedino and Sandra Pehilj from International and Exchange Student Centre at Western University, who work tirelessly to create supportive, positive, and welcoming atmosphere for all international students and volunteers, making every one of us feel included into a family-like community.

I am thankful to Western University, Government of Canada, and Government of Ontario for allowing me to come to Canada and awarding me with Ontario Graduate Scholarship.

Finally, I am grateful to my mother, who has always supported me.

Contents

Abstract ii

Summary for Lay Audience iii

Co-Authorship Statement iv

Acknowledgements v

List of Figures x

List of Tables xiii

1 Introduction 1

1.1 Motivation and Applications 1

1.2 Literature Review 2

1.2.1 Types of drilling systems 2

1.2.2 Structure of a rotary drilling system 3

1.2.3 Models of rotary drilling systems 5

1.2.4 Communication between the borehole and the surface 6

1.2.5 Control strategies for vibrations suppression and stabilization 7

1.3 Thesis Contribution 10

1.4 Thesis Outline 11

2 Algorithm for Power Stabilization in Rotary Drilling Systems 12

2.1 Abstract 12

2.2 Introduction 12

2.3 Mathematical model of the drilling system 14

2.4 Problem formulation and assumptions 18

2.5 Control design 19
2.6 Simulation results 25
2.7 Conclusions 26

3 Regulation of Penetration Rate and Drilling Power in Rotary Drilling Systems 28
3.1 Abstract 28
3.2 Introduction 28
3.3 Mathematical model of the drilling system 30
3.3.1 Rotational dynamics 31
3.3.2 Translational dynamics 32
3.3.3 Bit-rock interaction 32
3.4 Problem formulation and assumptions 34
3.5 Control design 35
3.6 Simulation results 44
3.6.1 Rate of penetration regulation 46
3.6.2 Drilling power regulation 47
3.7 Conclusions 47

4 Control of Penetration Rate in Distributed Parameter Rotary Drilling Systems 51
4.1 Abstract 51
4.2 Introduction 52
4.3 Mathematical model of the drilling system 53
4.3.1 Rotational dynamics 54
4.3.2 Translational dynamics 55
4.3.3 Bit-rock interaction 56
4.4 Problem formulation and assumptions 57
4.5 Control design 58
4.6 Simulation results 66
4.7 Conclusions 67

5 Observer-Based Control of Vertical Penetration Rate in Rotary Drilling Systems 71
5.1 Abstract 71
5.2 Introduction 72

5.3 Mathematical model of the drilling system . . . 74
5.4 Problem formulation and assumptions . . . 78
5.4.1 Problem formulations . . . 78
5.4.2 Assumptions . . . 78
5.5 Control design . . . 79
5.5.1 Step 1: Design for the reference angular velocity . . . 79
5.5.2 Step 2: Tracking of the reference angular velocity . . . 83
5.5.3 Step 3: HOSM observers design . . . 84
5.5.4 Step 4: Overall control algorithm . . . 87
5.6 Simulation results . . . 89
5.6.1 Calculation of parameters . . . 89
5.6.2 Simulation results for piecewise constant parameters of the environment 92
5.6.3 Simulation results in the case of random variations of intrinsic specific energy . . . 94
5.6.4 Simulation results for a distributed parameter model of the drilling system 95
5.7 Conclusions . . . 101

6 Sliding Mode Control of Rotary Drilling Systems with Full Parametric Uncertainty 105

6.1 Abstract . . . 105
6.2 Introduction . . . 106
6.3 Model of the drilling system . . . 107
6.3.1 Components of the system . . . 107
6.3.2 Model of rotational dynamics . . . 107
6.3.3 Model of translational dynamics . . . 109
6.3.4 Model of bit-rock interaction . . . 109
6.4 Control goal and assumptions . . . 111
6.5 Identification of drillstring parameters . . . 111
6.6 Estimation of non-measured variables . . . 115
6.7 Control design . . . 117
6.7.1 Algorithm for reference angular velocity . . . 117
6.7.2 Tracking of the reference velocity . . . 118

6.8 Simulation results 120
6.9 Conclusions 123

7 Conclusions **127**
7.1 Summary 127
7.2 Future Work 128

Bibliography **130**

Appendix A. Reprint Permissions **142**

Curriculum Vitae **144**

List of Figures

1.1 The structure of the rotary drilling system [1] 3

2.1 The structure of the drilling system [2] 14
2.2 Weight-on-bit W, the torque-on-bit T, the vertical penetration velocity v, and the rotational velocity ω. 16
2.3 Drilling power $P(t)$ (left plot); vertical velocity of the drill bit $v(t)$ (right plot). . 26
2.4 Output rotational velocity of the drill bit $\omega(t)$ vs. reference rotational velocity $\omega_d(t)$ (left plot); depth of cut $d(t)$ (right plot). 26
2.5 Intrinsic specific energy $\epsilon(t)$ (left plot); input control signal $V(t)$ (right plot). . . 27

3.1 The structure of the drilling system [3] 30
3.2 Structure of the closed-loop system 44
3.3 Rate of penetration regulation for $q = 1$ and different γ: rate of penetration $v(t)$ without anti-chattering filter (left plot), with filter (3.56)-(3.58) (right plot). . . . 46
3.4 Rate of penetration regulation: output angular velocity of the drill bit $\omega(t)$ vs. reference angular velocity $\omega_d(t)$ (left plot); rate of penetration $v(t)$ (right plot) for different q. 47
3.5 Rate of penetration regulation: intrinsic specific energy $\epsilon(t)$ (left plot); input control signal $V(t)$ for different q (right plot). 48
3.6 Rate of penetration regulation: torque-on-bit $T(t)$ (left plot) and depth of cut $d(t)$ (right plot) for different q. 49
3.7 Drilling power regulation: drilling power $P(t)$ (left plot); output angular velocity of the drill bit $\omega(t)$ vs. reference angular velocity $\omega_d(t)$ (right plot) for different q. 49
3.8 Drilling power regulation: torque-on-bit $T(t)$ (left plot); input control signal $V(t)$ (right plot) for different q. 50

3.9 Drilling power regulation: depth of cut $d(t)$ (left plot); rate of penetration $v(t)$ (right plot) for for different q. 50

4.1 The structure of the drilling system 53
4.2 The structure of the control system 66
4.3 The aggregated structure 66
4.4 Rate of penetration $v(t)$ 68
4.5 Output angular velocity of the drill bit $\phi_t(1,t)$ vs. reference angular velocity $\omega_d(t)$ (left plot); disturbance $\tau(t)$ vs. its estimate $\hat{\tau}(t)$ (right plot). 68
4.6 Angular velocity along the drillstring $\phi_t(x,t)$ (left plot); error between the reference and the actual angle of rotation $\tilde{g}(x,t) = \phi(x,t) - g(x,t)$ (right plot). . . . 69
4.7 Intrinsic specific energy $\epsilon(t)$ (left plot); input control signal $I(t)$ (right plot). . . 69
4.8 Torque-on-bit $T(t)$ (left plot); depth of cut $d(t)$ (right plot). 70

5.1 The structure of the drilling system 74
5.2 Structure of the control system 88
5.3 Piecewise constant parameters: actual and estimated output angular velocity of the drill bit $\omega(t)$, $\hat{\omega}(t)$ vs. reference angular velocity $\omega_d(t)$ (left plot); rate of penetration $v(t)$ (right plot). 93
5.4 Piecewise constant parameters: intrinsic specific energy $\epsilon(t)$ (left plot); input control signal $V(t)$ (right plot). 93
5.5 Piecewise constant parameters: actual torque on bit $T(t)$ vs. estimated torque-on-bit $\hat{T}(t)$ (left plot); depth of cut $d(t)$ (right plot). 94
5.6 Piecewise constant parameters: actual angular difference $\tilde{\phi}(t)$ vs. estimated angular difference $\hat{\tilde{\phi}}(t)$ (left plot); armature current $I(t)$ (right plot). 94
5.7 Maximum achievable penetration rate in steady state for a drilling system with parameters from Table 5.1 and maximum armature voltage 810 V. 95
5.8 The case of small random variations of the intrinsic specific energy: actual and estimated output angular velocity of the drill bit $\omega(t)$, $\hat{\omega}(t)$ vs. reference angular velocity $\omega_d(t)$ (left plot); rate of penetration $v(t)$ (right plot). 96
5.9 The case of small random variations of the intrinsic specific energy: intrinsic specific energy $\epsilon(t)$ (left plot); input control signal $V(t)$ (right plot). 96

5.10 The case of small random variations of the intrinsic specific energy: actual torque on bit $T(t)$ vs. estimated torque-on-bit $\hat{T}(t)$ (left plot); depth of cut $d(t)$ (right plot). 97
5.11 The case of small random variations of the intrinsic specific energy: actual angular difference $\tilde{\phi}(t)$ vs. estimated angular difference $\hat{\tilde{\phi}}(t)$ (left plot); armature current $I(t)$ (right plot). 97
5.12 Distributed parameter model: actual and reference vertical rate of penetration $v(t)$, $v_d(t)$ (left plot); actual, estimated and reference angular velocity of the drill bit $\omega(t)$, $\hat{\omega}(t)$, $\omega_d(t)$ (right plot). 99
5.13 Distributed parameter model: actual and estimated angular difference $\tilde{\phi}(t)$, $\hat{\tilde{\phi}}(t)$ (left plot); actual and estimated torque-on-bit $T(t)$, $\hat{T}(t)$(right plot). 100
5.14 Transient processes in the distriputed parameter model: Actual and reference rate of penetration $v(t)$, $v_d(t)$ (left plot); actual, estimated and reference angular velocity of the drill bit $\omega(t)$, $\hat{\omega}(t)$, $\omega_d(t)$(right plot). 101
5.15 Transient processes in the distriputed parameter model: Armature current $I(t)$ (left plot); actual and estimated torque-on-bit and additional torque $T(t)$, $\hat{T}(t)$(right plot). 101

6.1 The structure of the drilling system 107
6.2 Actual, nominal, and estimated coefficients of the rotational dynamics model $a_1, a_2, a_3, a_4, a_5, d_1$ 124
6.3 Rate of penetration v (left plot); actual, estimated, and reference rotational velocity of the drill bit ω, $\hat{\omega}$, ω_d (right plot) 125
6.4 Control voltage V (left plot); armature current I (right plot) 125
6.5 Depth of cut d (left plot); actual and estimated torque-on-bit T, $\hat{T}$ (right plot) . . 126
6.6 Sliding variable σ (left plot); intrinsic specific energy of the rock ϵ (right plot) . 126

7.1 Reprint permission from Journal of Process Control 142
7.2 Reprint permission from IEEE conference proceedings 143

List of Tables

2.1 Numerical values of the parameters used in simulations (Chapter 2) 25

3.1 Numerical values of the parameters used in simulations (Chapter 3) 45

4.1 Numerical values of the parameters used in simulations (Chapter 4) 67

5.1 Numerical values of the drilling system and environment parameters (Chapter 5) 90
5.2 Numerical values of the drilling controller parameters (Chapter 5) 91

6.1 Numerical values of the parameters used in simulations (Chapter 6) 122

Chapter 1

Introduction

1.1 Motivation and Applications

Drilling is an important area of engineering which can be traced at least 2500 years back [4]. Recent technological advances allow for drilling boreholes up to 10 km of depth using complex drilling mechanisms. Recently, the problem of control design for drilling processes have been recognized as important by mining and control engineers, and the amount of research in this area have substantially increased over the last several years (see, for example, [5]). The ultimate goal of these works is design of a system which, for a given set of parameters (such as vertical velocity of drilling, pressure in the wellbore, or a trajectory of the drill bit), is able to perform drilling operations automatically in an optimal way in spite of any factors that may intervene.

Today, potential drilling applications are numerous. In addition to conventional oil and gas extraction, it includes mineral excavation, offshore exploration [6], archaeological research [7], and automated extraterrestrial mining (on the Moon [8], asteroids and/or other planets). Implementation of new methods and control algorithms for drilling processes can bring substantial benefits into these fields. Moreover, the results can potentially be extended to other areas of technology, such as industrial assembly lines [9] and medical applications [10].

This research is focused on drilling automation. Many challenges exist in automated drilling today [1], and the ones that are addressed in this thesis are the following:

1. While there exists a large number of mathematical models of drilling systems, those that are closest to reality are rather complex, highly nonlinear, and characterized by both parametric and non-parametric uncertainties. Therefore, pertinent solutions to the

drilling control problem require applications of advanced theories and methods for nonlinear adaptive, and robust control design.

2. The drilling process is characterized by simultaneous applications of cutting and friction forces acting on a drill bit. Parameters of the model that describes these forces are unknown beforehand, and may depend on many factors that may change during the drilling process, including sharpness of the drill bit, characteristics of the material cut, etc. Uncertainty of these cutting/friction processes involved in drilling should be taken into account in control design.

3. The actual drilling may be performed at depths of up to 10 km, while the majority of the control equipment is located at the surface. Communication process between the downhole and the surface in drilling applications is typically subject to substantial constraints including time delays, limited bandwidth, noise, and information losses. Some measurements can only be performed at a very low sampling rate. Design of control systems that are operational in the presence of the above mentioned measurement/communication constraints is difficult and require application of sophisticated observers.

The main goal of this thesis is to design automatic control solutions that are able to guarantee stable and high-performance drilling operation in the presence of uncertainties, nonlinearities, and measurement/communication constraints.

1.2 Literature Review

1.2.1 Types of drilling systems

First, it is important to note that several types of drilling systems exist in modern industry [11], such as

- Percussive drilling systems [12], where the drill bit is continuously lifted and dropped, thus creating pressure waves that crush the rock.

- Rotary drilling systems, where the bit is rotated under the constant pressure, while its blades cut the rock.

- Combined rotary-percussive drilling systems [13], where the drilling process is enhanced to include both impact action on a rock and rotation of the bit in order to remove cuttings.

In this research, only rotary drilling systems are considered, as they are the most conventional and commonly used.

1.2.2 Structure of a rotary drilling system

A detailed structure of a rotary drilling system is presented in Figure 1.1, taken from [1]. A

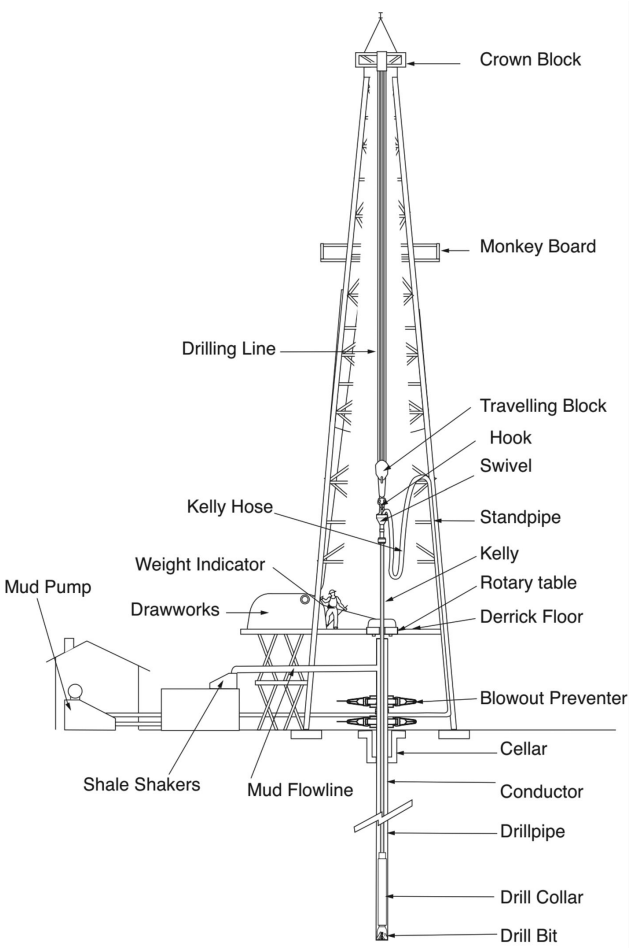

Figure 1.1: The structure of the rotary drilling system [1]

conventional drilling process is usually performed by means of a drilling rig [14] - a tower from which ground and underground equipment is operated. Its mechanical frame is called derrick; it provides sufficient vertical height of around 50 meters to perform operations with drill pipe sections. Translational operations (such as lifting, lowering, or applying a certain upward force

to the underground equipment) are functions of a hoisting system, whose hoisting mechanism is called drawworks. It is a large powerful winch that controls a drilling line by spooling it off or taking in. The drilling line is a wire rope that is connected to a hook; it passes through a crown block on top of the derrick and another set of pulleys (travelling block). The hook carries the weight of an underground part, and is coupled with the pipes through a swivel, which prevents rotation of the hook and the drilling line.

Rotation of the drillstring (drill pipes and other underground components) is performed by a rotary system which transfers the torque underground. There are two types of rotary systems: top-drive and rotary-table. The former implies a motor mounted on top of the drillstring, while in the latter a motor is geared to a rotary table, which is a heavy round platform located on a derrick floor. Rotary table is attached to a squared pipe in its center, which is called kelly. Kelly is then connected to the drillstring. When put in motion, rotary table rotates the whole drillstring underneath.

Underground, the drillstring consists of multiple sections of drill pipes, Bottom Hole Assembly (BHA) and a drill bit. BHA is a lower part which contains heavy collars that apply additional weight to the bit, and other equipment, such as sensors for measuring and transmitting necessary data, and stabilizers for keeping BHA in the center of the well. On the bottom end, the drill bit is located. It is a rigid body with cutting elements (blades) which perform the actual drilling of the rock. There are many types of drill bits, but the most common are roller cone, natural diamond, and Polycrystalline diamond compact (PDC) bits. Roller cone drill bits cut the rock by indention and gouging, performed by a number of teeth placed on rotating cones. Diamond bits show better performance and have either natural or polychrystalline diamonds embedded into their matrix. There exist other special types of drill bits, but PDC are the most widely used.

The last important component is a circulation system. Its main function is removal of drill cuttings, which is done by pumping a certain fluid (drilling mud) from the swivel down through the drill pipes and then up the annulus. On the surface, the mud goes through mud pits, where cuttings are removed, and the mud is conditioned for re-circulating. Through drilling mud, hydrostatic pressure is also applied in order to prevent other fluids from entering the annulus and to ensure stability of the hole. This pressure can also be controlled automatically during a process which is called Managed Pressure Drilling. Other functions of the drilling mud include cooling, lubrication, and often communication between downhole and surface levels.

1.2.3 Models of rotary drilling systems

The first problem in drilling analysis is the choice of a mathematical model of the drilling system. Typically, the models which are closest to reality are nonlinear and rather complicated. In the literature, models are typically defined separately for different components of the drilling system, such as drive model, drillstring model, and the model of bit-rock interaction.

The model of the drive usually includes dynamics of an electric motor, gearbox, and the rotary table. Underground components, however, are more complicated. The review presented in [15] classifies drill string models into three categories. The first category is lumped parameter models that represent the drill string as a finite-dimensional system with mass, spring, and damper elements, and describe it by ordinary differential equations. For example, a rather simple drive-drillstring model is presented in [16], where the drillstring is represented as a torsional pendulum and described by a system of linear differential equations. Drillstring dynamics can also be represented by a model with multiple degrees of freedom, as an interconnection of several segments [17]. In contrast, distributed parameter models take into account axial and torsional forces continuously along the string, resulting in a system of partial differential equations with the top and the bottom boundary conditions related to torsional and axial dynamics at the beginning and at the end of the drillstring [18]. The third category is neutral-type time-delay models, which are essentially input-output descriptions with omitted damping component. It describes the drillstring by means of differential equations with delays, where delays represent the time that is required for the torsional and axial waves to travel from one to the other extremity of the drillstring.

The third component is a model of bit-rock interaction which represents relationship between the weight-on-bit, the torque-on-bit, the rate of penetration, and the angular velocity of the bit, all of which constitute the drilling response. A considerable effort in drilling response description was undertaken by the research group of E. Detournay, who determined the model by considering the cutting and the frictional contact processes separately [19]. This approach is further developed in [20], where three phases of the response were identified, and the frictional contact model was expanded. Furthermore, the results were generalized to directional drilling [21], and an observer-based control strategy for directional drilling was proposed [22]. Another approach was presented in [23], where the drilling process is viewed as series of cycles that include feeding and cutting motions. The work [23] extends Nishimatsu model [24] which provided relations between the cutting forces and the rock strength, resulting in a more

detailed bit-rock interaction description.

Considering the frictional contact component, it is worth to mention that, in general, precise friction models are also nonlinear [15]. In particular, combination of static and Coulomb friction [25] as well as different modifications of Karnopp friction model [26], [27] can be taken into account in drilling response description.

1.2.4 Communication between the borehole and the surface

In order to obtain the desired behaviour of the drilling system, it is very important to get correct and timely information about the processes at the bottom of the borehole. For that purpose, special Measurement-While-Drilling (MWD) systems were developed [28]. MWD tools allow for transmission of various data from the borehole to the surface, which can be then used in the control algorithm. The most common transmission method is mud-pulse telemetry [29, 30], where the information is transmitted through modulation of pressure waves propagating along the drillstring. The bandwidth of mud pulse transmission can be as low as few bits per second in the cases of extreme drilling depths and high noise levels, and typically up to 100 bps in the most favourable conditions [31], although rates about 140 bps are reported for some state-of-the-art systems [32]. In addition to limited bandwidth, low sampling rates with sampling periods 3 sec or higher are typical [33]. Another substantial communication constraints typical for drilling systems are propagation delays. Propagation speed of pressure waves through the drilling mud depends on many factors, such as depth of a wellbore, pressure level in the annulus, mud composition, *etc.* Experiments show that propagation velocity of pressure waves through the drilling mud may vary between 40 m/s and 1250 m/s [34], which for typical drilling depths may result in communication delays anywhere from less than a second to tens of seconds.

In addition, there exist several problems that complicate restoration of the signal. In particular, it includes noises generated by mud pump and electrical equipment, signal echoes and reflections, signal attenuation and dispersion, rock formation particles and gas fractions in the mud flow [35], along with external disturbances [36]. A number of solutions was proposed in the literature to address these issues [29]. For example, wavelet transformation allows to decompose the original signal and identify the carrier's frequency characteristics in the presence of noise [37]. A number of low-pass filters with the use of improved Empirical Mode

Decomposition was proposed [38, 39]. A method of adaptive stochastic resonance can be used to detect weak mud pulses under low signal to noise ratio [40]. The researchers apply this method to transform part of noise energy into signal energy, while adjusting the parameters of the stochastic resonance system by a certain genetic algorithm. In [41], the authors proposed an adaptive differential noise cancellation algorithm, where the Recursive Least Squares filter is used to minimize the cost function of the output and generate the reference input signal, so that components in the primary input signal that correlate with the reference signal could be filtered out. Another approach is the use of artificial neural networks for signal recognition [42]. The method combines wavelet neural network with autoencoder, and is based on the deep learning techniques.

There are other types of telemetry as well. Electromagnetic telemetry is another way of getting the necessary information from the borehole by means of electromagnetic waves [43]. Even though it can be faster and more reliable, the signal is severely attenuated if comes through conductive formation (such as salt water). Another new method is acoustic telemetry technology, which can be used in deep wells with acoustic repeaters or even without them [44]. Data is transmitted by acoustic waves propagating through pipe walls. This technique is currently at experimental stage [45].

Finally, wired pipe telemetry [46] can offer the transmission rate of at least 57 kbps (for example, IntelliServ products [47]). The data is transmitted to the surface acquisition system on the ground through an electric cable, with repeaters every 300-400 m along the drill pipes. However, the use of such systems is limited due to high price and exploitation difficulties.

It is also worth to mention that some parameters, such as rock formation characteristic, cannot be measured directly. There exist many adaptive techniques for parameters estimation [48], [49], that can be used in the drilling control algorithms (see, for example, [50]).

1.2.5 Control strategies for vibrations suppression and stabilization

One more challenge that arises in drilling systems is vibrations, because they may lead to wearout or failure of bits and drill strings; therefore, vibration suppression is desirable. Axial, torsional and lateral vibrations can be induced during the drilling process. However, the most important type is torsional, which, under certain conditions, results in stick-slip oscillations. Torsional stick-slip oscillations can be described by periods when the bit stops completely and

periods when its angular velocity increases several times more than the desired value.

Starting from 1980s [51], researchers have investigated the vibration problem, and initially the proposed solutions considered the torsional dynamics only (for example, [16], [52]). However, this approach failed to explain many aspects of the stick-slip vibrations. The axial dynamics were taken into account in the subsequent research, and it was shown that the axial dynamics in fact cause stick-slip limit cycle [53]. The stick-slip vibrations can be described in terms of a lumped model of the drill string [53], a distributed model [54], as well as delay-differential equations [55]. Even though distributed parameter models typically provide a more realistic description of the dynamics, however, in many cases a lumped parameters approximation can be sufficient. Based on these models, researchers attempted to develop some strategies for control of vibrations. Two main categories of these strategies are passive and active methods. The former involve redesign of certain parts of drillstring or using specific devices at the bottom end to achieve better performance. We, however, are more interested in active methods that involve control algorithms based on feedback. The papers [56], [15] provide classification of the recent advances. The methods include:

- Soft Torque Rotary Systems [57, 58], where angular velocity is adjusted according to the drillstring torque variations, while the torque can be measured or estimated through the motor current;

- Adaptive PID control [59] which compensates a rotational velocity error and adjusts the dynamic response speed to improve the transition adjustment process;

- H_∞ control [60], where a controller is designed for a system with multiple degrees of freedom to ensure observability and controllability by solving corresponding Riccati equations;

- Active vibration damping at the bottom end [16] that provides a controller which, if properly tuned, can increase working range of rotational velocities where vibrations are attenuated;

- Sliding mode control [61] and sliding backstepping method [62], where an output is forced to evolve along a certain sliding surface (which typically involves tracking errors that, in turn, tend to zero);

- Weight-on-bit adjustment [63] depending on the rotational velocity of the bit, which reduces stick-slip, but does not guarantee lack of oscillations;
- Flatness-based control [64], where a control scheme is derived from the flatness property (*i.e.* all system variables can be parametrized through a so-called flat output). It solves the trajectory tracking problem and suppresses both axial and torsional vibrations;
- Torsional rectification controller [65] which solves the wave equation that describes vibration propagation, identifies "up" and "down" moving components, and maintains constant energy of the downward wave;
- PI-control [66], which ensures convergence of a rotational velocity to a desired value for a 3-DOF drilling system;
- Nonlinear friction compensation [67] through feedback linearization;
- Model-based controller [68] which predicts the vibration intensity and adjusts rotational velocity and weight on bit accordingly.
- Fuzzy Smith predictor–based control [69], where the state observer is combined with the predictor in order to compensate for the torque transmission delay, and a fuzzy online correction contributes to robustness under bit load uncertainty;
- Robust μ-synthesis [70], which optimizes robustness towards parametric uncertainty, measurement noise and actuator constraints, ensuring stability and robust performance of the closed-loop system.
- Infinite dimensional backstepping [71], where a control law is defined through a certain state transformation which brings the original system to an exponentially stable target system.

Even though the above listed methods successfully address some aspects of vibration suppression, they often rely on simplifying assumptions, such as availability of the downhole measurements, knowledge of parameters of the environment, or model simplifications. Moreover, the problem is often formulated as regulation of rotational velocity instead of vertical penetration rate. Further developments are still beneficial, especially in terms of balance between simplicity and effectiveness.

1.3 Thesis Contribution

In this thesis, we overcome challenges described in section 1.1 by designing several advanced drilling control algorithms that are able to ensure stability of a closed-loop system, mitigating vibrations and disturbances. In particular, we are solving the problem of regulation of vertical penetration rate (i.e., ensuring that it is converged to the desired value in a reasonable time) and, in some cases, regulation of drilling power. Stability, performance, and efficiency of the developed drilling control algorithms is investigated analytically and tested in simulations.

The main contributions are as follows:

- The problem of drilling power regulation is solved for the case of finite-dimensional model of the rotational dynamics, known parameters of the environment, and available downhole measurements. A novel two-step control algorithm is introduced: first, reference rotational velocity of the drill bit is calculated from the desired level of drilling power, and then its tracking and disturbance rejection is ensured through proportional control together with high-order sliding mode (HOSM) observers.

- Similar approach is extended to the case where parameters of the environment are unknown. Here, speed gradient algorithm is used in order to generate reference rotational velocity; however, its stability is only proved for vertical velocity regulation and a limited case of drilling power regulation.

- One more control scheme is designed for regulation of penetration rate, using a more sophisticated model of the rotational dynamics with distributed parameters. This model is closer to the reality than a finite-dimensional one, therefore, provides more precision. The solution still uses similar cascaded structure with first step being a speed gradient algorithm for reference angular velocity, but for the tracking part an infinite-dimensional reference model and a disturbance observer are utilized.

- The problem of vertical velocity regulation is solved with further relaxation of simplifying assumptions: the case where only ground-level measurements are available is considered. Again, a cascaded controller is used, together with a HOSM observer for estimation of non-measurable signals. This scheme is designed for a finite-dimensional model of the rotational dynamics, but tested in simulations with a distributed-parameter model, proving that it works effectively in real world.

- Finally, we relax the assumptions to the case where even mechanical characteristics of the drilling system itself are not known precisely. Parameters are estimated by an observer in the first phase, and then the estimates are used for the design of the controller. We propose a different control scheme based on a super-twisting sliding mode algorithm for tracking of the reference rotational velocity.

1.4 Thesis Outline

This thesis is organized according to the published papers (see Co-Authorship Statement) and thesis contributions (see Section 1.3) in the following way:

- In **Chapter 2**, drilling power regulation problem is solved with an assumption that parameters of the drilling system and of the environment are known, and downhole measurements are available immediately and without interruptions.
- In **Chapter 3**, control algorithms are designed for the case where parameters of the environment are unknown. Vertical velocity regulation problem is considered, as well as a limited case of drilling power regulation.
- In **Chapter 4**, a problem of regulation of vertical penetration rate is solved for a more complicated infinite-dimensional model of the drilling system.
- In **Chapter 5**, previous approach presented in Chapter 3 is extended to the case where downhole measurements are unavailable.
- In **Chapter 6**, a new control strategy is proposed for regulation of penetration rate for drilling systems with unknown mechanical characteristics, parameters of the environment, and unavailable measurements from downhole.
- In **Chapter 7**, results are summarized, and conclusions are given.

Chapter 2

Algorithm for Power Stabilization in Rotary Drilling Systems

This chapter is based on the following article:

Maksim V. Faronov and Ilia G. Polushin. Algorithm for power stabilization in rotary drilling systems. In *2019 IEEE 15th International Conference on Automation Science and Engineering (CASE)*, pp. 867–872, Vancouver, Canada, August 2019.

2.1 Abstract

This paper deals with synthesis of a control algorithm for regulation of drilling power in rotary drilling systems. Under some simplifying assumptions, we present a two-steps control design approach where the drilling power is stabilized to a prescribed level through an appropriate control algorithm for angular velocity of the drill bit. Simulation results for the case of nonzero bluntness of the bit are presented that illustrate the validity of the proposed design approach.

2.2 Introduction

Automatic control of the drilling process is an important problem in drilling practice, as it allows to free a human operator from constant and direct engagement into this work. The research of this topic can be traced back to 1950s [72], with focus on development of mathe-

matical models of drilling systems and their applications to improving performance of drilling operations. In particular, in [19, 20], mathematical models for drilling response of a drill bit were developed that take into account the effect of both cutting and frictional contact processes. Recently, the problem of automatic control of drilling processes attracted increased attention in control systems literature [73, 50, 74, 36]. Possible applications of the automatic drilling may include exploration and mineral excavation, oil and gas extraction, extra-terrestrial mining [75, 76], as well as medical applications to dentistry and orthopaedic surgery.

In this paper, the problem of design a control algorithm for stabilization of drilling power in rotary drilling systems is addressed. The approach is based on some preliminary developments presented in [50], where the problem of stabilization of the vertical velocity to the desired value defined by a human operator was addressed. One of the main drawbacks of the approach of [50] is high probability of quick wearout of the bit. This may occur because the exact structure of the rock layers is not always known, and there exists a possibility that the bit can hit very hard rock while the control system sill maintaining high vertical velocity of drilling. In this paper, we instead consider a problem of drilling power stabilization. For a constant drilling power, increase in rock hardness automatically results in decrease of the vertical velocity of drilling, which makes stabilization of constant power more appropriate control objective as compared to stabilization of the vertical velocity. Moreover, in [50] the drill bit was assumed ideally sharp and friction forces were not taken into account. In this paper, we utilize a more detailed model of interaction between the rock and the drill bit [20], which takes into account friction forces and non-ideal sharpness of the drill bit. The algorithms in this paper are developed under simplifying assumptions that all parameters are known and the measurements are performed continuously and available to the control system without delays.

The structure of the paper is as follows. In Section 2.3 the mathematical model of the drilling system is described. Based on the model, the drilling power stabilization problem is formulated in Section 2.4. Design of the control algorithm is presented in Section 2.5. Simulation results which illustrate efficiency of the proposed algorithm are given in Section 2.6. Finally, in Section 2.7 conclusions are made and possible future directions are outlined.

2.3 Mathematical model of the drilling system

In this section, a mathematical model of the drilling system is described; this model is used for control design in the subsequent sections. The general structure of a drilling system is shown in Figure 2.1. It consists of a hoisting system, a rotational system, drill pipes, and the Bottom Hole Assembly (BHA). The drill bit is located at the very end of the BHA. In the

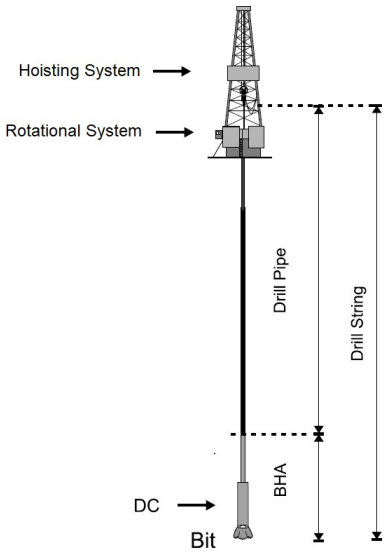

Figure 2.1: The structure of the drilling system [2]

literature, there exist a large number of mathematical models describing drilling systems. In this work, the model proposed in [16] is used, where the the drill string is modeled as a torsional pendulum and the drill pipes as a torsional spring; similar models was also used in [50]. The model in [16] is based on several simplifying assumptions, including the assumption that the drill collars (which are thick-walled tubes in the BHA) behave as a rigid body.

Under this assumption, the dynamics of the drill string can be described by the following equation:

$$J_1\ddot{\phi} + c_1\dot{\phi} + k(\phi - \phi_r) + T = 0, \tag{2.1}$$

where ϕ is the angular position of the drill bit, ϕ_r is the angular position of the rotary table, $J_1 > 0$ is the equivalent moment of inertia of the BHA and the drill pipes, $c_1 \geq 0$ is the equivalent viscous damping coefficient, $k > 0$ is the equivalent torsional stiffness of the drill pipes, and T is the torque-on-bit generated as a result of the rock cutting process. On the other

hand, the dynamics of the rotary table and drive system are described as follows:

$$J_2\ddot{\phi}_r + c_2\dot{\phi}_r - k(\phi - \phi_r) - nT_m = 0, \tag{2.2}$$

where $J_2 > 0$ is the combined equivalent moment of inertia of the rotary table and the rotor of the drive, $c_2 \geq 0$ is the equivalent viscous damping coefficient of all components of the drive system, and T_m is the motor torque. In the above equation (2.2), the motor is assumed to be coupled with a gearbox with a gear ratio $1 : n$. The drilling system is assumed to be powered by an electric DC motor which is described by the following equations

$$L\dot{I} + RI - V_b - V = 0, \quad V_b = K_m n\dot{\phi}_r, \quad T_m = K_m I, \tag{2.3}$$

where I is the armature current, L is an equivalent armature inductance, R is an equivalent armature resistance, V_b is the back emf, V is the armature voltage, and K_m is a constant which depends on the motor characteristics. Introducing a new variable $\tilde{\phi} := \phi_r - \phi$, and using notation $\omega := \dot{\phi}$, $\omega_r := \dot{\phi}_r$, the model (2.1)–(2.3) can be represented in the following matrix form [50]:

$$\begin{bmatrix} \dot{\omega} \\ \dot{\tilde{\phi}} \\ \dot{\omega}_r \\ \dot{I} \end{bmatrix} = \begin{bmatrix} -\frac{c_1}{J_1} & \frac{k}{J_1} & 0 & 0 \\ -1 & 0 & 1 & 0 \\ 0 & -\frac{k}{J_2} & -\frac{c_2}{J_2} & \frac{K_m n}{J_2} \\ 0 & 0 & -\frac{K_m n}{L} & -\frac{R}{L} \end{bmatrix} \begin{bmatrix} \omega \\ \tilde{\phi} \\ \omega_r \\ I \end{bmatrix} + \begin{bmatrix} -\frac{1}{J_1} \\ 0 \\ 0 \\ 0 \end{bmatrix} T + \begin{bmatrix} 0 \\ 0 \\ 0 \\ \frac{1}{L} \end{bmatrix} V. \tag{2.4}$$

The model (2.4) represents the rotational dynamics of the drilling system powered by an electric DC motor.

The translational dynamics of the drilling system are described by the following equation

$$M\dot{v} = W_0 - W - K_f v, \tag{2.5}$$

where v is the vertical penetration velocity of the drill bit, $M > 0$ is the combined mass of the drill string and BHA, W_0 is the difference between the submerged weight of the drilling system and the constant upward force applied at the top of the drilling rig, $K_f > 0$ is the viscous friction coefficient, and W is the weight-on-bit, which is a force applied in the vertical direction as a result of the interaction between the bit and the rock.

The rotational dynamics (2.4) and the translational dynamics (2.5) interact through the

process of rock cutting by a drill bit. The mathematical model of the drill bit cutting rocks used in our work is based on the drilling response model proposed in [20]. The force interaction between the bit and the rock is a sum of two components which are torque-on-bit T and weight-on-bit W. The weight-on-bit is applied in the vertical direction while the torque-on-bit is applied in the direction of rotation, as illustrated in Figure 2.2. Both torque-on-bit and weight-

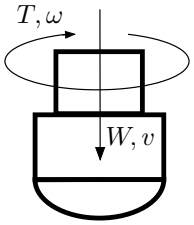

Figure 2.2: Weight-on-bit W, the torque-on-bit T, the vertical penetration velocity v, and the rotational velocity ω.

on-bit can be decomposed into its cutting and frictional components, as follows

$$T = T^c + T^f, \quad W = W^c + W^f, \tag{2.6}$$

where the superscripts c and f correspond to the cutting and frictional components, respectively. Assuming the drill bit is full, which means that there are no hollow regions inside the bit, and the ratio of the inner to the outer bit radius is zero, the cutting components are described as follows [19, 20]:

$$T^c := \frac{1}{2}a^2\epsilon d, \quad W^c := a\zeta\epsilon d, \tag{2.7}$$

where $a > 0$ is the radius of the drill bit, $\epsilon \geq 0$ is the intrinsic specific energy which is defined as the amount of energy needed for cutting a unit volume of the material by an ideally sharp bit, ζ represents the ratio of the vertical force to the horizontal force between the rock and the cutter contact surfaces, which in practice is usually in the range 0.5 – 0.8, and $d \geq 0$ represents the depth of cut per revolution.

To define the frictional components, it is necessary to consider three phases of the drilling process [20]. The phases are defined based on the value of the depth of cut. In the beginning, the contact forces increase proportionally to the depth of cut as a result of increase of the contact area between the cutters' wear flat and the rock. In the second phase (which occurs after the depth of cut exceeds some critical value), the contact area reaches its limit, and contact forces

stay constant. The third phase is characterized by further increase of the contact surface due to insufficient cleaning of the cut material.

Overall, the frictional components are described by the following formulas:

$$T^f := \begin{cases} (a^2/2) \cdot \mu\gamma\sigma\kappa d, & \text{for } d < d_*, \\ (a^2/2) \cdot \mu\gamma\sigma\kappa d_*, & \text{for } d_* \le d \le d_b, \\ (a/2) \cdot \mu\gamma(\frac{d-d_b}{\beta} + a\sigma\kappa d_*), & \text{for } d > d_b, \end{cases} \tag{2.8}$$

$$W^f := \begin{cases} a\sigma\kappa d, & \text{for } d < d_*, \\ a\sigma\kappa d_*, & \text{for } d_* \le d \le d_b, \\ \frac{d-d_b}{\beta} + a\sigma\kappa d_*, & \text{for } d > d_b, \end{cases} \tag{2.9}$$

where $\mu > 0$ is the friction coefficient defined as a ratio between parallel and normal components of the cutter force which acts along the wear flat, $\gamma > 0$ is the bit constant which depends on the bit design and determines the distribution and orientation of the contact forces, $\sigma > 0$ is the contact strength defined as a limiting value of the normal stress that can be transmitted by the wear flat, $\kappa > 0$ is the rate of change of contact length with d, $d_* > 0$ is the critical value of d when contact forces are fully mobilized, which depends on the bit bluntness, $d_b > d_*$ is the critical value of d when the contact surface between the bit and the rock increases (due to insufficient cleaning), which depends on the bit geometry and mud and rock properties, and β is a coefficient characterizing the slope of W^f at the phase 3. Equations (2.4)-(2.9) describe the overall mathematical model of the drilling system under consideration.

Remark 1. It is frequently convenient to use notions of the drilling specific energy E and the drilling specific strength S, defined as follows [19]:

$$E := \frac{2T}{a^2 d}, \quad S := \frac{W}{ad}. \tag{2.10}$$

Both E and S have dimension of stress and describe the amount of effort that is required to cut a rock of unit depth; in particular, E and S increase as hardness of the rock cut increases. •

Remark 2. In the normal mode of operation, where the angular velocity of the drill bit $\omega > 0$ is sufficiently separated from zero, the depth of cut d can be approximately calculated

based on the vertical velocity of drilling v and ω according to the formula

$$d = 2\pi\frac{v}{\omega}, \tag{2.11}$$

see for example [20, 50]. •

2.4 Problem formulation and assumptions

Our goal is to design a control algorithm which brings the system (2.4)-(2.9) into a prescribed steady-state mode of drilling. Mathematically, this corresponds to regulation (*i.e.*, stabilization of a prescribed constant value) of a certain control variable. In [50], the vertical velocity of the drill bit was chosen as the regulated variable. This choice, however, is inappropriate in certain cases, in particular, keeping constant vertical velocity in the situation where the stiffness/hardness of the rock suddenly increases is dangerous and may lead to breakdown of the drill bit. In this work, our goal is to design a control algorithm that regulates the drilling power. The drilling power is defined by the formula

$$P = T\omega, \tag{2.12}$$

where T and ω are the torque-on-bit and the angular velocity of the drill bit, respectively, as defined above in Section 2.3. Taking into account (2.10) and (2.11), one concludes that

$$P = \pi a^2 E v, \tag{2.13}$$

where E is the drilling specific energy, and v is the vertical velocity. It is clear that, in the case of constant power, increase in E (which corresponds to increase of rock hardness) results in decrease of the vertical velocity v, which makes regulation of drilling power more appropriate control objective as compared to regulation of the vertical velocity.

The problem of regulation of drilling power, however, appears to be substantially more involved as compared to that of stabilization of the vertical drilling velocity. In this work, we solve the drilling power regulation problem under a number of simplifying assumptions. These include assumptions that torque-on-bit and weight-on-bit are continuously measurable, all parameters of the drilling system and the environment are known and can be directly used

for calculation of the desired values, and that the results of these measurements are available to control system immediately, *i.e.*, all communication delays are negligible.

2.5 Control design

In this section, we discuss the design of a control algorithm that stabilizes the drilling power (2.12) to a prescribed constant value under the assumptions described above in Section 2.4. Our approach to the control design that achieves the above defined goal consists of two steps described as follows. During the first step, we exclude the rotational dynamics (2.4) from consideration, and design a control algorithm that stabilizes the drilling power of the system (2.5)-(2.9) assuming ω is a constant but otherwise arbitrary control input which can be assigned at will. In the second step, we design a control algorithm for the rotational dynamics (2.4) that stabilizes the angular velocity of the drill bit ω to the desired constant value while rejecting the (measurable) disturbances T.

Step 1(a): Steady-state analysis

Consider the equation of translational dynamics (2.5). In the steady state ($\dot{v} = 0$), it gives $v = (W_0 - W(d))/K_f$. On the other hand, equation (2.11) in steady state gives $d \cdot \omega = 2\pi v$. Combining these two formulas, one obtains

$$\omega = \frac{2\pi (W_0 - W(d))}{K_f d}, \tag{2.14}$$

which describes the steady-state relationship between the angular velocity ω and the depth of cut d. Combining the last equation (2.14) with formula for power (2.12), we get the following expression for power in the steady state:

$$P = \frac{2\pi T(d) (W_0 - W(d))}{K_f d}. \tag{2.15}$$

One can conclude that, in the steady state, the drilling power is a function of depth of cut d. Power regulation, therefore, can be achieved through regulation of depth of cut. Specifically, given a desired value of the drilling power $P_d > 0$, the desired value of the depth of cut $d_d > 0$

can be calculated by inversion of the formula (2.15), as follows.

$$d_d = \begin{cases} \frac{\pi a^2 W_0(\epsilon+\mu\gamma\sigma\kappa)-K_f P_d}{\pi a^3(\zeta\epsilon+\sigma\kappa)(\epsilon+\mu\gamma\sigma\kappa)}, & \text{for } P_d > P(d_*), \\ \frac{-z_1+\sqrt{z_1^2-z_2}}{2\pi a^3\zeta\epsilon^2}, & \text{for } P(d_*) \geq P_d \geq P(d_b), \\ \frac{-z_3+\sqrt{z_3^2-z_4}}{2\pi a(1+a\beta\epsilon\zeta)(a\beta\epsilon+\mu\gamma)}, & \text{for } P_d < P(d_b), \end{cases}$$

where

$$\begin{aligned} z_1 =& K_f P_d + a^2\pi\epsilon\,(a\sigma\kappa d_* - W_0) + a^3\pi\zeta\epsilon\mu\gamma\sigma\kappa d_*, \\ z_2 =& 4\pi^2 a^5\zeta\epsilon^2\mu\gamma\sigma\kappa d_*\,(a\sigma\kappa d_* - W_0)\,, \\ z_3 =& K_f P_d\beta^2 - \pi a\,(\mu\gamma(2d_b + W_0\beta) - a^2 d_*\beta^2\epsilon\sigma\kappa(1+\mu\gamma\zeta) + a\beta\epsilon(d_b + W_0\beta + db\mu\gamma\zeta) - \\ & 2a\beta\mu\gamma\sigma\kappa d_*)\,, \\ z_4 =& 4\pi^2 a^2\mu\gamma(1+a\beta\epsilon\zeta)(a\beta\epsilon+\mu\gamma)(d_b - a\beta\sigma\kappa d_*)\cdot(d_b + \beta W_0 - a\beta\sigma\kappa d_*), \end{aligned}$$

Step 1(b): Desired depth of cut stabilization

At this step, we assume that we have direct control over the angular velocity ω. In this case, the exponential convergence of the depth of cut $d(t)$ to a given desired value $d_d > 0$ can be achieved by an appropriate choice of a constant angular velocity $\omega = \omega_d > 0$, as follows. From (2.11), for $\omega > 0$ one obtains

$$\dot{d} = 2\pi\frac{\dot{v}\omega - v\dot{\omega}}{\omega^2}. \tag{2.16}$$

Also, using (2.11), equation (2.5) can be rewritten in the form:

$$\dot{v} = M^{-1}\left(W_0 - W(d) - \frac{K_f\cdot d\cdot\omega}{2\pi}\right). \tag{2.17}$$

Substituting (2.17) into (2.16), one gets the following differential equation which describes the dynamics of the depth of cut:

$$\dot{d} = \frac{2\pi\,(W_0 - W(d))}{M\omega} - \left(\frac{K_f}{M} + \frac{\dot{\omega}}{\omega}\right)d. \tag{2.18}$$

Given $d_d > 0$, denote

$$\omega_d := \frac{2\pi\,(W_0 - W(d_d))}{K_f d_d}. \tag{2.19}$$

Assuming $\omega \equiv \omega_d$, and taking into account that $\dot{\omega}_d \equiv 0$, equation (2.18) becomes

$$\dot{d} = \frac{2\pi\,(W_0 - W(d))}{M\omega_d} - \frac{K_f}{M} d. \tag{2.20}$$

Taking into account (2.19), equation (2.20) can be rewritten in the form

$$\dot{d} = \frac{2\pi\,(W_0 - W(d_d))}{M\omega_d} + \frac{2\pi\,(W(d_d) - W(d))}{M\omega_d} - \frac{K_f}{M} d = -\frac{K_f}{M}\,(d - d_d) + \frac{2\pi\,(W(d_d) - W(d))}{M\omega_d},$$

and using notation $\tilde{d} := d - d_d$, one gets:

$$\dot{\tilde{d}} = -\frac{K_f}{M}\tilde{d} + \frac{2\pi\,(W(d_d) - W(d))}{M\omega_d}. \tag{2.21}$$

It is easy to see that $\tilde{d}(t) \to 0$ exponentially. Indeed, it follows from (2.6), (2.7), (2.9), that $W(d)$ satisfies

$$K_1\,(d_1 - d_2) \le W(d_1) - W(d_2) \le K_2\,(d_1 - d_2) \tag{2.22}$$

for some constants $0 < K_1 \le K_2$ and for any $d_1 \ge d_2 \ge 0$, therefore $\tilde{d}\cdot(W(d_d) - W(d)) \le -K_1\tilde{d}^2$. Choosing a Lyapunov function $V := \tilde{d}^2/2$, and calculating its derivative along the trajectories of (2.21), one gets

$$\dot{V} = -\frac{K_f}{M}\tilde{d}^2 + \tilde{d}\frac{2\pi\,(W(d_d) - W(d))}{M\omega_d} \le -\frac{K_f\omega_d + 2\pi K_1}{M\omega_d}\tilde{d}^2,$$

i.e.,

$$\dot{V} \le -\frac{2K_f\omega_d + 4\pi K_1}{M\omega_d} V,$$

which implies that the system (2.21) is exponentially stable, *i.e.*, $d(t) \to d_d$ exponentially as long as $\omega(t) \equiv \omega_d$. Finally, taking into account that the exponential stability property of a system described by a differential equation (such as (2.20)) is robust with respect to small perturbations of the right-hand side (see for example [77, Section 9.2]), one concludes that any

trajectory $d(t)$ of the system (2.18) with initial conditions from an arbitrary large compact set converges exponentially to an arbitrarily small neighbourhood of d_d as long as $\omega(t)$ is sufficiently close to ω_d and $\dot{\omega}(t)$ is sufficiently close to zero. More precisely, for any given δ, D such that $0 < \delta \leq D < \infty$, there exists $\epsilon > 0$ such that $|\omega(t) - \omega_d| \leq \epsilon$ and $|\dot{\omega}(t)| \leq \epsilon$ for all $t \geq t_0$ imply that any trajectory of (2.18) with initial condition $|d(t_0)| \leq D$ converges exponentially to a set $\{d : |d - d_d| \leq \delta\}$.

Step 2: Stabilization of the angular velocity ω

The goal of this section is to design a control algorithm that stabilizes the angular velocity ω to its desired value ω_d. Let us rewrite the system (2.4) in the standard state-space form

$$\begin{aligned} \dot{x} &= Ax + Bu + DT, \\ y &= Cx, \end{aligned} \tag{2.23}$$

where

$$A = \begin{bmatrix} -\frac{c_1}{J_1} & \frac{k}{J_1} & 0 & 0 \\ -1 & 0 & 1 & 0 \\ 0 & -\frac{k}{J_2} & -\frac{c_2}{J_2} & \frac{K_m n}{J_2} \\ 0 & 0 & -\frac{K_m n}{L} & -\frac{R}{L} \end{bmatrix}, \quad B = \begin{bmatrix} 0 \\ 0 \\ 0 \\ \frac{1}{L} \end{bmatrix}, \quad D = \begin{bmatrix} -\frac{1}{J_1} \\ 0 \\ 0 \\ 0 \end{bmatrix}, \quad C = \begin{bmatrix} 1 \\ 0 \\ 0 \\ 0 \end{bmatrix}^T, \tag{2.24}$$

$$x = \begin{bmatrix} \omega & \tilde{\phi} & \omega_r & I \end{bmatrix}^T, \quad u = V. \tag{2.25}$$

In the above model (2.23), $u = V$ is the control input while T is the disturbance to be rejected. We design a control algorithm of the form

$$u = -Kx + u_d + u_T, \tag{2.26}$$

where $K := \begin{bmatrix} k_1 & k_2 & k_3 & k_4 \end{bmatrix}$ is the feedback gain matrix chosen such that the state matrix of the closed-loop system $A - BK$ has desired properties, u_d is the component of the control algorithm which guarantees tracking of the desired value of the output, and u_T is the component which ensures disturbance rejection. Substituting (2.26) into (2.23), one can calculate the transfer

matrix of the closed-loop system as follows

$$\Omega(s) = \begin{bmatrix} W_u(s) & W_T(s) \end{bmatrix} \begin{bmatrix} U_d(s) + U_T(s) \\ T(s) \end{bmatrix}, \tag{2.27}$$

where $\Omega(s)$ is the Laplace transform of the output $y = \omega$, and $W_u(s) := C\,[s\mathbb{I} - A + BK]^{-1}\,B$, $W_T(s) := C\,[s\mathbb{I} - A + BK]^{-1}\,D$ are transfer functions that correspond to a part of the control input $u_d + u_T$ and the disturbance input T, respectively. Let $\Omega_d(s)$ denote the Laplace transform of $\omega_d(t)$. From (2.27), it follows that the choice of control inputs

$$U_T(s) = -\frac{W_T(s)}{W_u(s)} T(s), \tag{2.28}$$

$$U_d(s) = \frac{1}{W_u(s)} \Omega_d(s), \tag{2.29}$$

results in $\Omega(s) = \Omega_d(s)$. However, taking into account the fact that ω_d is a constant signal (*i.e.*, $\Omega_d(s) = s^{-1}\omega_d$), and applying the final value theorem, one concludes that, instead of using (2.29), the control signal u_d can be chosen in a simpler form, as follows

$$u_d = G \cdot \omega_d, \tag{2.30}$$

where $G := \lim\limits_{s\to 0} W_u^{-1}(s)$. For our model, where the matrices A, B, and C are given by (2.24), and the feedback matrix has a form $K := \begin{bmatrix} k_1 & k_2 & k_3 & k_4 \end{bmatrix}$, direct calculations reveal that

$$G := \lim_{s\to 0} W_u^{-1}(s) = \frac{(k_4 + R)(c_1 + c_2)}{K_m n} + \frac{c_1 k_2}{k} + k_1 + k_3 + K_m n. \tag{2.31}$$

On the other hand, calculating the transfer function in the right-hand side of (2.28), one obtains

$$-\frac{W_T(s)}{W_u(s)} = \beta(s) = \beta_3 s^3 + \beta_2 s^2 + \beta_1 s + \beta_0, \tag{2.32}$$

where $\beta_3 = \frac{J_2 L}{k K_m n}$, $\beta_2 = \frac{J_2(k_4+R)+c_2 L}{k K_m n}$, $\beta_1 = \frac{c_2(k_4+R)+K_m n(k_3+K_m n)+kL}{k K_m n}$, $\beta_0 = \frac{k(k_4+R)+k_2 K_m n}{k K_m n}$.

Therefore, implementation of (2.28) requires knowledge of up to the third time derivative of $T(t)$. To obtain estimates of the time derivatives, one can use a hybrid differentiator proposed in [78]. It combines two components: high-order sliding mode (HOSM) differentiator and a classic high-gain differentiator. The HOSM component ensures exact differentiation of a

continuous input signal as well as robustness with respect to high-frequency measurement noise. The second component provides faster convergence and improves the behaviour of the estimates. The differentiator is described by the following equations:

$$\begin{aligned}
\dot{z}_0 &= -\lambda_4 L^{\frac{1}{5}} |z_0 - T|^{\frac{4}{5}} \operatorname{sign}(z_0 - T) - \mu_4 \sigma(z_0 - T) + z_1, \\
\dot{z}_1 &= -\lambda_3 L^{\frac{1}{4}} |z_1 - \dot{z}_0|^{\frac{3}{4}} \operatorname{sign}(z_1 - \dot{z}_0) - \mu_3 \sigma(z_1 - \dot{z}_0) + z_2, \\
\dot{z}_2 &= -\lambda_2 L^{\frac{1}{3}} |z_2 - \dot{z}_1|^{\frac{2}{3}} \operatorname{sign}(z_2 - \dot{z}_1) - \mu_2 \sigma(z_2 - \dot{z}_1) + z_3, \\
\dot{z}_3 &= -\lambda_1 L^{\frac{1}{2}} |z_3 - \dot{z}_2|^{\frac{1}{2}} \operatorname{sign}(z_3 - \dot{z}_2) - \mu_1 \sigma(z_3 - \dot{z}_2) + z_4, \\
\dot{z}_4 &= -\lambda_0 L \operatorname{sign}(z_4 - \dot{z}_3) - \mu_0 \sigma(z_4 - \dot{z}_3),
\end{aligned} \tag{2.33}$$

where $z \in \mathbb{R}^5$ is the state of the estimator, a vector of estimates of T and its time derivatives, specifically $z_i(t)$ is an estimate of i-th derivative of $T(t)$, $i = 0, \ldots, 4$, L is a sufficiently large number, $\lambda_i > 1$, $i = 0, \ldots, 4$, are HOSM differentiator parameters that may be chosen recursively [79], $\mu_i > 0$, $i = 0, \ldots, 4$ are coefficients chosen such that the polynomial $\alpha(s) = s^5 + \mu_4 s^4 + \mu_4\mu_3 s^3 + \mu_4\mu_3\mu_2 s^2 + \mu_4\mu_3\mu_2\mu_1 s + \mu_4\mu_3\mu_2\mu_1\mu_0$ is Hurwitz, and $\sigma > 0$ is a gain which can be adjusted in order to ensure the desired dynamic properties.

The obtained estimates can be used in place of T in the controller (2.28), specifically,

$$u_T = \begin{bmatrix} \beta_3 & \beta_2 & \beta_1 & \beta_0 \end{bmatrix} \begin{bmatrix} z_3 & z_2 & z_1 & z_0 \end{bmatrix}^T, \tag{2.34}$$

where $\beta_0, \ldots, \beta_3$ are defined after equation (2.32).

It is known [79], that observer (2.33) achieves exact differentiation of $T(t)$ as long as the corresponding derivatives are well-defined. It is worth to mention that the existence of derivatives of $T(t)$ within each phase of the drilling process is guaranteed by our mathematical model. Specifically, taking into account that within each drilling phase both torque-on-bit T and weight-on-bit W are linear functions of the depth of cut d, the fact that derivatives of $T(t)$ are well defined can be easily established by comparing equations (2.4) and (2.18) and using induction arguments (*e.g.*, equation (2.4) implies that $\dot{\omega}$ is well defined, therefore equation (2.18) implies that $\dot{d}$ is well defined and so are $\dot{T}$, $\dot{W}$, therefore equation (2.4) implies that $\ddot{\omega}$ is well-defined, etc.) Thus, in the noise-free case, the observer (2.33) allows for exact reconstruction of derivatives of T and consequently exact compensation of the effect of T on the rotational dynamics (2.4). In the presence of measurement noise, it is known [79, Theorem 6]

Table 2.1: Numerical values of the parameters used in simulations (Chapter 2)

Parameter	Value	Parameter	Value
Parameters set by human			
P_d, W	1500		
Drilling system parameters			
J_1, kgm^2	400	n	5.7
J_2, kgm^2	2516	W_0, N	4000
c_1, Nms	51	M, kg	49300
c_2,Nms	396	K_f, Nm	15
k, Nm	526	a, m	0.089
R, Ω	0.019	ζ	0.8
L, H	0.003	d_*, m	$2 \cdot 10^{-3}$
K_m, Vs	8.4	$\mu\gamma$	2.86
Drilling controller parameters			
$s_1 \dots s_4$	$\begin{bmatrix} -7 & -2.5 & -5 & -1.2 \end{bmatrix}$		
$\mu_0 \dots \mu_4$	$\begin{bmatrix} 0.438 & 1.218 & 2.647 & 5.667 & 15 \end{bmatrix}$		
$\lambda_0 \dots \lambda_4$	$\begin{bmatrix} 1.1 & 1.5 & 2 & 3 & 5 \end{bmatrix}$		
L	10000		
σ	15		
Parameters of the environment			
ϵ, J/m^3	$5 \cdot 10^6/2 \cdot 10^7/6 \cdot 10^7$		
$\sigma\kappa$, N/m^2	0.07ϵ		

that small magnitude of the noise results in small deviations of the derivatives' estimates from their actual values, which would result in approximate compensation of the effect of T on the rotational dynamics. Detailed investigation of the effect of measurement noise is outside of the scope of this paper and will be addressed in our future research.

2.6 Simulation results

In this section, we present an example of simulations of the power stabilization algorithm in the drilling control system. Numerical values of the parameters used in the simulations are given in Table 2.1. Based on the parameters of the drilling system and the desired poles of the closed-loop system ($s_1 \dots s_4$ in Table 2.1), the parameters of the control law (2.26), (2.30), (2.34) are calculated as follows: $K = [-1.912; 20.764; -35.826; 0.027]$, $G = 12.5876$, $\beta_0 = 0.04, \beta_1 = 0.024, \beta_2 = 0.005, \beta_3 = 0.0003$.

Simulation results for the overall system are presented in Figures 2.3 - 2.5. We simulate drilling through several rock layers with different intrinsic specific energies. It can be seen that for the given parameters the system demonstrates rather good performance: the drilling power converges to the reference value for each layer in around 5 seconds with some undershoot or overshoot at the border of the layers. The control scheme also ensures rather fast convergence of the angular velocity to its reference value.

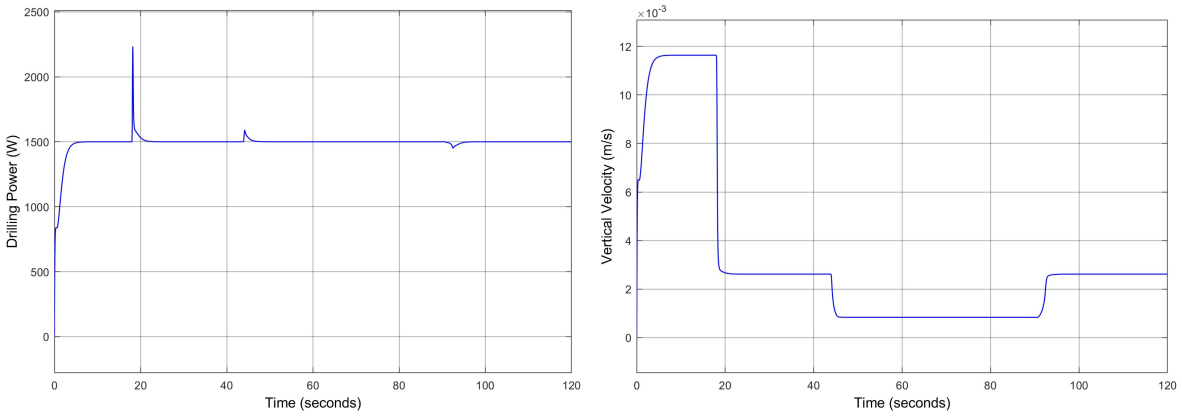

Figure 2.3: Drilling power $P(t)$ (left plot); vertical velocity of the drill bit $v(t)$ (right plot).

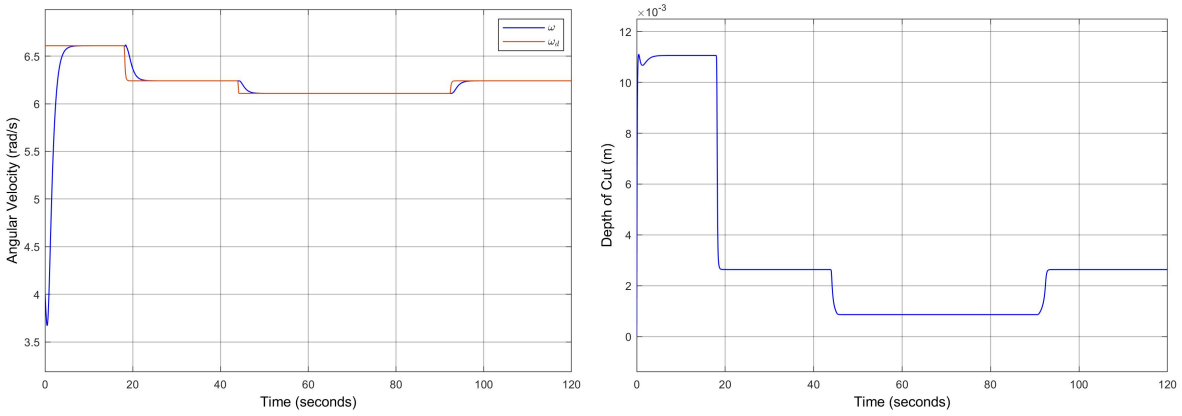

Figure 2.4: Output rotational velocity of the drill bit $\omega(t)$ vs. reference rotational velocity $\omega_d(t)$ (left plot); depth of cut $d(t)$ (right plot).

2.7 Conclusions

In this paper, a control algorithm for power stabilization in rotary drilling systems is presented. The proposed method is based on a constant tracking and disturbance rejection scheme

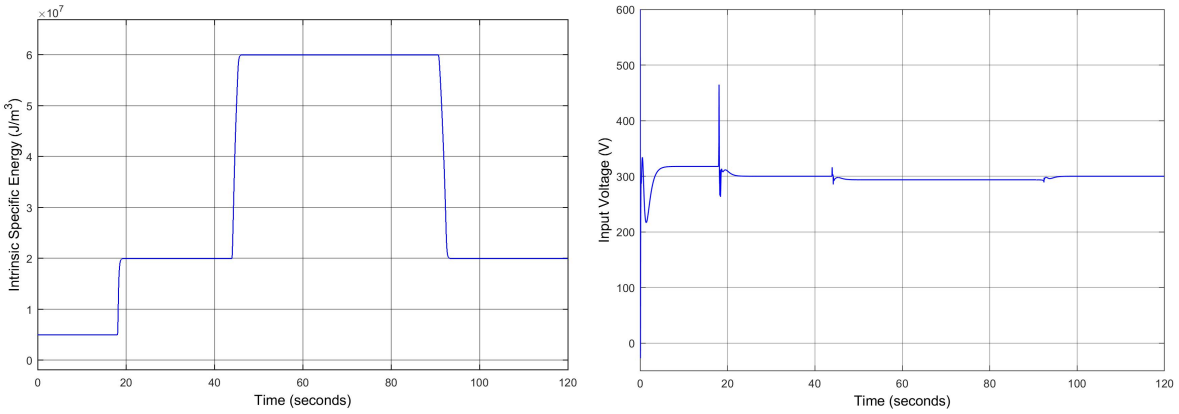

Figure 2.5: Intrinsic specific energy $\epsilon(t)$ (left plot); input control signal $V(t)$ (right plot).

which, in particular, requires measurability of the parameters at the bit level, such as torque on bit and the angular velocity of the bit. The reference angular velocity of the drill bit is then calculated such that the drilling power converges to its reference value. Simulation results demonstrate feasibility of the proposed approach and good performance of the closed-loop system. The goals of future work include relaxation and/or complete elimination of some technical assumptions used in this paper which may not necessarily hold in real life applications, including knowledge of all system's parameters, continuous noise-free measurability of torque-on-bit and weight-on-bit, and the absence of communication delays within the closed-loop system.

Chapter 3

Regulation of Penetration Rate and Drilling Power in Rotary Drilling Systems

This chapter is based on the following article:

Maksim V. Faronov and Ilia G. Polushin. Regulation of penetration rate and drilling power in rotary drilling systems. In *IEEE 16th International Workshop on Advanced Motion Control (AMC 2020)*, pp. 97–104, Kristiansand, Norway, September 2020.

3.1 Abstract

The problems of regulation of penetration rate and drilling power in rotary drilling systems are addressed. Regulation algorithms are proposed which do not require knowledge of majority of the parameters of the drilling systems and those of the rock-bit interaction. The algorithms are designed using a two-step process, where first the target angular velocity is generated using the speed-gradient control algorithms, and subsequently tracking of the target angular velocity is achieved using tracking and disturbance rejection scheme. Simulation results are presented which illustrate the efficiency of the proposed control design.

3.2 Introduction

Drilling automation is an important part of the drilling practice [80]. First attempts to create automatic feed control of the drill bit can be traced back to 1860s [81], however, early research

was mostly concentrated on mathematical models of the drilling process and appropriate choice of drilling techniques rather than actual control design [72], [82]. Recently, an increasing number of results have been reported in the literature related to applications of control systems methods and techniques to different aspects of drilling problems [73, 31, 50, 74, 36].

In this paper, we address problems related to design of control algorithms for rotary drilling systems. Specifically, we address the problems of regulation of the vertical rate of penetration as well as regulation of the drilling power in the case where majority of the parameters that describe the drilling system's dynamics and the bit-rock interaction are unknown. We provide a complete solution to the problem of regulation of the vertical rate of penetration, and partially extend it to regulation of the drilling power. To solve these problems, we implement a two-step approach to the control design where, in the first step, we design control algorithms assuming that the angular velocity of the drill bit is directly available for control. This step is performed using speed-gradient control design method [49]. In the second step, we use the desired angular velocity signal generated during step one as a reference, and implement a control algorithm that guarantees tracking of the reference angular velocity with disturbances attenuations. For implementation of the latter algorithm, a number of derivatives of the reference signal as well as those of the disturbance input are required which are not available for direct measurement. For this purpose, we use a hybrid differentiator proposed in [78] which combines theoretically perfect estimation of derivatives and robustness with respect to measurement noise. Simulation results are presented which illustrate the applicability of the proposed methods. The results of this paper can be considered an extension of the previous work of the authors [83], where the problem of drilling power regulation was solved under the assumption that all the system's parameters as well as the parameters of rock-bit interaction are known.

The paper is organized as follows. The mathematical model of the drilling system is described in Section 3.3. In Section 3.4, the control problems are formulated, and assumptions are stated. Design of the control algorithms is addressed in Section 3.5. Simulation results which illustrate feasibility and efficiency of the proposed algorithms are presented in Section 3.6. Finally, in Section 3.7, conclusions are made and future work directions are outlined.

3.3 Mathematical model of the drilling system

In this section, we present a mathematical model of the vertical rotary drilling system. Its structure is shown in Figure 3.1. The set consists of a part located on the ground and the underground components. The former is represented by a drilling rig which carries, among other equipment, a rotational system and a hoisting system. The rotational system contains a rotary table and an electric drive that rotates the underground components by generating a torque and transferring it down. The hoisting system controls a hook, which is installed at some level, and may lift or drop the underground part, if necessary. A rigid body equipped with blades which performs the rock cutting process is called a drill bit; it is located at the very bottom of the borehole. The bit is attached to the Bottom Hole Assembly (BHA), which contains some additional equipment and applies pressure on the bit. The rotary table and the BHA are connected by hollow tubes called drill pipes. Altogether, the underground part of the drilling system constitutes the drill string. The model of the drilling system used in this paper

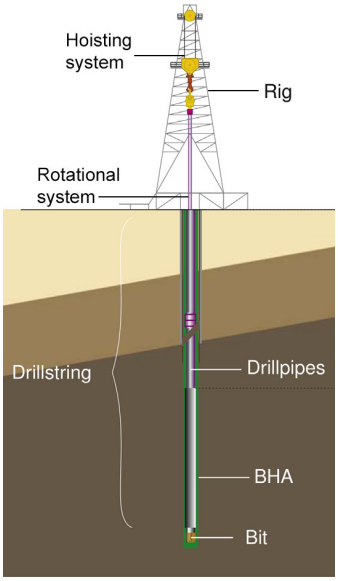

Figure 3.1: The structure of the drilling system [3]

is similar to the one utilized previously in [83]. It consists of three parts: rotational dynamics, translational dynamics, and the interaction between the bit and the rock.

3.3.1 Rotational dynamics

The rotational dynamics are described by a simplified finite-dimensional model introduced in [16], where the dynamics of the drill string are represented by those of a torsional pendulum. Assuming that the BHA behaves as a rigid body, dynamics of the drill string are described by the following equation

$$J_1\ddot{\phi} + c_1\dot{\phi} + k(\phi - \phi_r) + T = 0, \tag{3.1}$$

where ϕ is the angular position of the drill bit, ϕ_r is the angular position of the rotary table, $J_1 > 0$ is the equivalent moment of inertia of the BHA and the drill pipes, $c_1 \geq 0$ is the equivalent viscous damping coefficient, $k > 0$ is the equivalent torsional stiffness of the drill pipes, and T is the torque-on-bit generated as a result of the rock cutting process. The dynamics of the rotary table and the top drive system are described as follows:

$$J_2\ddot{\phi}_r + c_2\dot{\phi}_r - k(\phi - \phi_r) - nT_m = 0, \tag{3.2}$$

where $J_2 > 0$ is the combined equivalent moment of inertia of the rotary table and the rotor of the drive, $c_2 \geq 0$ is the equivalent viscous damping coefficient of all components of the drive system, and T_m is the motor torque. The motor is coupled with a gearbox with a gear ratio $1 : n$. The following formulas describe the DC motor with an independent excitation:

$$L\dot{I} + RI + V_b - V = 0, \quad V_b = K_m n\dot{\phi}_r, \quad T_m = K_m I, \tag{3.3}$$

where I is the armature current, L is an equivalent armature inductance, R is an equivalent armature resistance, V_b is the back emf, V is the armature voltage, and $K_m > 0$ is a motor constant which depends on its characteristics. The model (3.1)-(3.3) can be written in the state-space form [50, 83]:

$$\begin{bmatrix} \dot{\omega} \\ \dot{\tilde{\phi}} \\ \dot{\omega}_r \\ \dot{I} \end{bmatrix} = \begin{bmatrix} -\frac{c_1}{J_1} & \frac{k}{J_1} & 0 & 0 \\ -1 & 0 & 1 & 0 \\ 0 & -\frac{k}{J_2} & -\frac{c_2}{J_2} & \frac{K_m n}{J_2} \\ 0 & 0 & -\frac{K_m n}{L} & -\frac{R}{L} \end{bmatrix} \begin{bmatrix} \omega \\ \tilde{\phi} \\ \omega_r \\ I \end{bmatrix} + \begin{bmatrix} -\frac{1}{J_1} \\ 0 \\ 0 \\ 0 \end{bmatrix} T + \begin{bmatrix} 0 \\ 0 \\ 0 \\ \frac{1}{L} \end{bmatrix} V, \tag{3.4}$$

where we use notation $\tilde{\phi} := \phi_r - \phi$, $\omega := \dot{\phi}$, $\omega_r := \dot{\phi}_r$.

3.3.2 Translational dynamics

The translational dynamics describe the vertical movements of the drilling system. They are modeled by the following differential equation

$$M\dot{v} = W_0 - W - K_f v, \tag{3.5}$$

where v is the vertical velocity of the drill bit, $M > 0$ is the combined mass of the drill pipes and the BHA, W_0 is the difference between the submerged weight of the drilling system and the constant upward force applied by a hoisting system at the top of the drilling rig, $K_f > 0$ is the viscous friction coefficient, and W is the weight-on-bit, which is a reaction force applied to the bit in the vertical direction.

3.3.3 Bit-rock interaction

The bit-rock interaction is defined by the drilling response [20], which is the relationship between torque-on-bit, weight-on-bit, and rotational and vertical velocities of the drill bit. Both torque and weight-on-bit are induced as a reaction to the rock cutting process and applied in the direction of rotation and the vertical direction, respectively. An important parameter in the drilling response model is the depth of cut. This parameter represents the vertical displacement of the bit per revolution. Usually, when the angular velocity of the drill bit ω is sufficiently large, it may be assumed constant during one revolution; this allows for the following approximate calculation of d [20]:

$$d = 2\pi\frac{v}{\omega}. \tag{3.6}$$

Both torque-on-bit and weight-on-bit consist of cutting and frictional components:

$$T = T^c + T^f, \quad W = W^c + W^f, \tag{3.7}$$

where the superscripts c and f correspond to the cutting and frictional components, respectively. In case where no hollow areas exist inside the bit, the cutting components are described

as follows [19, 20]:

$$T^c := \frac{1}{2}a^2\epsilon d, \quad W^c := a\zeta\epsilon d, \tag{3.8}$$

where $a > 0$ is the radius of the drill bit, $\epsilon \geq 0$ is the intrinsic specific energy, which is the amount of energy needed for cutting a unit volume of the material by an ideally sharp bit, ζ represents the ratio of the vertical force to the horizontal force between the rock and the cutter contact surfaces, and $d > 0$ is the depth of cut per revolution.

Unlike the cutting components, frictional components are different for each of the three phases of drilling [20], where the latter are defined by the depth of cut. In the first phase, the contact forces increase with the depth of cut. After the contact forces reach the limit at some critical value of d, in the next phase the frictional components stay constant regardless of d. With further increase of the depth of cut, at some point contact surface increases again due to poor cleaning of the cut rock. At this stage, the bit response may vary, as it depends on the loading path. Generally, the frictional components can be expressed by the following equations:

$$T^f := \begin{cases} (a^2/2)\cdot\mu\gamma\sigma\kappa d, & \text{for } d < d_*, \\ (a^2/2)\cdot\mu\gamma\sigma\kappa d_*, & \text{for } d_* \leq d \leq d_b, \\ (a/2)\cdot\mu\gamma(\frac{d-d_b}{\beta} + a\sigma\kappa d_*), & \text{for } d > d_b, \end{cases} \tag{3.9}$$

$$W^f := \begin{cases} a\sigma\kappa d, & \text{for } d < d_*, \\ a\sigma\kappa d_*, & \text{for } d_* \leq d \leq d_b, \\ \frac{d-d_b}{\beta} + a\sigma\kappa d_*, & \text{for } d > d_b, \end{cases} \tag{3.10}$$

where $\mu > 0$ is the friction coefficient defined as a ratio between parallel and normal components of the cutter force which acts along the wear flat, $\gamma > 0$ is the bit constant which depends on the bit design and determines the distribution and orientation of the contact forces, $\sigma > 0$ is the contact strength defined as a limiting value of the normal stress that can be transmitted by the wear flat, $\kappa > 0$ is the rate of change of contact length with d, $d_* > 0$ is the critical value of d (which depends on the bit bluntness) at which the contact forces are fully mobilized, $d_b > d_*$ is the critical value of d when the contact surface between the bit and the rock increases (due

to insufficient cleaning), which depends on the bit geometry and mud and rock properties, and β is a coefficient characterizing the slope of W^f in phase 3. Equations (3.4)-(3.10) describe the overall mathematical model of the drilling system.

Remark 3.1 *The cut material can also be characterized by means of the drilling specific energy E and the drilling specific strength S [19]:*

$$E := \frac{2T}{a^2 d}, \quad S := \frac{W}{ad}. \tag{3.11}$$

Both E and S characterize hardness of the cut rock together with the amount of energy dissipated due to friction.•

3.4 Problem formulation and assumptions

In this paper, we address the following two problems:

- *Problem 1: Regulation of the vertical rate of penetration.* Given $v_d > 0$, find a control algorithm that achieves

$$v(t) \to v_d \quad \text{as } t \to \infty. \tag{3.12}$$

- *Problem 2: Regulation of the drilling power:* The drilling power P can be defined as follows

$$P = T\omega, \tag{3.13}$$

where T is the torque-on-bit, and ω is the angular velocity of the drill bit. Taking into account (3.11) and (3.6), it can be seen that

$$P = \pi a^2 E v, \tag{3.14}$$

where E is the drilling specific energy, and v is the vertical velocity. The problem is to design a control law that guarantees

$$P(t) \to P_d \quad \text{as } t \to \infty. \tag{3.15}$$

The motivation behind this goal is the fact that in this case the vertical velocity of the bit is inversely proportional to the drilling specific energy, which can be seen from (3.14). This prevents the bit from breaking or excessive wearout in case of sudden increase of the hardness of the rock.

Below, we solve Problem 1; we also solve Problem 2 under the assumption that the process of drilling is happening in phase 1, *i.e.*, where $d \leq d_*$ in (3.9), (3.10). Both Problem 1 and Problem 2 are solved under the assumption that the parameters of the environment and of the drill bit are unknown. More precisely, the combined mass $M > 0$ of drill pipes and the BHA, the viscous friction coefficient $K_f > 0$, the intrinsic specific energy $\epsilon > 0$, force ratio $\zeta > 0$, radius of drill bit $a > 0$, friction coefficient $\mu > 0$, bit constant $\gamma > 0$, contact strength $\sigma > 0$, rate of change of contact length $\kappa > 0$, phase boundaries $0 < d_* < d_b$, and slope coefficient $\beta > 0$ are all assumed unknown. Additionally, both Problems 1 and 2 are solved assuming the upward force applied by the hoisting system at the top of drilling rig is constant (*i.e.*, we do not use this force as a control variable). Some simplifying assumptions used in our work include knowledge of the parameters of the drilling system model (3.1)-(3.3) (equivalently, model (3.4)). In addition, it is assumed that the torque-on-bit, rotational velocity, vertical velocity and angular displacement of the bit are continuously measurable, and there are no communication delays between the borehole and the ground level, where the controller is located.

3.5 Control design

The general approach to the control design used in this paper is similar to that of [83]. Specifically, we first design the control algorithms that achieve the control goals formulated above under the assumption that the angular velocity of the drill bit ω can be controlled directly. In other words, we design an auxiliary control signal ω_d such that setting $\omega \equiv \omega_d$ solves the corresponding control problem. As a second step, we design a control algorithm for armature voltage V which guarantees that ω tracks ω_d while simultaneously rejects the disturbances which in our case is torque-on-bit T.

Step 1: Design for the desired angular velocity ω_d

At this first step, we design control algorithms that solve Problems 1 and 2 assuming the angular velocity of the drill bit ω can be controlled directly. As described above in Section 3.4, we do this under the assumption that all the parameters entering the equation of the translational dynamics (3.5) as well as the formulas that describe the rock-bit interaction (3.7)-(3.10) are constant and unknown. Under these assumptions, we solve Problems 1 and 2 using the speed-gradient method [49].

Problem 1: Rate of penetration regulation. We begin with deriving the equations that relate the angular velocity ω to the translational dynamics (3.5). Taking into account (3.7), (3.8), and (3.10), one can write

$$W(d) = a_w d + b_w, \tag{3.16}$$

where $a_w > 0$ and b_w are the coefficients that depend on the phase of drilling and the parameters of the rock-bit interaction model. Substituting (3.16) into (3.5), one can write

$$\dot{v} = -\left(\frac{K_f}{M} + \frac{2\pi a_w}{M\omega}\right)v + \frac{W_0 - b_w}{M}, \tag{3.17}$$

and using notation $K_1 := \frac{K_f}{M} > 0$, $K_2 := \frac{2\pi a_w}{M} > 0$, $K_3 := \frac{W_0 - b_w}{M} > 0$, equation (3.17) can be written in the form

$$\dot{v} = -(K_1 + K_2\omega^{-1})v + K_3. \tag{3.18}$$

It is clear that for any constant $\omega(t) \equiv \omega_* > 0$, equation (3.18) has a globally exponentially stable equilibrium at

$$v_* = \frac{K_3}{K_1 + K_2\omega_*^{-1}}. \tag{3.19}$$

Conversely, given $v_* \in (0; \frac{K_3}{K_1})$, the choice $\omega(t) \equiv \omega_*$ where

$$\omega_* = \frac{K_2 v_*}{K_3 - K_1 v_*}, \tag{3.20}$$

makes v_* the globally exponentially stable equilibrium of (3.18). Let $v_d > 0$ be a desired vertical rate of penetration, and let $\omega_* > 0$ be found from (3.20) by setting $v_* = v_d$. Denote $\theta := K_1 + K_2\omega^{-1}$, $\theta_* := K_1 + K_2\omega_*^{-1}$, and $\tilde{\theta} := \theta - \theta_*$. From (3.19) one can see that $K_3 = \theta_* v_d$. Equation (3.18) becomes

$$\dot{v} = -\theta v + \theta_* v_d. \tag{3.21}$$

Using notation $\tilde{v} := v - v_*$, one can write

$$\dot{\tilde{v}} = -(\tilde{\theta} + \theta_*)v + \theta_* v_d = -\tilde{\theta} v - \theta_* \tilde{v}. \tag{3.22}$$

In order to apply the speed-gradient method to equation (3.22), consider a family of goal functions

$$Q_{v,q} := \frac{1}{q} \cdot |\tilde{v}|^q, \quad \text{where } q = 1, 2, \ldots \tag{3.23}$$

Calculating the time derivative of $Q_{v,q}$ along the trajectories of (3.22), one obtains

$$\dot{Q}_{v,q} = |\tilde{v}|^{q-1} \operatorname{sign}\{\tilde{v}\}\, \dot{\tilde{v}} = |\tilde{v}|^{q-1} \operatorname{sign}\{\tilde{v}\} \left(-\tilde{\theta} v - \theta_* \tilde{v}\right) = -\tilde{\theta} v\, |\tilde{v}|^{q-1} \operatorname{sign}\{\tilde{v}\} - q\, Q_{v,q} \theta_*. \tag{3.24}$$

Taking into account $\tilde{\theta} := \theta - \theta_*$, one can calculate

$$\frac{\partial \dot{Q}_{v,q}}{\partial \theta} = -v \cdot |\tilde{v}|^{q-1} \operatorname{sign}\{\tilde{v}\}, \tag{3.25}$$

and the corresponding family of speed-gradient algorithms [49, Chapter 3] can be obtained as follows

$$\dot{\theta} = -\gamma_1 \frac{\partial \dot{Q}_{v,q}}{\partial \theta} = \gamma_1\, v\, |\tilde{v}|^{q-1} \operatorname{sign}\{\tilde{v}\}, \quad q = 1, 2, \ldots \tag{3.26}$$

Sufficient conditions for algorithms (3.26) to guarantee convergence $Q_{v,q}(t) \to 0$ as $t \to +\infty$ are given for example in [49, Theorem 3.1]. It is easy to check that all conditions of [49, Theorem 3.1] are satisfied for the system (3.22) and any of the goal functions $Q_{v,q}$, $q = 1, 2, \ldots$ Thus, any algorithm of the form (3.26) guarantees that $Q_{v,q}(t) \to 0$ as $t \to +\infty$ and, therefore, solves the problem of regulation of the rate of penetration (Problem 1). On the other hand, we

have $\theta = K_1 + K_2\omega^{-1}$, and therefore

$$\dot{\theta} = -K_2 \frac{\dot{\omega}}{\omega^2}. \tag{3.27}$$

Using (3.27), we see that (3.26) is equivalent to the following algorithms for the desired rotational velocity ω_d:

$$\dot{\omega}_d = -\gamma\, \omega_d^2\, v\, |\tilde{v}|^{q-1}\, \mathrm{sign}\{\tilde{v}\}, \quad q = 1, 2, \ldots \tag{3.28}$$

where $\gamma := \gamma_1 / K_2 > 0$.

Problem 2: Drilling power regulation. The algorithm (3.28) generates the desired angular velocity that guarantees regulation of the rate of penetration. The method used above can be extended to solve the problem of regulation of the drilling power in phase 1 of the drilling process ($d \leq d_*$ in (3.9), (3.10)). Combining formula for power (3.13) with the model of the rock-bit interaction (3.7)-(3.10), and using relationship (3.6), it is easy to conclude that, in phase 1 of drilling, the drilling power P is proportional to the rate of penetration v, *i.e.*, $P = \bar{c}_1 v$, where $\bar{c}_1 > 0$ is a constant which depends on parameters of the rock-bit interaction. Let $P_d > 0$ be a desired value of the drilling power, and denote $\tilde{P} := P - P_d$. We have

$$\tilde{P} = \bar{c}_1 \tilde{v}. \tag{3.29}$$

Consider the following family of goal functions:

$$Q_{P,q} := \frac{1}{q} |\tilde{P}|^q, \quad \text{where } q = 1, 2, \ldots \tag{3.30}$$

Calculating the time derivative of (3.30) along the trajectories of (3.22) and using (3.29), one obtains

$$\dot{Q}_{P,q} = |\tilde{P}|^{q-1}\, \mathrm{sign}\{\tilde{P}\} \bar{c}_1 \left(-\tilde{\theta} v - \theta_* \tilde{v}\right) = -|\tilde{P}|^{q-1}\, \mathrm{sign}\{\tilde{P}\} P \tilde{\theta} - q Q_{P,q} \theta_*. \tag{3.31}$$

From (3.31), the family of speed gradient algorithms can be obtained as follows:

$$\dot{\theta} = -\frac{\partial \dot{Q}_{P,q}}{\partial \theta} = \gamma_2\, P |\tilde{P}|^{q-1}\, \mathrm{sign}\{\tilde{P}\}, \quad q = 1, 2, \ldots, \tag{3.32}$$

and using (3.27), one obtains

$$\dot{\omega}_d = -\gamma_0 \omega_d^2 P |\tilde{P}|^{q-1} \operatorname{sign}\{\tilde{P}\}, \quad q = 1, 2, \ldots, \tag{3.33}$$

where $\gamma_0 := \gamma_2 / K_2$. Alternatively, taking into account $P = \bar{c}_1 v$, the family of algorithms (3.33) can be written in the form

$$\dot{\omega}_d = -\gamma \omega_d^2 v |\tilde{P}|^{q-1} \operatorname{sign}\{\tilde{P}\}, \quad q = 1, 2, \ldots, \tag{3.34}$$

where $\gamma := \gamma_0 \bar{c}_1$. Again, it is straightforward to check that the system (3.22), (3.29) with any goal function of the form (3.30) satisfy all conditions of [49, Theorem 3.1] and, therefore, the family of algorithms (3.33) (equivalently (3.34)) solves the power regulation problem as long as the drilling process is in phase 1. Outside of phase 1, the relationship between power P, penetration rate v and rotational velocity ω becomes more complicated, and the power regulation problem apparently does not allow for direct solution using the speed-gradient methods. Development of the power regulation algorithms for phases 2 and 3 is a topic for future research.

Step 2: Tracking of the desired angular velocity

At this step, our goal is to design a control algorithm that guarantees that the angular velocity of the drill bit ω tracks its desired trajectory ω_d, where the latter was designed during the previous step. The control algorithm presented in this section is largely similar to the one of [83]; the difference is that in this paper ω_d is no longer a constant signal and therefore provisions must be made to guarantee tracking of time-varying $\omega_d(t)$. Let us rewrite the system (3.4) in the state-space form

$$\begin{aligned} \dot{x} &= Ax + Bu + DT, \\ y &= Cx, \end{aligned} \tag{3.35}$$

where

$$A = \begin{bmatrix} -\frac{c_1}{J_1} & \frac{k}{J_1} & 0 & 0 \\ -1 & 0 & 1 & 0 \\ 0 & -\frac{k}{J_2} & -\frac{c_2}{J_2} & \frac{K_m n}{J_2} \\ 0 & 0 & -\frac{K_m n}{L} & -\frac{R}{L} \end{bmatrix}, \quad B = \begin{bmatrix} 0 \\ 0 \\ 0 \\ \frac{1}{L} \end{bmatrix}, \quad D = \begin{bmatrix} -\frac{1}{J_1} \\ 0 \\ 0 \\ 0 \end{bmatrix}, \quad C = \begin{bmatrix} 1 & 0 & 0 & 0 \end{bmatrix}, \tag{3.36}$$

$$x = \begin{bmatrix} \omega & \tilde{\phi} & \omega_r & I \end{bmatrix}^T, \quad u = V. \tag{3.37}$$

In the above model, $u = V$ is the control input signal, and T is the disturbance which has to be rejected. The control algorithm has the following form

$$u = -Kx + u_d + u_T, \tag{3.38}$$

where $K := \begin{bmatrix} k_1 & k_2 & k_3 & k_4 \end{bmatrix}$ is the feedback gain matrix chosen such that the closed-loop system has desired dynamical properties, u_d is the component which is responsible for tracking of the desired value of the output, and u_T is the component which ensures disturbance rejection. In order to define these components, one can represent the system (3.35)-(3.38) in the input-output form:

$$\Omega(s) = \begin{bmatrix} W_u(s) & W_T(s) \end{bmatrix} \begin{bmatrix} U_d(s) + U_T(s) \\ T(s) \end{bmatrix}, \tag{3.39}$$

where $\Omega(s)$ is the Laplace transform of the output $y = \omega$, and $W_u(s) := C\left[s\mathbb{I} - A + BK\right]^{-1} B$, $W_T(s) := C\left[s\mathbb{I} - A + BK\right]^{-1} D$ are transfer functions that correspond to a part of the control input $u_d + u_T$ and the disturbance input T, respectively. Let $\Omega_d(s)$ denote the Laplace transform of $\omega_d(t)$. From (3.39), one concludes that the following control inputs

$$U_T(s) = -\frac{W_T(s)}{W_u(s)} T(s), \quad U_d(s) = \frac{1}{W_u(s)} \Omega_d(s), \tag{3.40}$$

result in $\Omega(s) = \Omega_d(s)$.

Assuming that the system's parameters are known, it is possible to calculate the transfer

functions in (3.40) directly. In this case, they can be represented as polynomials:

$$-\frac{W_T(s)}{W_u(s)} = \beta(s) = \beta_3 s^3 + \beta_2 s^2 + \beta_1 s + \beta_0, \tag{3.41}$$

$$\frac{1}{W_u(s)} = \alpha(s) = \alpha_4 s^4 + \alpha_3 s^3 + \alpha_2 s^2 + \alpha_1 s + \alpha_0, \tag{3.42}$$

where

$$\beta_3 = \frac{J_2 L}{k K_m n}, \tag{3.43}$$

$$\beta_2 = \frac{J_2(k_4 + R) + c_2 L}{k K_m n}, \tag{3.44}$$

$$\beta_1 = \frac{c_2(k_4 + R) + K_m n(k_3 + K_m n) + kL}{k K_m n}, \tag{3.45}$$

$$\beta_0 = \frac{k(k_4 + R) + k_2 K_m n}{k K_m n}, \tag{3.46}$$

$$\alpha_4 = \frac{J_1 J_2 L}{k K_m n}, \tag{3.47}$$

$$\alpha_3 = \frac{L(c_2 J_1 + c_1 J_2) + J_1 J_2(k_4 + R)}{k K_m n}, \tag{3.48}$$

$$\alpha_2 = \frac{1}{k K_m n}(J_1 K_m n(k_3 + K_m n) + kL(J_1 + J_2) + c_1 c_2 L + (c_1 J_2 + c_2 J_1)(k_4 + R)), \tag{3.49}$$

$$\alpha_1 = \frac{1}{k K_m n}(K_m n(c_1 k_3 + c_1 K_m n + J_1 k_2) + kL(c_1 + c_2) + (c_1 c_2 + kJ_1 + kJ_2)(k_4 + R)), \tag{3.50}$$

$$\alpha_0 = \frac{k(c_1 + c_2)(k_4 + R) + c_1 k_2 K_m n}{k K_m n} + k_1 + k_3 + K_m n. \tag{3.51}$$

It follows from (3.41), (3.42) that in order to implement perfect tracking and disturbance rejection, knowledge of up to the third time derivative of $T(t)$ and up to the fourth derivative of $\omega_d(t)$ is necessary. In order to estimate these derivatives, we use a hybrid differentiator proposed in [78]. It consists of two parts: high-order sliding mode (HOSM) differentiator and a classical high-gain differentiator. The HOSM component ensures exact differentiation of a continuous input signal as well as robustness with respect to measurement noise. The high-gain

component contributes to faster convergence of the estimates. Two differentiators are necessary to implement: one for T and another for ω_d. They have the following form:

$$\dot{z}_{0i} = -\lambda_4 L_i^{\frac{1}{5}} |z_{0i} - \Gamma_i|^{\frac{4}{5}} \operatorname{sign}(z_{0i} - \Gamma_i) - \mu_4 \sigma_i (z_{0i} - \Gamma_i) + z_{1i},$$

$$\dot{z}_{1i} = -\lambda_3 L_i^{\frac{1}{4}} |z_{1i} - \dot{z}_{0i}|^{\frac{3}{4}} \operatorname{sign}(z_{1i} - \dot{z}_{0i}) - \mu_3 \sigma_i (z_{1i} - \dot{z}_{0i}) + z_{2i},$$

$$\dot{z}_{2i} = -\lambda_2 L_i^{\frac{1}{3}} |z_{2i} - \dot{z}_{1i}|^{\frac{2}{3}} \operatorname{sign}(z_{2i} - \dot{z}_{1i}) - \mu_2 \sigma_i (z_{2i} - \dot{z}_{1i}) + z_{3i},$$

$$\dot{z}_{3i} = -\lambda_1 L_i^{\frac{1}{2}} |z_{3i} - \dot{z}_{2i}|^{\frac{1}{2}} \operatorname{sign}(z_{3i} - \dot{z}_{2i}) - \mu_1 \sigma_i (z_{3i} - \dot{z}_{2i}) + z_{4i},$$

$$\dot{z}_{4i} = -\lambda_0 L_i \operatorname{sign}(z_{4i} - \dot{z}_{3i}) - \mu_0 \sigma_i (z_{4i} - \dot{z}_{3i}), \tag{3.52}$$

where $i = 1, 2$, $i = 1$ corresponds to the estimator for $T(t)$, $i = 2$ corresponds to the estimator for $\omega_d(t)$, $\Gamma_1 = T$, $\Gamma_2 = \omega_d$, $z_i \in \mathbb{R}^5$ are the state variables of the estimators, specifically, $z_{1j}(t)$ is an estimate of j-th derivative of $T(t)$, $z_{2j}(t)$ is an estimate of j-th derivative of $\omega_d(t)$, $j = 0, \ldots, 4$, $L_i > 0$ are sufficiently large numbers, $\lambda_j > 1$, $j = 0, \ldots, 4$, are HOSM differentiators parameters that may be chosen recursively [79], $\mu_j > 0$, $j = 0, \ldots, 4$ are coefficients chosen such that the polynomial $r(s) = s^5 + \mu_4 s^4 + \mu_4\mu_3 s^3 + \mu_4\mu_3\mu_2 s^2 + \mu_4\mu_3\mu_2\mu_1 s + \mu_4\mu_3\mu_2\mu_1\mu_0$ is Hurwitz, and $\sigma_i > 0$ are gains which can be adjusted in accordance with the desired dynamic properties. The obtained estimates are used in the expressions (3.40)-(3.42) instead of the actual derivatives, specifically,

$$u_T = \begin{bmatrix} \beta_3 & \beta_2 & \beta_1 & \beta_0 \end{bmatrix} \begin{bmatrix} z_{31} & z_{21} & z_{11} & z_{01} \end{bmatrix}^T, \tag{3.53}$$

$$u_d = \begin{bmatrix} \alpha_4 & \alpha_3 & \alpha_2 & \alpha_1 & \alpha_0 \end{bmatrix} \begin{bmatrix} z_{42} & z_{32} & z_{22} & z_{12} & z_{02} \end{bmatrix}^T \tag{3.54}$$

where $\beta_0, \ldots, \beta_3, \alpha_0, \ldots, \alpha_4$ are given by (3.43)-(3.51). Overall, the algorithm for stabilization of angular velocity of the drill bit has the form (3.38), where u_T, u_d are calculated according to (3.52) - (3.54), and $\beta_0, \ldots, \beta_3, \alpha_0, \ldots, \alpha_4$ by (3.43)-(3.51).

Remark 3.2 *It is proven in [79] that the filter* (3.52) *provides exact differentiation of* $T(t)$*,* $\omega_d(t)$ *as long as noise is absent, sample time tends to zero, and the corresponding derivatives*

exist. It is possible to demonstrate that, within each phase of the drilling process and within each layer, the derivatives of $T(t)$ are well-defined. The bit-rock interaction model implies that $T(t)$, $W(t)$ are piecewise-linear functions of d. Therefore, $\dot{T}$ id defined by $\dot{d}$, which can be represented as follows:

$$\dot{d} = \frac{2\pi\,(W_0 - W(d))}{M\omega} - \left(\frac{K_f}{M} + \frac{\dot{\omega}}{\omega}\right) d. \tag{3.55}$$

One can establish by induction, using equations (3.55) *and* (3.4)*, that higher derivatives of $T(t)$ are well-defined as well. Therefore, the hybrid HOSM differentiator ensures exact compensation of the disturbance $T(t)$ in the noise-free case and small sampling time. If the measurement noise is present, [79, Theorem 6] shows that small magnitude of the noise results in small deviations of the derivatives' estimates from their actual values, which would result in approximate compensation of the effect of T on the rotational dynamics.*•

Step 3: Anti-chattering filtration

Simulations of response of the closed-loop system with the control law (3.38), (3.43)-(3.54), (3.33) with $q = 1$ reveal presence of some chattering in the steady state (see Section 3.6). Chattering magnitude grows with the increase of the coefficient γ. It happens because of imperfect tracking of ω_d, as the estimates of derivatives are not always exact due to non-zero step size and derivatives' uncertainty at the switching moments. Therefore, it is desirable to reduce chattering in the steady state. In order to reduce the number of switches, first a small dead zone is introduced, *i.e.*, the following approximation of the sign function is used:

$$\operatorname{sign}_d \tilde{f} := \begin{cases} -1, & \text{for } \tilde{f} < -\Delta f, \\ 0, & \text{for } -\Delta f \le \tilde{f} \le \Delta f, \\ 1, & \text{for } \tilde{f} > \Delta f, \end{cases} \tag{3.56}$$

where f is either v or P depending on the task, and $\Delta f \ge 0$ is the size of the dead zone defined by designer. A simple anti-chattering filter was proposed in [84], which, when applied to our model, can be written as follows:

$$\dot{\omega}_d = -(\gamma|\eta| + \delta)\omega_d^2 v \operatorname{sign}_d \tilde{f}, \tag{3.57}$$

$$\tau\dot{\eta} + \eta = \text{sign}_d \tilde{f}, \tag{3.58}$$

where f is either v or P depending on the task, $\gamma > 0$ is an arbitrary number, $\delta > 0$ is a sufficiently small design parameter, η is an average value of $\text{sign}_d \tilde{f}$, and $\tau > 0$ is the time constant of the averaging filter. The structure of the overall system is shown in Figure 3.2.

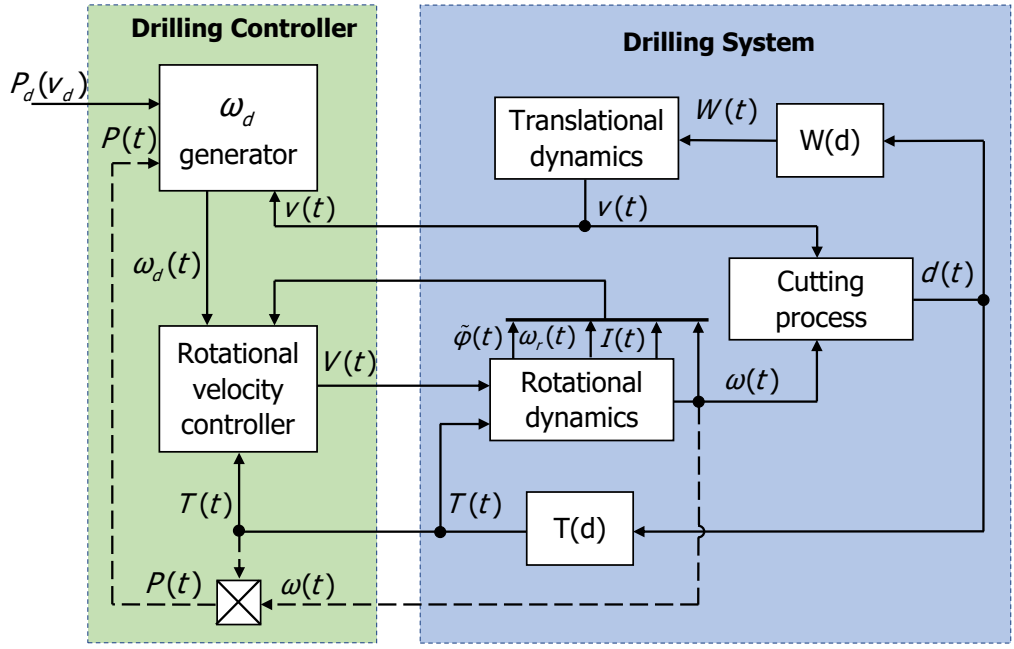

Figure 3.2: Structure of the closed-loop system

3.6 Simulation results

In this section, we present samples of simulation results of the rate of penetration and drilling power regulation schemes developed above. Numerical values of all parameters used in the simulations are presented in Table 3.1. The parameters of the drilling controller are calculated using the drilling system parameters and the desired poles of the closed-loop system ($s_1 \dots s_4$ in Table 3.1). Their values are the following: $K = [-1.397; 8.792; -46.962; 0.012]$, $\beta_0 = 15.83 \cdot 10^{-3}$, $\beta_1 = 9.95 \cdot 10^{-3}$, $\beta_2 = 2.12 \cdot 10^{-3}$, $\beta_3 = 1.48 \cdot 10^{-4}$, $\alpha_0 = 5.032$, $\alpha_1 = 8.798$, $\alpha_2 = 4.662$, $\alpha_3 = 0.96$, $\alpha_4 = 0.067$.

Table 3.1: Numerical values of the parameters used in simulations (Chapter 3)

Parameter	Value	Parameter	Value
Parameters set by operator			
P_d, W	6000	v_d, m/s	0.02
Drilling system parameters			
J_1, kgm^2	450	n	6.9
J_2, kgm^2	2236	W_0, N	4200
c_1, Nms	46	M, kg	48500
c_2,Nms	415	K_f, Nm	21
k, Nm	575	a, m	0.095
R, Ω	0.016	ζ	0.75
L, H	0.002	d_*, m	0.0015 / 0.01
K_m, Vs	7.6	$\mu\gamma$	2.23
Drilling controller parameters			
$s_1 \dots s_4$	$\begin{bmatrix} -6.5 & -2.9 & -4 & -1 \end{bmatrix}$		
$\mu_0 \dots \mu_4$	$\begin{bmatrix} 0.438 & 1.218 & 2.647 & 5.667 & 15 \end{bmatrix}$		
$\lambda_0 \dots \lambda_4$	$\begin{bmatrix} 1.1 & 1.5 & 2 & 3 & 5 \end{bmatrix}$		
L_1	10^4	L_2	10
σ_1	15	σ_2	10
q	1 / 2 / 4	τ	1.2
δ	0.001		
ΔP, W	15	Δv, m/s	0.0005
Parameters of the environment			
ϵ, J/m^3	$5 \cdot 10^6 / 1 \cdot 10^7 / 2 \cdot 10^7$		
$\sigma\kappa$, N/m^2	0.9ϵ		

3.6.1 Rate of penetration regulation

In this part of simulations, the desired value of the vertical rate of penetration is set to $v_d = 0.02$ m/s, and the velocity control algorithms described in the previous section are implemented. Figure 3.3 shows vertical velocity of the drill bit for $q = 1$ for different layers with and without an anti-chattering filter. One can observe that in the presence of the filter chattering is reduced significantly. All subsequent plots with $q = 1$ are simulated with the filter. Simulation results for different q are presented in Figures 3.4 - 3.6. Analyzing the plots, one can observe that there are more oscillations when $q = 1$; this is because of the presence of chattering. However, in each layer, this chattering is quickly filtered out. It is also possible to make the following observation: with the increase of q, processes around the border of the layers become faster, which is caused by larger magnitude of the control signal, but the subsequent convergence of v to its desired value v_d turns out to be slower. Combining these facts, we conclude that $q = 2$ seems to be an optimal value in the case of rate of penetration regulation.

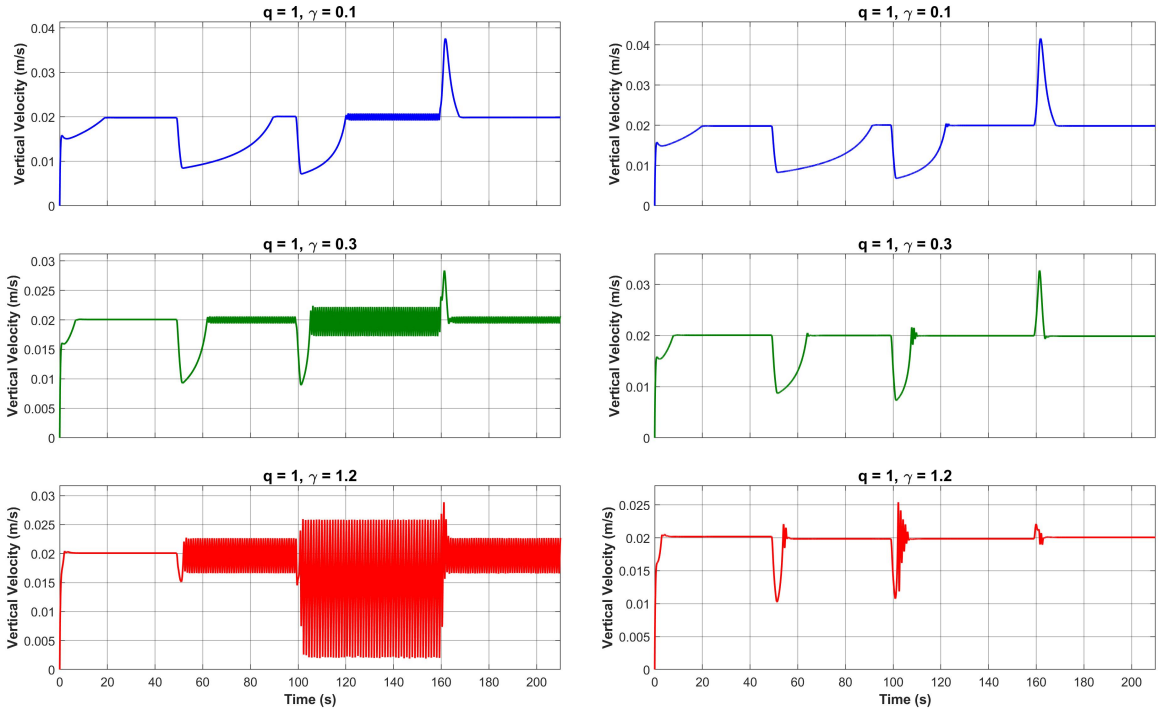

Figure 3.3: Rate of penetration regulation for $q = 1$ and different γ: rate of penetration $v(t)$ without anti-chattering filter (left plot), with filter (3.56)-(3.58) (right plot).

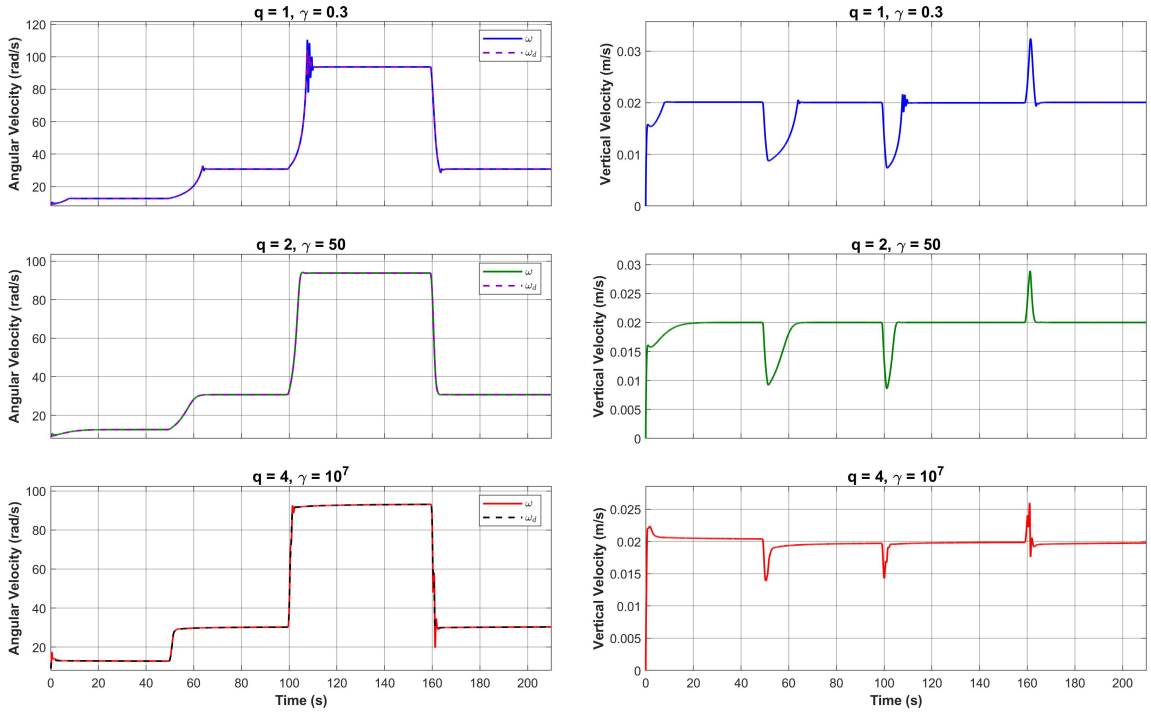

Figure 3.4: Rate of penetration regulation: output angular velocity of the drill bit $\omega(t)$ vs. reference angular velocity $\omega_d(t)$ (left plot); rate of penetration $v(t)$ (right plot) for different q.

3.6.2 Drilling power regulation

In this section, the power regulation algorithm is simulated assuming the drilling process is in phase 1. The desired value of the drilling power is set to $P_d = 6000$ W. Results of simulations of the algorithm (3.34), (3.57), (3.58) for different q are shown in Figures 3.7 - 3.9. It can be seen that, in every case, the drilling power converges to its desired value. Similarly to the velocity regulation case, the choice $q = 2$ seems to result in a smoother response and overall better behaviour as compared to other values of q. Additionally, one can observe that, in the first phase of drilling, the desired and the actual angular velocities of the drill bit remain approximately constant, regardless of the rock hardness.

3.7 Conclusions

In this paper, algorithms for regulation of the rate of penetration and the drilling power in rotary drilling systems are proposed. The speed gradient method is implemented for the purpose of generation of reference signal, while the latter is subsequently fed into a tracking

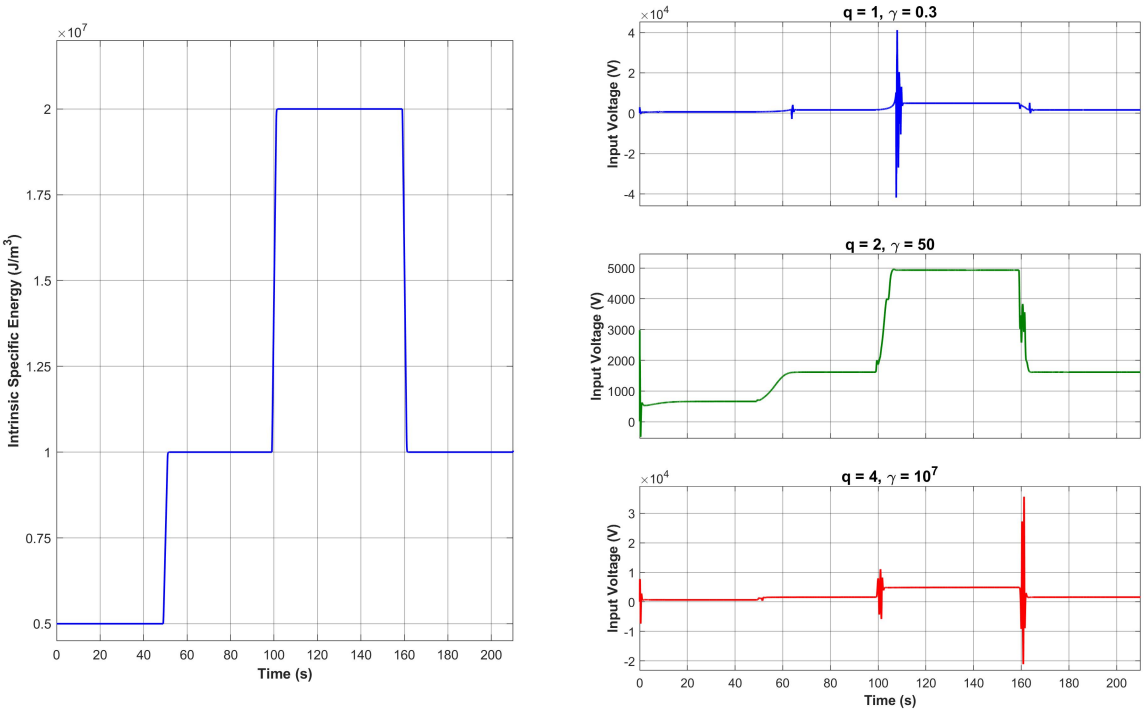

Figure 3.5: Rate of penetration regulation: intrinsic specific energy $\epsilon(t)$ (left plot); input control signal $V(t)$ for different q (right plot).

and disturbance rejection scheme. Regulation is achieved without knowledge of majority of system's parameters, including parameters of the bit-rock interaction as well as parameters that describe the translational dynamics of the drilling system. The control algorithms in this work are designed under some simplifying assumptions, including absence of communication delays between the bottom and the ground levels, as well as continuous and noise-free measurements. Elimination or relaxation of these assumptions constitutes the goal of future research.

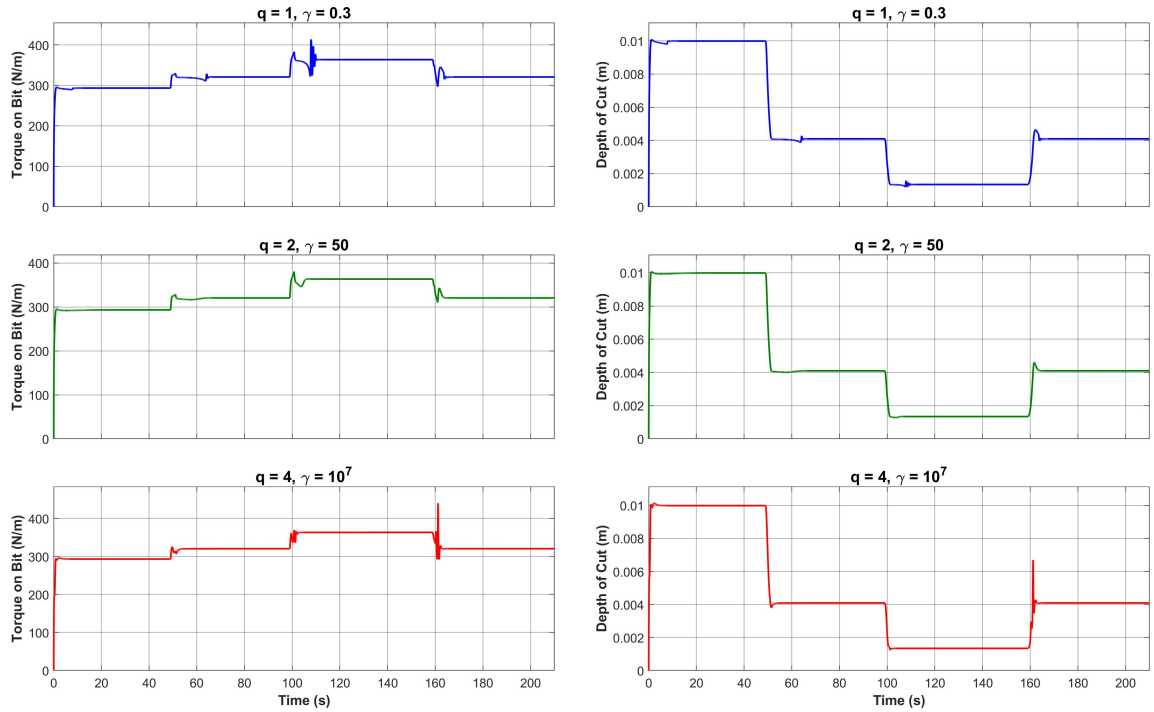

Figure 3.6: Rate of penetration regulation: torque-on-bit $T(t)$ (left plot) and depth of cut $d(t)$ (right plot) for different q.

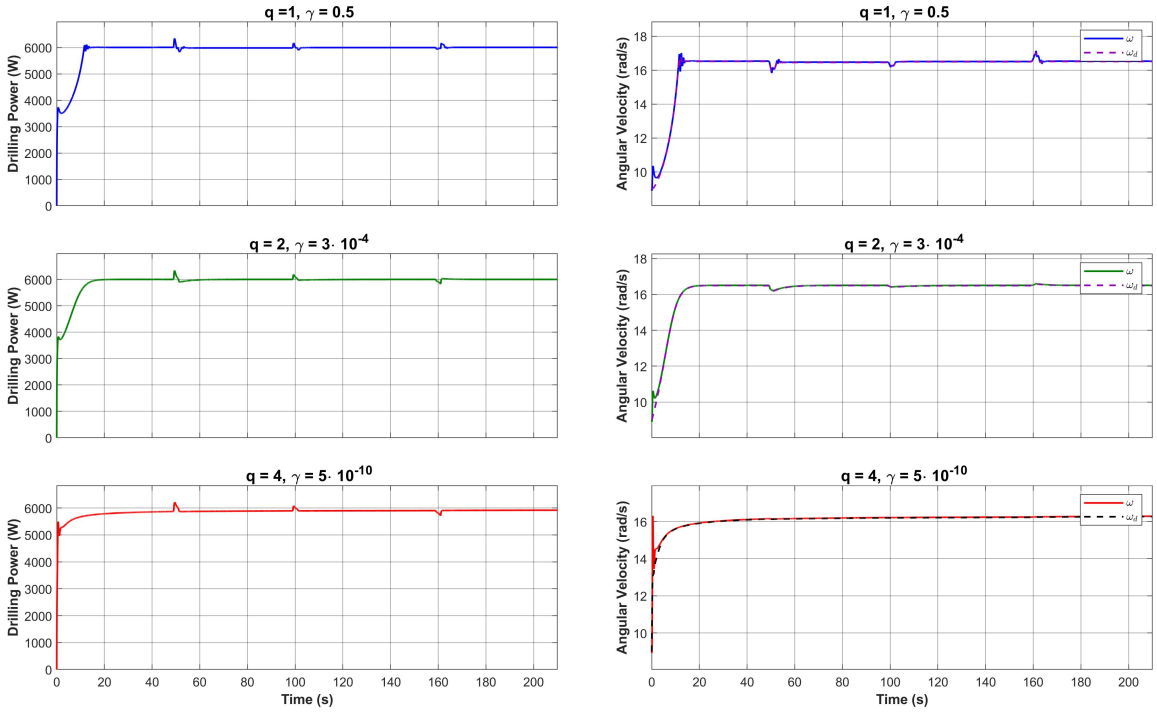

Figure 3.7: Drilling power regulation: drilling power $P(t)$ (left plot); output angular velocity of the drill bit $\omega(t)$ vs. reference angular velocity $\omega_d(t)$ (right plot) for different q.

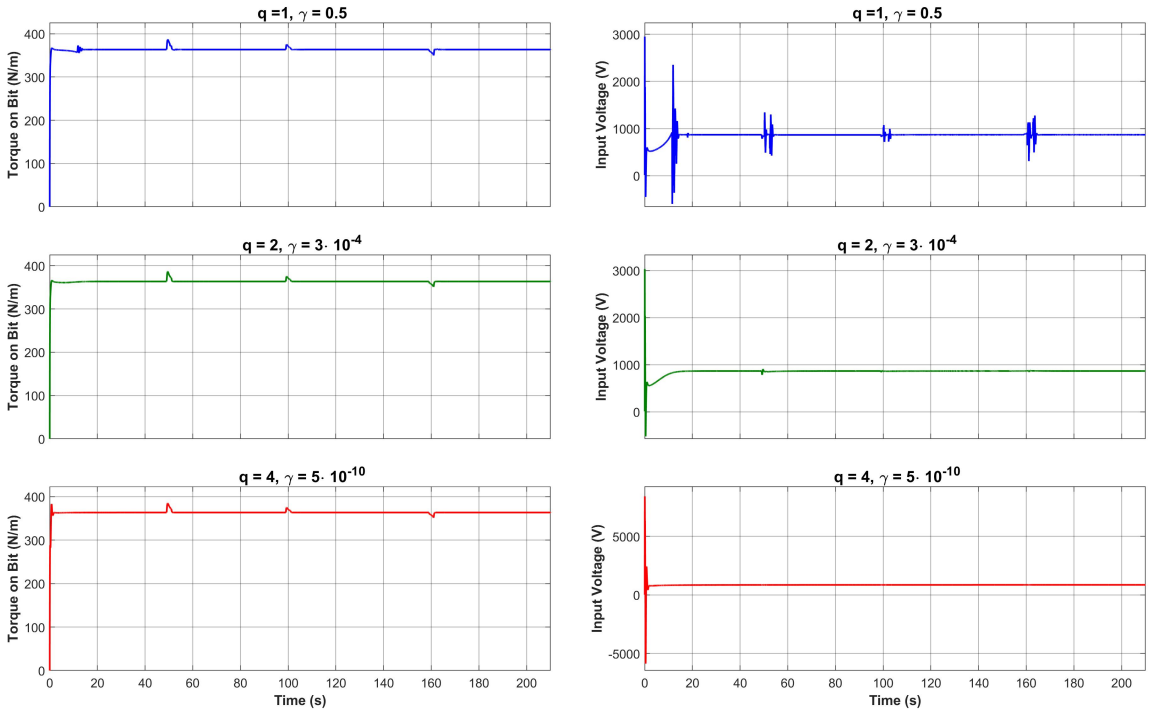

Figure 3.8: Drilling power regulation: torque-on-bit $T(t)$ (left plot); input control signal $V(t)$ (right plot) for different q.

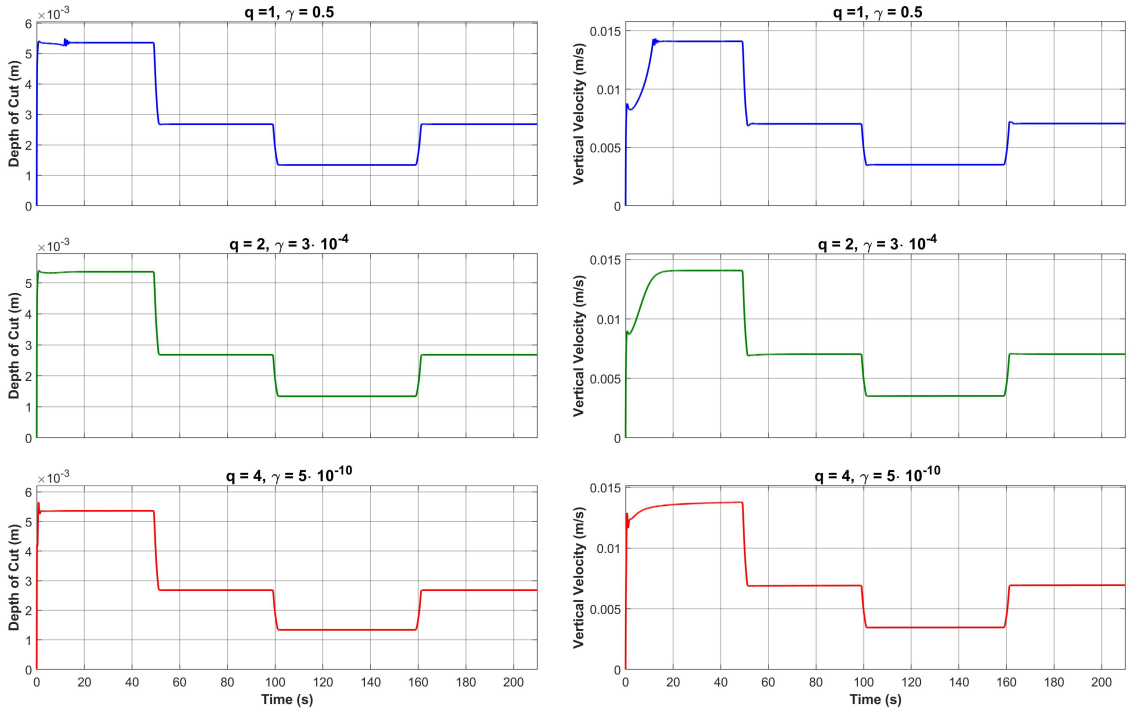

Figure 3.9: Drilling power regulation: depth of cut $d(t)$ (left plot); rate of penetration $v(t)$ (right plot) for for different q.

Chapter 4

Control of Penetration Rate in Distributed Parameter Rotary Drilling Systems

This chapter is based on the following article:

Maksim V. Faronov and Ilia G. Polushin. Control of penetration rate in distributed parameter rotary drilling systems. In *2021 IEEE Conference on Control Technology and Applications (CCTA)*, pp. 1095–1102, San Diego, USA, August 2021.

4.1 Abstract

This paper deals with control of vertical penetration rate in a spatially distributed rotary drilling system with limited measurements at the bottom level and unknown parameters of the rock-bit interaction. Rotational dynamics of the drilling system are represented using an infinite-dimensional model. A control algorithm which allows for regulation of the vertical penetration rate to a desired constant level is presented. The proposed algorithm has a cascaded structure and consists of two parts. First, a reference signal for the rotational velocity of the drill bit is derived based on the speed gradient method. Second, an algorithm for tracking of reference velocity signal by the distributed parameters rotational dynamics is designed which involves an infinite-dimensional reference model and a disturbance observer. Stability of the closed-loop system is proved using Lyapunov method. Efficiency of the obtained results is illustrated by simulations.

4.2 Introduction

Drilling automation is an important area of control engineering which was a subject of active research over recent decades [80, 31]. Advanced results were obtained in many specific areas of drilling automation including conventional vertical and directional drilling [20, 22], offshore drilling [36], extraterrestial drilling [85], *etc.* However, efficient automatic control of drilling systems remains an open challenge due to complexity of the drilling models as well as the fact that drilling systems operate in unknown and frequently unpredictable environmental conditions.

In authors' previous works [83, 86], control algorithms for regulation of vertical velocity and drilling power were developed based on simplified finite-dimensional drilling models. However, more realistic mathematical models of drilling systems are infinite-dimensional and use partial differential equations (PDEs) with control action applied at the boundary. In the literature, a number of methods were presented which deal with boundary control of distributed-parameter systems of similar type. In [87, 88], backstepping design methods were developed for systems described by PDEs with and without damping and for various boundary conditions. The paper [89] specifically deals with the problem of control of drilling systems with distributed parameters, however, a simplified model of the drilling response was used and only the problem of tracking of constant angular velocity was addressed. A number of works deal with boundary control of wave PDEs with disturbances [90, 91, 92]. Most of these results, however, are limited to the case of input disturbances which act on the same extremity as the control input, while in drilling systems the disturbances mostly appear at the drill bit level and the control action is applied at the opposite end of the drillstring located on the surface. An alternative approach was used in [15], where the authors apply a special transformation which transforms a distributed parameter model of drilling system into a finite-dimensional model with delays (neutral-type time-delay equations), and subsequently design control algorithms that use motor torque and hook force as control variables.

In this paper, we address the problem of regulation of the vertical penetration rate with disturbance rejection in rotary drilling systems. We extend our previous results [86] to a more realistic (and also substantially more difficult) case where the rotational dynamics are described by a distributed parameters model. Combining it with a detailed nonlinear model of the rock-bit interaction developed in [20] and a model of translational dynamics from [93], we present a

cascaded control design approach, where the vertical penetration velocity is regulated through tracking of the reference angular velocity of the drill bit. The paper is organized as follows. Section 4.3 presents the mathematical model of the drilling system. In Section 4.4, the control problem is formulated and the assumptions are stated. The control design approach is presented in Section 4.5. Numerical simulations which illustrate efficiency of the proposed solution are demonstrated in 4.6. Finally, in Section 4.7, conclusions are presented and possible future research is outlined.

4.3 Mathematical model of the drilling system

The structure of a vertical drilling system is shown in Figure 4.1. The system includes

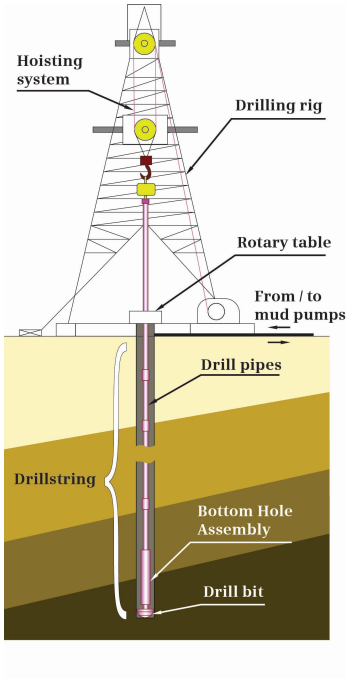

Figure 4.1: The structure of the drilling system

a drilling rig, which is located above the ground, and an underground drillstring. A drilling process itself is conducted at the bottom hole by a drill bit. The Bottom Hole Assembly (BHA) is located close to the bit, and its function is to apply additional pressure and carry the necessary equipment, such as sensors. The BHA is connected to a rotary table on the ground through drill pipes joined together via threaded connectors. The rotational system is equipped with a powerful motor which generates torque, transferring it underground and rotating the whole

drillstring. The string is also connected to a hoisting system that regulates a vertical force by lifting or dropping the underground components.

The mathematical model of the drilling system consists of three parts which are the rotational dynamics, the translational dynamics, and the model of interaction between the bit and the rock.

4.3.1 Rotational dynamics

For the rotational dynamics of the rotary drilling system, we use a distributed parameter model adapted from the one in [15]. Let $x \in [0, 1]$ denote a normalized distance between the ground level and the corresponding point along the drillstring; in particular, $x = 0$ and $x = 1$ correspond to positions of the rotary table and the drill bit, respectively. By $\phi(x, t)$ we denote the angle of rotation along the drillstring as a function of normalized distance x and time t. Following standard practice, we use subscripts to denote partial derivatives; for example, $\phi_t(x, t) := \partial\phi(x, t)/\partial t$, $\phi_x(x, t) := \partial\phi(x, t)/\partial x$, $\phi_{tt}(x, t) := \partial^2\phi(x, t)/\partial t^2$, etc. The rotational dynamics are described by the following partial differential equation (PDE) [15]:

$$\rho J_2 \phi_{tt}(x, t) = \frac{GJ_2}{L^2}\phi_{xx}(x, t) + \frac{\epsilon_\phi}{L^2}\phi_{txx}(x, t) - \gamma_\phi \phi_t(x, t), \tag{4.1}$$

where $L > 0$ is the length of the drillsting, $G > 0$ is the shear modulus, $\rho > 0$ is density of the drillstring material, $J_2 > 0$ is geometric moment of inertia of the drill pipes ($J_2 = I_p/\rho$, where I_p is the moment of inertia), $\epsilon_\phi \geq 0$ is the rotational viscoelastic Kelvin-Voigt internal damping coefficient, and $\gamma_\phi \geq 0$ is the rotational viscous damping coefficient. The boundary conditions for PDE (4.1) are of the form

$$\frac{GJ_2}{L}\phi_x(0, t) = -I_T \phi_{tt}(0, t) - nT_m(t), \tag{4.2}$$

$$\frac{GJ_B}{L}\phi_x(1, t) = -I_B \phi_{tt}(1, t) - T(t), \tag{4.3}$$

where $I_T > 0$ and $I_B > 0$ are lumped moments of inertia at the rotary table and the drill bit levels, respectively, $J_B := I_B/\rho$ is the geometric moment of inertia at the BHA/bit level, $T_m(t)$ is motor torque, n is a gearbox ratio, and $T(t)$ is the torque-on-bit which represents a reaction

torque that appears as a result of rock cutting. The torque generated by the DC motor in (4.2) is proportional to the armature current:

$$T_m(t) = K_m I(t), \tag{4.4}$$

where $K_m > 0$ is a motor constant, $I(t)$ is armature current. Thus, the control variable here is current through the motor armature, and since the control variable enters the boundary condition (4.2) the control problem is that of boundary control [87].

In a number of recent works [89, 15, 56], the damping torques, *i.e.*, the last two term in the right-hand side of (4.1), are assumed zero. The motivation is that majority of energy dissipation in drilling systems is due to the rock-bit interaction, and therefore dissipation due to damping torques acting on the drillstring can be considered negligible. In this work, we assume that the Kelvin-Voigt internal damping is null (*i.e.*, $\epsilon_\phi = 0$), however, the viscous damping is generally speaking non-negligible ($\gamma_\phi > 0$). Under these assumptions, one can rewrite the model (4.1)-(4.4) in the following form:

$$\phi_{tt}(x,t) = c^2\phi_{xx}(x,t) - k_1\phi_t(x,t), \tag{4.5}$$

$$\phi_x(0,t) = -k_2\phi_{tt}(0,t) - k_3 I(t), \tag{4.6}$$

$$\phi_x(1,t) = -q\phi_{tt}(1,t) + \tau(t), \tag{4.7}$$

where $c := \frac{1}{L}\sqrt{G/\rho} > 0$, $k_1 := \frac{\gamma_\phi}{\rho J_2} > 0$, $k_2 := \frac{I_T L}{G J_2} > 0$, $k_3 := \frac{K_m n L}{G J_2} > 0$, $q := \frac{\rho L}{G} > 0$ are known coefficients, and $\tau(t) = -\frac{L}{G J_B} T(t)$ is a non-measurable disturbance.

4.3.2 Translational dynamics

In this work, we address the case where the longitudinal deformations of the drillstring are assumed negligible. Therefore, for the translational dynamics, we use a lumped parameter model of the form [93]:

$$M\dot{v}(t) = W_0 - W(t) - K_f v(t), \tag{4.8}$$

where $v(t)$ is the vertical rate of the bit penetration, $M > 0$ is the overall mass of the drillstring, W_0 is the difference between the submerged weight of the drilling system and the force applied by the hoisting system, $K_f > 0$ is the viscous friction coefficient, and $W(t)$ is the weight-on-bit which is a reaction force generated in response to the drillstring's pressure applied to the bottom hole.

4.3.3 Bit-rock interaction

To describe the interaction between the drill bit and the rock, we use a mathematical model for the drilling response developed in [20, 19]. The drilling response model relates the torque-on-bit T and the weight-on-bit W to the vertical rate of penetration v and the rotational velocity of the bit $\omega := \phi_t(1, t)$. To obtain these relations, one can decompose T and W into their cutting and frictional components, as follows

$$T = T^c + T^f, \quad W = W^c + W^f, \tag{4.9}$$

where the superscripts c and f denote the cutting and the frictional components, respectively. The cutting components are given by the following formulas [20, 19]:

$$T^c := \frac{1}{2}a^2\epsilon d, \quad W^c := a\zeta\epsilon d, \tag{4.10}$$

where $a > 0$ is the bit radius, $\epsilon \geq 0$ is the intrinsic specific energy which represents the amount of energy spent for cutting a unit volume of the material by an ideally sharp bit, ζ is the ratio of the vertical force to the horizontal force between the rock and the cutter contact surfaces, and $d > 0$ is the depth of cut. The depth of cut d is an important variable which describes the vertical penetration distance per one revolution of the bit. In the steady state, it can be approximated using the following formula [20]

$$d = 2\pi\frac{v}{\omega}. \tag{4.11}$$

In contrast with the cutting components T^c, W^c, expressions that describe the frictional components T^f, W^f depend on the specific drilling phase [20]. The drilling phases are functions of the depth of cut d. There are three phases: phase 1 in which $d < d_*$, phase 2 where $d_* \leq d \leq d_b$, and phase 3 in which $d > d_b$, where $d_* > 0$ and $d_b > d_*$ are some critical (gener-

ally unknown) values of d that correspond to transitions between drilling phases. The frictional components T^f, W^f are described as follows

$$T^f := \begin{cases} (a^2/2) \cdot \mu\gamma\sigma\kappa d, & \text{for } d < d_*, \\ (a^2/2) \cdot \mu\gamma\sigma\kappa d_*, & \text{for } d_* \le d \le d_b, \\ (a/2) \cdot \mu\gamma(\frac{d-d_b}{\beta} + a\sigma\kappa d_*), & \text{for } d > d_b, \end{cases} \tag{4.12}$$

$$W^f := \begin{cases} a\sigma\kappa d, & \text{for } d < d_*, \\ a\sigma\kappa d_*, & \text{for } d_* \le d \le d_b, \\ \frac{d-d_b}{\beta} + a\sigma\kappa d_*, & \text{for } d > d_b, \end{cases} \tag{4.13}$$

where $\mu > 0$ is a ratio between parallel and normal components of the cutter force which acts along the wear flat, $\gamma > 0$ is the bit constant which depends on the bit design, $\sigma > 0$ is the contact strength defined as a bound of the normal stress that can be transmitted by the wear flat, $\kappa > 0$ is the rate of change of contact length with d, and β is a coefficient characterizing the slope of W^f in phase 3.

4.4 Problem formulation and assumptions

In this paper, we address the problem of regulation of the vertical rate of penetration in the rotary drilling system described by the mathematical model (4.5)-(4.13). Specifically, we design a control algorithm which, for a given arbitrary desired constant value $v_d > 0$, guarantees that

$$v(t) \to v_d \quad \text{as } t \to \infty. \tag{4.14}$$

We solve the above formulated problem under the following assumptions.

Assumption 4.1 *Parameters in the equations* (4.5)-(4.7) *that describe the rotational dynamics of the drilling system (i.e., c, k_1, k_2, k_3, q) are constant and known.*

Assumption 4.2 *The angular velocity of the rotary table $\phi_t(0, t)$, the angular velocity of the drill bit $\phi_t(1, t)$, and the vertical rate of penetration $v(t)$ are continuously measured and available to the controller without delays.*

It is worth to mention that the parameters of the drill bit and the environment that enter the equations (4.8), (4.10), (4.12), (4.13), are assumed unknown. Also, the control algorithm presented below does not use real-time measurement of the torque-on-bit $T(t)$ and the weight-on-bit $W(t)$.

4.5 Control design

Step 1: Design for the desired angular velocity ω_d

At this step, our goal is to design a reference rotational velocity of the drill bit, which brings the vertical velocity to a desired constant level v_d. In doing so, we use the speed gradient approach, details of which can be found in our previous paper [86]. The algorithm for the reference rotational velocity ω_d is defined as follows:

$$\dot{\omega}_d = -\gamma_v \, \omega_d^2 \, v \, |\tilde{v}|^{z-1} \operatorname{sign}\{\tilde{v}\}, \tag{4.15}$$

where $z \in \{1, 2, \ldots\}$, $\gamma_v > 0$ is an arbitrary constant which impacts the speed of convergence, and $\tilde{v} := v - v_d$ is a vertical velocity error. It was demonstrated in [86] that $\omega(t) \equiv \omega_d(t)$ results in convergence $v(t) \to v_d$ as $t \to +\infty$. Moreover, taking into account the persistency of excitation property, which holds in this case, it can be shown that the system is globally uniformly asymptotically stable (the corresponding analysis is straightforward and can be based for example on [49, Theorem 3.10]).

Step 2: Tracking of the desired angular velocity

At this step, our goal is to design a control algorithm for the rotational dynamics (4.5)-(4.7) that guarantees exponential convergence of the angular velocity of the drill bit $\phi_t(1, t)$ to its desired value $\omega_d(t)$ as $t \to +\infty$, where $\omega_d(t)$ is generated by the algorithm (4.15). Our approach is based on that from [94], where a similar problem was solved for a wave equation with different boundary conditions and without damping. Consider the rotational dynamics (4.5)-(4.7), where the armature current I plays the role of control input. Let us redefine a control

input as follows

$$I = -k_3^{-1}\left[k_2\phi_{tt}(0,t) + \bar{u}\right], \tag{4.16}$$

where $\bar{u}$ is the new control input. Substitution of (4.16) into (4.5)-(4.7) results in the following equations of the rotational dynamics

$$\phi_{tt}(x,t) = c^2\phi_{xx}(x,t) - k_1\phi_t(x,t), \tag{4.17}$$

$$\phi_x(0,t) = \bar{u}, \tag{4.18}$$

$$\phi_x(1,t) = -q\phi_{tt}(1,t) + \tau(t). \tag{4.19}$$

In order to implement a control strategy for (4.17)-(4.19), we use a reference model and a disturbance observer. The reference model is of the form

$$g_{tt}(x,t) = c^2 g_{xx}(x,t) - k_1 g_t(x,t), \tag{4.20}$$

$$g_t(1,t) = \omega_d(t), \tag{4.21}$$

$$g_x(1,t) = -q\dot{\omega}_d(t) + \hat{\tau}(t), \tag{4.22}$$

where $\hat{\tau}$ is an estimate of disturbances τ at the bit level. The model (4.20)-(4.22) produces trajectories of the system that correspond to the reference (*i.e.*, desired) rotational velocity of the drill bit ω_d. An estimate $\hat{\tau}$ of disturbances τ used in (4.22) is obtained using a disturbance observer of the form

$$f_{tt}(x,t) = c^2 f_{xx}(x,t) - k_1 f_t(x,t), \tag{4.23}$$

subject to boundary conditions

$$f_x(0,t) = \bar{u}(t) - c_1\left(\phi_t(0,t) - f_t(0,t)\right), \tag{4.24}$$

$$f_t(1,t) = \phi_t(1,t), \tag{4.25}$$

where $c_1 > 0$ is a design parameter. An estimate $\hat{\tau}$ is subsequently generated according to the formula

$$\hat{\tau}(t) = q f_{tt}(1,t) + f_x(1,t). \tag{4.26}$$

Finally, the control input $\bar{u}$ applied to the right-hand side of (4.18) is

$$\bar{u}(t) = g_x(0,t) + c_2 \cdot \left[\phi_t(0,t) - g_t(0,t)\right], \tag{4.27}$$

where $c_2 > 0$ is a design parameter.

Using notation $\tilde{g}(\cdot) := \phi(\cdot) - g(\cdot)$, $\tilde{f}(\cdot) := \phi(\cdot) - f(\cdot)$, the equations for $\tilde{g}(\cdot)$, $\tilde{f}(\cdot)$ along the trajectories of the closed-loop system (4.17)-(4.27) are as follows

$$\tilde{g}_{tt}(x,t) = c^2 \tilde{g}_{xx}(x,t) - k_1 \tilde{g}_t(x,t), \tag{4.28}$$

$$\tilde{f}_{tt}(x,t) = c^2 \tilde{f}_{xx}(x,t) - k_1 \tilde{f}_t(x,t), \tag{4.29}$$

subject to conditions

$$\tilde{g}_x(0,t) = c_2\, \tilde{g}_t(0,t), \tag{4.30}$$

$$\tilde{f}_x(0,t) = c_1 \tilde{f}_t(0,t), \tag{4.31}$$

$$\tilde{g}_x(1,t) = -q\tilde{g}_{tt}(1,t) + \tilde{f}_x(1,t), \tag{4.32}$$

$$\tilde{f}_t(1,t) = 0, \tag{4.33}$$

where, in particular, equation (4.33) follows from (4.25), while (4.32) can be obtained by combining (4.19), (4.25), and (4.26).

In order to formulate the stability result, let us introduce the spatial $\mathcal{L}_2$-norms of signals $\tilde{g}_t$, $\tilde{g}_x$, according to the formulas $\|\tilde{g}_t(t)\|_2 := \left(\int_0^1 \tilde{g}_t^2(x,t)dx\right)^{1/2}$, $\|\tilde{g}_x(t)\|_2 := \left(\int_0^1 \tilde{g}_x^2(x,t)dx\right)^{1/2}$, and similarly for $\tilde{f}_t$, $\tilde{f}_x$. The following result is valid.

Theorem 4.5.1 *Consider the system* (4.28)-(4.33). *Suppose the coefficients c,* k_1 *that enter equation* (4.5) *satisfy the condition*

$$k_1 < c/2. \tag{4.34}$$

Then for any gains $c_1, c_2 > 0$, along the trajectories of the system (4.28)-(4.33), $\|\tilde{g}_t(t)\|_2 \to 0$, $\|\tilde{g}_x(t)\|_2 \to 0$, $\|\tilde{f}_t(t)\|_2 \to 0$, $\|\tilde{f}_x(t)\|_2 \to 0$ *exponentially as* $t \to +\infty$.

Remark 4.1 *The condition* (4.34) *means that the viscous damping along the drillstring is sufficiently small. The assumption is reasonable, in fact, in the literature the viscous damping is frequently assumed zero as majority of energy dissipation happens at the bit-rock interface (see for example [15, Section 2.2.2] and references therein).*

Proof Consider the following Lyapunov functional candidate:

$$V := K \cdot V_f + V_g, \tag{4.35}$$

where

$$\begin{aligned} V_f := \frac{1}{2}\int_0^1 \tilde{f}_t^2(x,t)dx + \frac{c^2}{2}\int_0^1 \tilde{f}_x^2(x,t)dx \\ -\beta_1 \int_0^1 x\tilde{f}_t(x,t)\tilde{f}_x(x,t)dx - \beta_2 \int_0^1 (1-x)\tilde{f}_t(x,t)\tilde{f}_x(x,t)dx, \end{aligned} \tag{4.36}$$

and

$$V_g := \frac{1}{2}\int_0^1 \tilde{g}_t^2(x,t)dx + \frac{c^2}{2}\int_0^1 \tilde{g}_x^2(x,t)dx + \frac{qc^2}{2}\tilde{g}_t^2(1,t) + \beta_3 \int_0^1 (x-2)\tilde{g}_t(x,t)\tilde{g}_x(x,t)dx. \tag{4.37}$$

In the above functional, the parameters $K > 0, \beta_1 > 0, \beta_2 > 0, \beta_3 > 0$ are chosen such that

$$\beta_2 < \min\left\{c, \frac{2c^2c_1}{1+c^2c_1^2}\right\}, \tag{4.38}$$

$$\beta_3 < \min\left\{\frac{c}{2}, \frac{c^2c_2}{1+c^2c_2^2}\right\}, \tag{4.39}$$

$$\beta_1 < \beta_2\left(1 - \frac{k_1}{c}\right), \tag{4.40}$$

$$K > \frac{c^2}{\beta_1\beta_3}. \tag{4.41}$$

It is easy to verify that V_f, V_g are positive definite; more precisely, there exist κ_{1f}, κ_{2f}, κ_{1g},

$\kappa_{1g} > 0$ such that

$$\kappa_{1f}\left(\|\tilde{f}_t\|_2^2 + \|\tilde{f}_x\|_2^2\right) \le V_f \le \kappa_{2f}\left(\|\tilde{f}_t\|_2^2 + \|\tilde{f}_x\|_2^2\right), \tag{4.42}$$

$$\kappa_{1g}\left(\|\tilde{g}_t\|_2^2 + \|\tilde{g}_x\|_2^2\right) \le V_g \le \kappa_{2g}\left(\|\tilde{g}_t\|_2^2 + \|\tilde{g}_x\|_2^2\right). \tag{4.43}$$

Indeed, collecting the terms in (4.36), we have

$$V_f = \int_0^1 \left[\frac{1}{2}\tilde{f}_t^2 + \frac{c^2}{2}\tilde{f}_x^2 + ((\beta_2 - \beta_1)x - \beta_2)\,\tilde{f}_t\tilde{f}_x\right] dx. \tag{4.44}$$

From (4.40), (4.38), it follows that $0 < \beta_1 < \beta_2 < c$. Taking into account $0 \le x \le 1$, we see that $c^2 - ((\beta_2 - \beta_1)x - \beta_2)^2 > 0$. The latter implies that the expression under the integral in (4.44) is a positive definite quadratic form, which implies (4.42). Similarly, (4.39) implies (4.43).

In the derivations below, the arguments (x, t) will be omitted unless $x = 0$ or $x = 1$. The time derivative of the Lyapunov function (4.36) is

$$\dot{V}_f = \int_0^1 \left(\tilde{f}_t\tilde{f}_{tt} + c^2\tilde{f}_x\tilde{f}_{xt}\right) dx - \beta_1 \int_0^1 x\left(\tilde{f}_{tt}\tilde{f}_x + \tilde{f}_t\tilde{f}_{xt}\right) dx - \beta_2 \int_0^1 (1-x)\left(\tilde{f}_{tt}\tilde{f}_x + \tilde{f}_t\tilde{f}_{xt}\right) dx.$$

Using (4.29), and integrating by parts, one gets

$$\begin{aligned}\dot{V}_f = {} & c^2\tilde{f}_x\tilde{f}_t\Big|_0^1 - \frac{c^2\beta_1}{2}x\tilde{f}_x^2\Big|_0^1 - \frac{\beta_1}{2}x\tilde{f}_t^2\Big|_0^1 - \frac{c^2\beta_2}{2}(1-x)\tilde{f}_x^2\Big|_0^1 - \frac{\beta_2}{2}(1-x)\tilde{f}_t^2\Big|_0^1 \\ & - \left(\frac{\beta_2}{2} - \frac{\beta_1}{2} + k_1\right)\int_0^1 \tilde{f}_t^2 dx - c^2\left(\frac{\beta_2}{2} - \frac{\beta_1}{2}\right)\int_0^1 \tilde{f}_x^2 dx - k_1\int_0^1 ((\beta_2 - \beta_1)x - \beta_2)\,\tilde{f}_t\tilde{f}_x dx \\ = {} & c^2\tilde{f}_x(1)\tilde{f}_t(1) - c^2c_1\tilde{f}_t^2(0) - \frac{c^2\beta_1}{2}\tilde{f}_x^2(1) - \frac{\beta_1}{2}\tilde{f}_t^2(1) + \frac{c^2\beta_2c_1^2}{2}\tilde{f}_t^2(0) + \frac{\beta_2}{2}\tilde{f}_t^2(0) \\ & - \left(\frac{\beta_2}{2} - \frac{\beta_1}{2} + k_1\right)\int_0^1 \tilde{f}_t^2 dx - c^2\left(\frac{\beta_2}{2} - \frac{\beta_1}{2}\right)\int_0^1 \tilde{f}_x^2 dx - k_1\int_0^1 ((\beta_2 - \beta_1)x - \beta_2)\,\tilde{f}_t\tilde{f}_x dx.\end{aligned}$$

Taking advantage of the fact that $\tilde{f}_t(1) = 0$, we obtain

$$\dot{V}_f = -\left(c^2 c_1 - \frac{\beta_2}{2} - \frac{\beta_2 c^2 c_1^2}{2}\right)\tilde{f}_t^2(0) - \frac{\beta_1 c^2}{2}\tilde{f}_x^2(1) - \left(\frac{\beta_2}{2} - \frac{\beta_1}{2} + k_1\right)\int_0^1 \tilde{f}_t^2 dx - c^2\left(\frac{\beta_2}{2} - \frac{\beta_1}{2}\right)\int_0^1 \tilde{f}_x^2 dx - k_1\int_0^1 ((\beta_2 - \beta_1)x - \beta_2)\,\tilde{f}_t\tilde{f}_x dx.$$

Next, the time derivative of V_g is

$$\dot{V}_g = \int_0^1 \tilde{g}_t\tilde{g}_{tt}dx + c^2\int_0^1 \tilde{g}_x\tilde{g}_{xt}dx + qc^2\tilde{g}_t(1)\tilde{g}_{tt}(1) + \beta_3\int_0^1 (x-2)\tilde{g}_{tt}\tilde{g}_x dx + \beta_3\int_0^1 (x-2)\tilde{g}_t\tilde{g}_{xt}dx.$$

After integration, one can see that

$$\dot{V}_g = c^2\tilde{g}_x\tilde{g}_t\Big|_0^1 + qc^2\tilde{g}_t(1)\tilde{g}_{tt}(1) + \frac{c^2\beta_3}{2}(x-2)\tilde{g}_x^2\Big|_0^1 + \frac{\beta_3}{2}(x-2)\tilde{g}_t^2\Big|_0^1 - \left(\frac{\beta_3}{2} + k_1\right)\int_0^1 \tilde{g}_t^2 dx - \frac{c^2\beta_3}{2}\int_0^1 \tilde{g}_x^2 dx - k_1\beta_3\int_0^1 (x-2)\tilde{g}_t\tilde{g}_x dx$$

$$= c^2\tilde{g}_t(1)\tilde{f}_x(1) - c^2c_2\tilde{g}_t^2(0) - \frac{c^2\beta_3}{2}(-q\tilde{g}_{tt}(1) + \tilde{f}_x(1))^2 - \frac{\beta_3}{2}\tilde{g}_t^2(1) + c^2\beta_3 c_2^2\tilde{g}_t^2(0) + \beta_3\tilde{g}_t^2(0) - \left(\frac{\beta_3}{2} + k_1\right)\int_0^1 \tilde{g}_t^2 dx - \frac{c^2\beta_3}{2}\int_0^1 \tilde{g}_x^2 dx - k_1\beta_3\int_0^1 (x-2)\tilde{g}_t\tilde{g}_x dx.$$

and using Young's quadratic inequality $\tilde{g}_t(1)\tilde{f}_x(1) \leq \frac{\delta_1}{2}\tilde{g}_t^2(1) + \frac{1}{2\delta_1}\tilde{f}_x^2(1)$ which holds for an arbitrary $\delta_1 > 0$, one obtains:

$$\dot{V}_g \leq -(c^2c_2 - \beta_3 - \beta_3 c^2 c_2^2)\tilde{g}_t^2(0) - \frac{c^2\beta_3}{2}(-q\tilde{g}_{tt}(1) + \tilde{f}_x(1))^2 - \left(\frac{\beta_3}{2} - \frac{c^2\delta_1}{2}\right)\tilde{g}_t^2(1) + \frac{c^2}{2\delta_1}\tilde{f}_x^2(1) - \left(\frac{\beta_3}{2} + k_1\right)\int_0^1 \tilde{g}_t^2 dx - \frac{c^2\beta_3}{2}\int_0^1 \tilde{g}_x^2 dx - \frac{c^2\beta_3}{2}\int_0^1 \tilde{g}_x^2 dx - k_1\beta_3\int_0^1 (x-2)\tilde{g}_t\tilde{g}_x dx.$$

Now, for the overall Lyapunov function(al) candidate (4.35), we would like to show that

there exists $\sigma > 0$, such that $\dot{V} + \sigma V < 0$. We have:

$$\dot{V} + \sigma V = K\dot{V}_f + \dot{V}_g + \sigma K V_f + \sigma V_g$$
$$\leq -K\left(c^2c_1 - \frac{\beta_2}{2} - \frac{\beta_2 c^2 c_1^2}{2}\right)\tilde{f}_t^2(0) - (\frac{K\beta_1 c^2}{2} - \frac{c^2}{2\delta_1})\tilde{f}_x^2(1) - (c^2c_2 - \beta_3 - \beta_3 c^2 c_2^2)\tilde{g}_t^2(0)$$

$$- \frac{c^2\beta_3}{2}(-q\tilde{g}_{tt}(1) + \tilde{f}_x(1))^2 - \frac{\beta_3 - c^2\delta_1 - \sigma q c^2}{2}\tilde{g}_t^2(1) - \frac{K\beta_2 - K\beta_1 - \sigma}{2}\int_0^1 \tilde{f}_t^2 dx$$
$$- \frac{c^2}{2}(K\beta_2 - K\beta_1 - \sigma)\int_0^1 \tilde{f}_x^2 dx + (\sigma - Kk_1)\int_0^1 ((\beta_2 - \beta_1)x - \beta_2)\,\tilde{f}_t\tilde{f}_x dx - \frac{\beta_3 - \sigma}{2}\int_0^1 \tilde{g}_t^2 dx$$
$$- \frac{c^2}{2}(\beta_3 - \sigma)\int_0^1 \tilde{g}_x^2 dx + (\sigma - k_1)\beta_3\int_0^1 (x-2)\tilde{g}_t\tilde{g}_x dx.$$

It can be shown that, if the conditions (4.34)-(4.41) are met, the inequality $\dot{V} + \sigma V < 0$ is satisfied with

$$\sigma = \min\left\{\frac{\beta_3 - c^2\delta_1}{qc^2}, \frac{(c + 2k_1\,\mathrm{sign}\{\beta_3 - k_1\})\beta_3}{2\beta_3\,\mathrm{sign}\{\beta_3 - k_1\} + c}, \frac{cK(\beta_2 - \beta_1) + Kk_1\beta_2\,\mathrm{sign}\{\beta_2 - \beta_1 - k_1\}}{\beta_2\,\mathrm{sign}\{\beta_2 - \beta_1 - k_1\} + c}\right\}.$$

Thus, $\dot{V} \leq -\sigma V$, which implies $V(t) \leq V(0)e^{-\sigma t}$, and the statement of theorem follows from (4.35), (4.42), and (4.43). •

Theorem 4.5.1, in particular, states that $\|\tilde{g}_t(t)\|_2^2 := \int_0^1 \tilde{g}_t^2(x,t)dx \to 0$ exponentially as $t \to +\infty$. Taking into account the uniform boundedness of $\tilde{g}_{tx} = \tilde{g}_{xt}$ along the trajectories of the closed-loop system, this implies $\tilde{g}_t(1,t) := \phi_t(1,t) - \omega_d(t) \to 0$ exponentially as $t \to +\infty$. Indeed, integrating by parts, one obtains

$$\int_0^1 \tilde{g}_t^2(x,t)dx = \tilde{g}_t^2(x,t)\,x\Big|_{x=0}^1 - 2\int_0^1 x\tilde{g}_t(x,t)\tilde{g}_{tx}(x,t)dx = \tilde{g}_t^2(1,t) - 2\int_0^1 x\tilde{g}_t(x,t)\tilde{g}_{tx}(x,t)dx,$$

and therefore

$$\tilde{g}_t^2(1,t) = \int_0^1 \tilde{g}_t^2(x,t)dx + 2\int_0^1 x\tilde{g}_t(x,t)\tilde{g}_{tx}(x,t)dx \le \|\tilde{g}_t(t)\|_2^2 + 2\left(\int_0^1 \tilde{g}_t^2(x,t)dx\right)^{\frac{1}{2}}\left(\int_0^1 x^2\tilde{g}_{tx}^2(x,t)dx\right)^{\frac{1}{2}}$$

$$\le \|\tilde{g}_t(t)\|_2^2 + 2\left(\int_0^1 \tilde{g}_t^2(x,t)dx\right)^{\frac{1}{2}}\left(\int_0^1 \tilde{g}_{tx}^2(x,t)dx\right)^{\frac{1}{2}} = \|\tilde{g}_t(t)\|_2^2 + 2\cdot\|\tilde{g}_t(t)\|_2\cdot\|\tilde{g}_{tx}(t)\|_2,$$

where we used the Cauchy-Schwartz inequality and an (obvious) fact that $x^2 \le 1$ for all $x \in [0,1]$. From the last string of inequalities, it follows that uniform boundedness of $\tilde{g}_{tx}(x,t)$ together with the fact that $\|\tilde{g}_t(t)\|_2 \to 0$ exponentially as $t \to +\infty$ imply $\tilde{g}_t(1,t) := \phi_t(1,t) - \omega_d(t) \to 0$ exponentially as $t \to +\infty$.

Step 3: The overall stability analysis

Now, in order to justify the stability properties of the overall drilling control systems, consider a block diagram shown in Figure 4.2. Assuming $\tilde{g}_t(1,t) \equiv 0$, the feedback loop consisting of translational dynamics and speed-gradient control algorithm (4.15) is globally uniformly asymptotically stable (Section 4.5 Step 1). On the other hand, as shown in Section 4.5, Step 2, the output $\tilde{g}_t(1,t) := \phi_t(1,t) - \omega_d(t)$ of the controlled rotational dynamics exponentially converges to zero for arbitrary bounded signals $\omega_d, \dot{\omega}_d$. Thus, the overall system can be represented as a cascade interconnection of a driving subsystem whose output converges exponentially to zero and a globally uniformly asymptotically stable driven subsystem (Figure 4.3). Under mild technical assumptions, such a cascade is globally asymptotically stable [95, Corollary 1]. In addition, the initial conditions for the driving system (*i.e.*, the controlled rotational dynamics) can be set equal to zero by resetting the initial states of the model (4.20)-(4.22), the observer (4.23)-(4.25), as well as that of the speed gradient controller (4.15). This would theoretically result in the output of the controlled rotational dynamics being totally equal to zero, *i.e.*, $\tilde{g}_t(1,t) \equiv 0$, which effectively reduces the overall cascade dynamics to those of the driven system (*i.e.* the controlled translational dynamics) which are globally uniformly asymptotically stable.

Remark 4.2 *As it was mentioned before, the angular acceleration on the upper extremity* $\phi_{tt}(0,t)$ *is used in the control algorithm* (4.16)*. Due to the assumption that only* $\phi_t(0,t)$ *and* $\phi_t(1,t)$ *are measurable but their derivatives are not, this acceleration should be estimated. It*

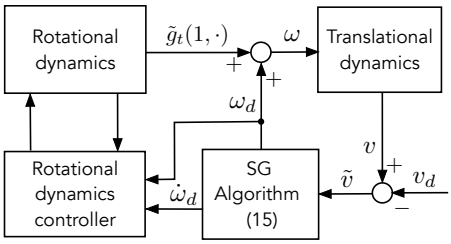

Figure 4.2: The structure of the control system

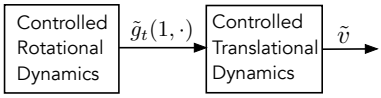

Figure 4.3: The aggregated structure

can be done by using a high order sliding mode (HOSM) observer, which theoretically can provide perfect real-time differentiation while staying robust to noises. Adapting the result from [78], one can use the following structure:

$$\dot{\phi}_1 = -\lambda_1 M_0^{1/2} |\phi_1 - \phi_t(0,t)|^{1/2} \operatorname{sign}\{\phi_1 - \phi_t(0,t)\} - \mu_1 \sigma(\phi_1 - \phi_t(0,t)) + \phi_2,$$

$$\dot{\phi}_2 = -\lambda_2 M_0 \operatorname{sign}\{\phi_2 - \dot{\phi}_1\} - \mu_2 \sigma(\phi_2 - \dot{\phi}_1), \tag{4.45}$$

where $M_0 > 0$ is a sufficiently large number, $\lambda_i > 1$ are HOSM differentiator parameters that may be chosen recursively [79], $\mu_i > 0$ are arbitrary positive coefficients, and $\sigma > 0$ is an adjustable gain. An estimate of the second time derivative is defined by $\hat{\phi}_{tt}(0,t) = \phi_2(t)$. This signal can be used in place of the real value in (4.16)*.*

4.6 Simulation results

In this section, we present an example of simulation results of the drilling system with the proposed control algorithm. For simulation of PDEs, we use a simple implicit finite difference method. A discrete version of the algorithm for reference rotational velocity (4.15) (with $z = 2$) is obtained using second-order Taylor method [96]:

$$\omega_d(j+1) = \omega_d(j) - \gamma \omega_d^2(j) v(j) \tilde{v}(j) \Delta t + \gamma^2 \omega_d^3(j) v^2(j) \tilde{v}^2(j) \Delta t^2.$$

Table 4.1: Numerical values of the parameters used in simulations (Chapter 4)

Parameter	Value	Parameter	Value
Parameters set by operator			
$v_d, m/s$	0.025	c_1	0.1
c_2	1200	γ_v	50
Drilling system parameters			
$G, N/m^2$	$79.3 \cdot 10^9$	$\rho, kg/m^3$	8000
L, m	1400	W_0, N	4150
I_b, kgm^2	352	M, kg	52000
I_B,kgm^2	110	K_f, Nm	28
I_T, kgm^2	91	a, m	0.093
I_p, kgm^2	2317	ζ	0.82
n	5	d_*, m	0.002
K_m, Vs	8.6	$\mu\gamma$	2.7
γ_ϕ, Ns	100		
Parameters of the environment			
$\epsilon, J/m^3$	$5 \cdot 10^6/1 \cdot 10^7/2 \cdot 10^7$		
$\sigma\kappa, N/m^2$	0.89ϵ		

The exact discretization of the (linear) equation of the translational dynamics (4.8) is obtained as follows:

$$v(j+1) = e^{-\frac{K_f}{M}\Delta t} v(j) - \frac{W_0 - W(j)}{K_f}\left(e^{-\frac{K_f}{M}\Delta t} - 1\right).$$

Numerical values of all parameters that are used in the simulations are presented in Table 4.1. We simulate the drilling process through several rock layers with different intrinsic specific energy. Simulation results obtained using time step $\Delta t = 0.15$ s and spatial discretization step of $\Delta x = 7$ m are presented in Figures 4.4 - 4.8. It can be seen that the proposed controller solves the regulation problem, specifically the rate of penetration converges to its desired value $v_d = 0.025 m/s$ in a reasonable time. Rotational velocity of the drill bit $\phi_t(x,t)$ tracks the reference rotational velocity $\omega_d(t)$ almost ideally, and the disturbance is estimated rather precisely. Also, the error $\tilde{g}(x,t)$ converges to a small neighborhood of zero in each layer.

4.7 Conclusions

In this paper, the problem of regulation of the vertical penetration rate in rotary drilling systems is addressed in the situation where the parameters of the rock-bit interaction are un-

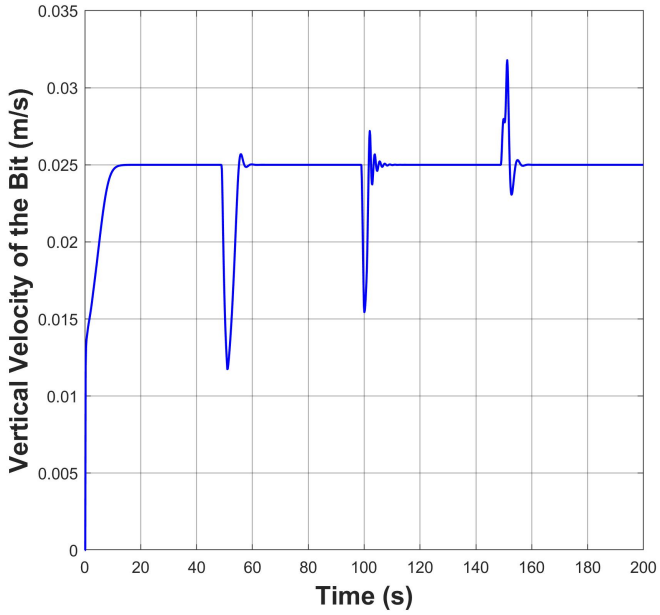

Figure 4.4: Rate of penetration $v(t)$

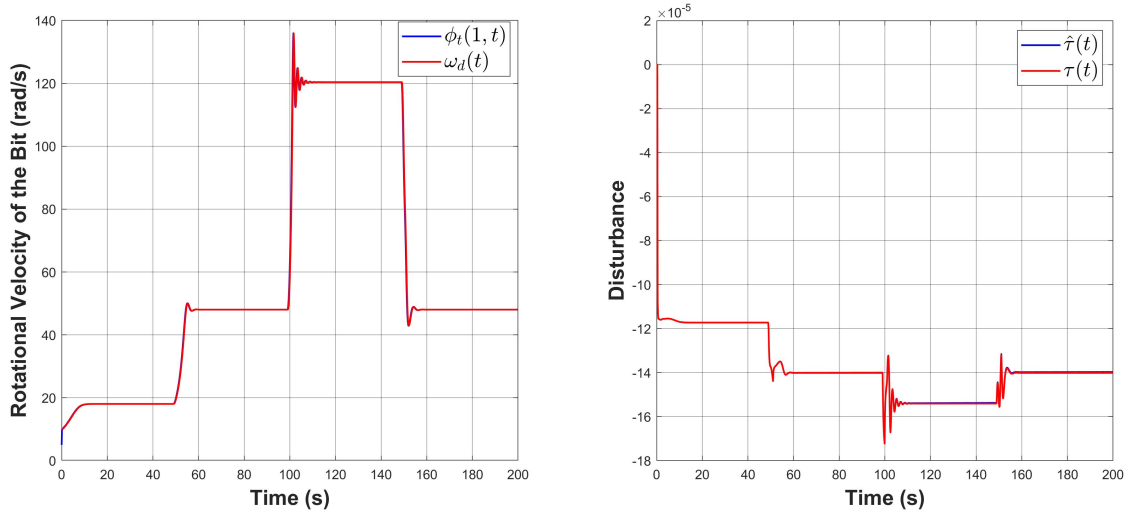

Figure 4.5: Output angular velocity of the drill bit $\phi_t(1,t)$ vs. reference angular velocity $\omega_d(t)$ (left plot); disturbance $\tau(t)$ vs. its estimate $\hat{\tau}(t)$ (right plot).

known. The rotational dynamics of the drilling system are assumed to be infinite-dimensional and modeled using partial differential equations. A cascaded approach for control of translational dynamics is developed which is based on regulation of the angular velocity of the drill bit using a distributed parameter reference model, where unmeasured variables at the bit level are estimated using a distributed parameter observer. The convergence is proved using Lya-

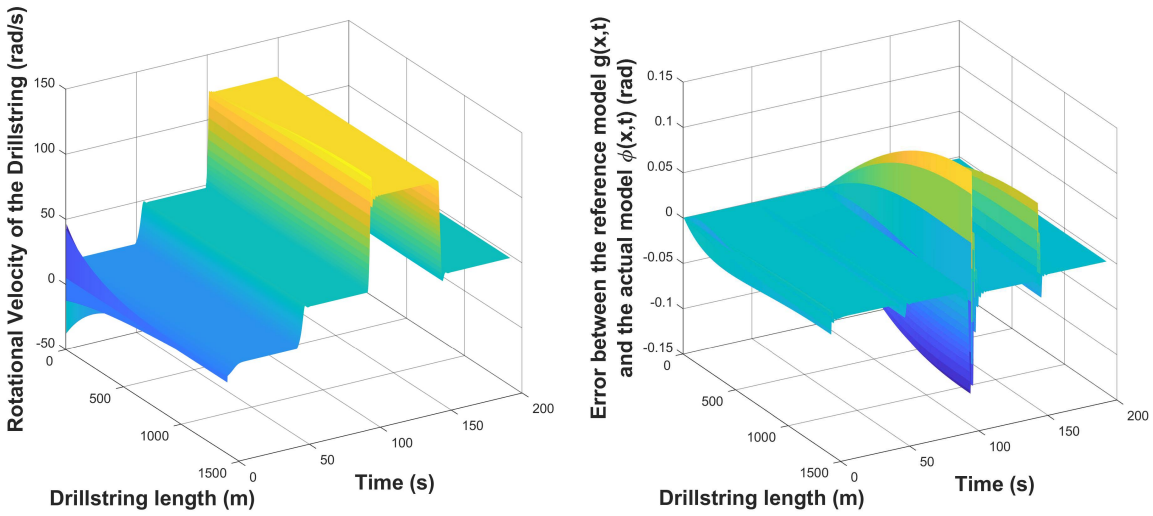

Figure 4.6: Angular velocity along the drillstring $\phi_t(x,t)$ (left plot); error between the reference and the actual angle of rotation $\tilde{g}(x,t) = \phi(x,t) - g(x,t)$ (right plot).

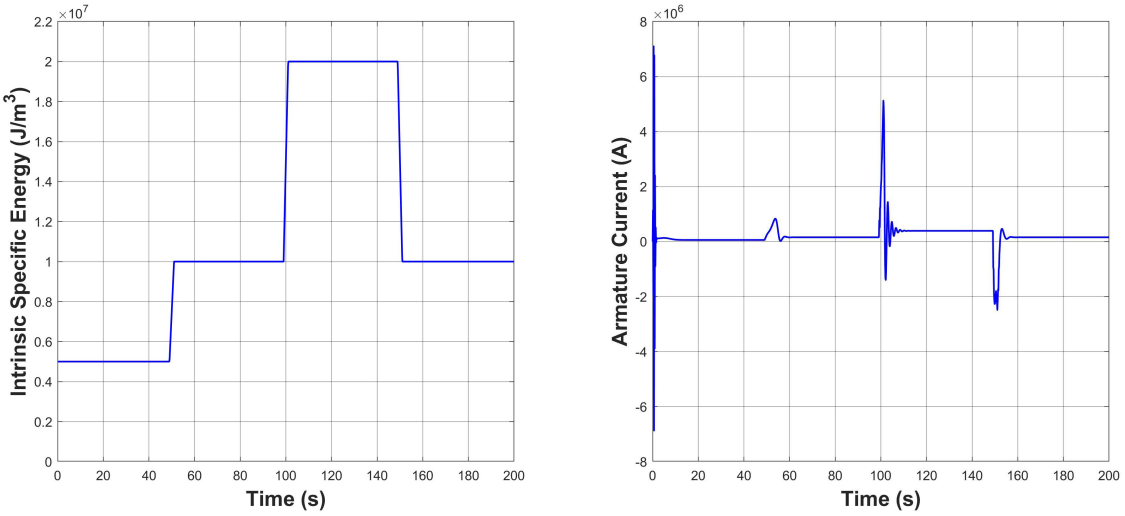

Figure 4.7: Intrinsic specific energy $\epsilon(t)$ (left plot); input control signal $I(t)$ (right plot).

punov methods. An example of simulations is presented which demonstrate the validity and efficiency of the proposed results. Future research will deal with investigation of robust properties of the proposed algorithm and possible development of adaptive versions in the case where parameters of the system are unknown and/or subject to change.

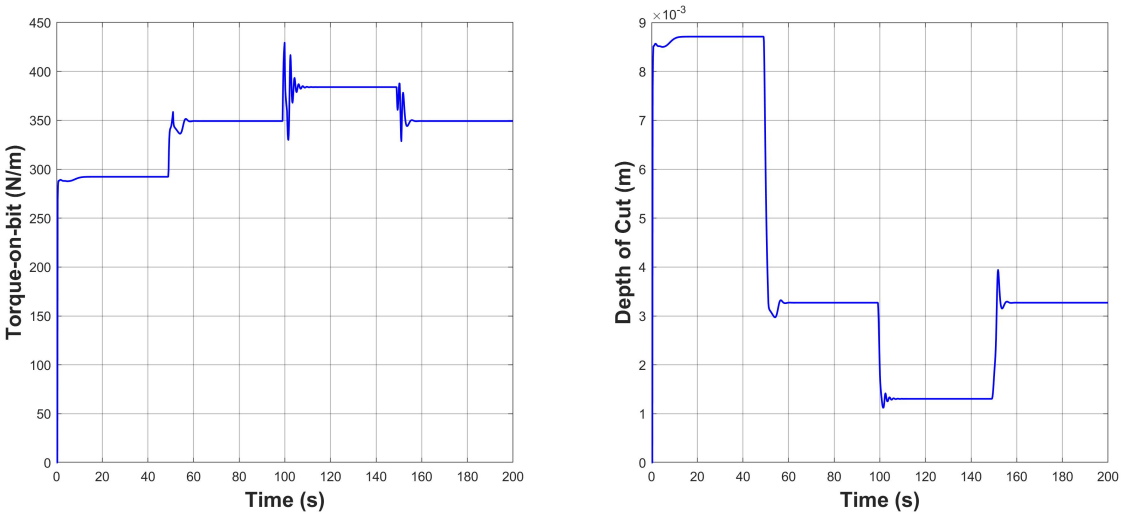

Figure 4.8: Torque-on-bit $T(t)$ (left plot); depth of cut $d(t)$ (right plot).

Chapter 5

Observer-Based Control of Vertical Penetration Rate in Rotary Drilling Systems

This chapter is based on the following article:

Maksim V. Faronov and Ilia G. Polushin. Observer-based control of vertical penetration rate in rotary drilling systems. Journal of Process Control, Volume 106, pp. 29–43, 2021.

5.1 Abstract

An algorithm for regulation of the vertical penetration rate in rotary drilling systems is developed under the assumption that parameters of the rock-bit interaction as well as those of the translational dynamics are unknown. The control design utilizes a multi-step approach, where the vertical penetration velocity is regulated through an appropriate assignment of a reference rotational velocity signal, while the tracking of the latter is achieved using tracking with disturbance rejection scheme. In contrast with the existing results, the algorithm does not require real-time measurement and communication to the ground level of the downhole variables, such as angular position, rotational velocity, and torque-on-bit. This is achieved through the use of high-order sliding mode observers which estimate the required downhole variables based on measurements performed at the ground level. Simulation results are presented which confirm efficiency of the proposed control method.

5.2 Introduction

In modern drilling systems, automation is an important component which allows for safer, cheaper, and more efficient operations [5]. Industrial companies currently employ drilling automation systems with different degrees of autonomy, from monitoring to fully automated solutions [97]. Over the recent decades, researchers have worked on different aspects of automatic drilling, such as modeling and control of the drill bit in conventional vertical drilling [98, 56], trajectory control for directional drilling [99, 100], pressure control in managed pressure drilling [36, 101], and other challenges. However, many areas of drilling automation remain underdeveloped [31], and the existing solutions can be made more effective by introduction of new methods and elimination of simplifying assumptions.

One of the typical tasks in automatic control of drilling systems is to bring the drilling operation to a certain desired stable mode and maintain it automatically while suppressing vibrations and rejecting disturbances. A number of approaches to modeling and control of the drilling systems have been developed over the years (see [102]). Models of the drilling process differ substantially in their complexity. On one end of the complexity spectrum are finite-dimensional lumped parameter models [16, 68]. Even though these models do not typically describe the processes happening in the wellbore in full detail, they nevertheless allow for design of observers and control algorithms that were proven practically effective. Examples of such controllers include soft torque algorithm [57], impedance matching [58], $\mathcal{H}_\infty$-based method [103], and others. On the other end of the complexity spectrum are infinite-dimensional models which allow for more realistic description of the drilling systems [15], where the most complex models combine distributed torsional dynamics with axial [104] as well as lateral [105] dynamics. In particular, infinite-dimensional models reveal complex dynamics and patterns of behavior of the drillstrings which are impossible to predict using lumped-parameter models [18, 106]. The control approaches for infinite-dimensional drilling models include flatness based feedforward control with disturbance rejection [107], observer-based robust stabilization of interconnections that involve hyperbolic partial differential equations [108], prediction-based adaptive backstepping-like controller [89], and the use of a transformation which transforms partial differential equations into a system of finite-dimensional neutral-type time delay equations [15]. Recently in [109], a design of observer for parameters of the bit-rock interaction law is presented based on an infinite-dimensional model for torsional

dynamics.

Previously in [86], we addressed the problems of regulation of the vertical penetration rate and the drilling power in rotary drilling systems in the situation where the process of rock-bit interaction is described by the nonlinear drilling response model [20], parameters of which are assumed unknown. We presented a two-step control design that solves the problem of regulation of the vertical penetration rate, while also solving the drilling power regulation problem under the assumption that the drilling process is in the phase 1 [20]. The major limitation of the control design presented in [86] is the assumption that the angular position and the rotational velocity of the drill bit, as well as the torque-on-bit are continuously and precisely measured and available to the ground-level controller without delays. This assumption is unrealistic [31]; in fact, in real life drilling automation systems, the borehole measurements are noisy, and the communication process between the bottom hole and the ground level is subject to severe data rate limitations as well as latency and jitter.

In this paper, we address the problem of regulation of the vertical penetration rate in rotary drilling system assuming unknown parameters of the rock-bit interaction process. We improve upon the results developed in [86] by completely removing the assumptions of direct measurement of the angular position and the rotational velocity of the drill bit, as well as that of the torque-on-bit. This is achieved through design of a hybrid high-order sliding mode observer which generates theoretically exact estimates of the dynamic variables at the downhole level as well as those of input disturbances including torque-on-bit and its time derivatives. Since these estimates are generated based on measurements performed at the ground level, the proposed approach also allows for complete elimination of any and all assumptions related to real-time communication between the downhole and the ground levels. The design approach used in our work utilizes a lumped parameter model of the drilling system dynamics which allows for use of tools from finite-dimensional observer and control theory. The designed control and observation algorithm is subsequently simulated in conjunction with infinite-dimensional distributed parameter model of drillstring rotational dynamics similar to that of [15], and the simulation results demonstrate validity of the design approach. A preliminary version of some of the results from this paper is reported in [110].

The paper is organized as follows. In Section 5.3, the mathematical model of the drilling system is described, including rotational dynamics, translational dynamics, and the rock-bit interaction model. In Section 5.4, the control problem is formulated, and the assumptions are

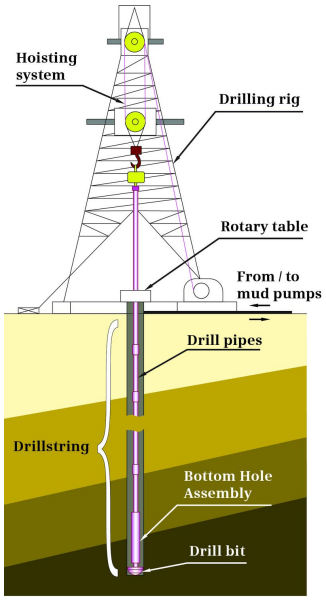

Figure 5.1: The structure of the drilling system

stated. The design of control/observation algorithm is discussed in Section 5.5. Simulation results are presented in Section 5.6, while in Section 5.7 concluding remarks are given.

5.3 Mathematical model of the drilling system

The purpose of the drilling system is to create a borehole by rotating a drill bit which crushes the surrounding rock. The structure of a vertical rotary drilling system is shown in Figure 5.1. The system consists of ground components, which include a drilling rig together with the drive and the hoisting systems, and the underground parts which include the drillstring and the Bottom Hole Assembly (BHA). On the ground, a large rotary table controlled by a powerful DC motor is connected to the drillstring. The drive system generates torque, and the drillstring transfers the torque to the drill bit. The drillstring mainly consists of hollow drill pipes. The upper end of the drill string is attached to the hoisting system, which controls the hook and applies a specified upward force. The BHA is attached to the lower end of the drillstring, and contains the drill bit as well as other components such as sensors.

The mathematical model of the drilling system that we use includes three major components: rotational dynamics, translational dynamics, and the interaction between the bit and the

rock. The rotational dynamics are described by the following equations [16]:

$$J_1\ddot{\phi} + c_1\dot{\phi} + k(\phi - \phi_r) + T = 0, \tag{5.1}$$

$$J_2\ddot{\phi}_r + c_2\dot{\phi}_r - k(\phi - \phi_r) - nT_m = 0, \tag{5.2}$$

where (5.1) describes the dynamics of BHA and the drill pipes while (5.2) those of the rotary table and the drive. In these equations, ϕ denotes the angular position of the drill bit, ϕ_r is the angular position of the rotary table, $J_1 > 0$ is the equivalent combined moment of inertia of the BHA and the drill pipes while $J_2 > 0$ is that of the rotary table and the drive, $c_1, c_2 \geq 0$ are the equivalent nominal viscous damping coefficients, $k > 0$ is the equivalent torsional stiffness of the drill pipes, T_m is the torque generated by the motor, n is the gearbox ratio, and T is an equivalent torque applied to the drill bit which includes the "torque-on-bit" [20] (*i.e.*, the reaction torque generated due to rock cutting process) as well as an equivalent sum of all other torques due to different effects not accounted for in the model (5.1). The dynamics of the electric drive (a DC motor with a separated excitation circuit) are described by standard equations

$$L\dot{I} + RI - V_b - V = 0, \quad V_b = K_m n\dot{\phi}_r, \quad T_m = K_m I, \tag{5.3}$$

where I is the armature current, L is an equivalent armature inductance, R is an equivalent armature resistance, V_b is the back EMF, V is the armature voltage, and $K_m > 0$ is a motor constant which depends on its characteristics. Using notation $\tilde{\phi} := \phi_r - \phi$, $\omega := \dot{\phi}$, $\omega_r := \dot{\phi}_r$, the rotational dynamics (5.1)-(5.3) can be represented in the state-space form [50, 83, 86], as follows

$$\begin{bmatrix} \dot{\omega} \\ \dot{\tilde{\phi}} \\ \dot{\omega}_r \\ \dot{I} \end{bmatrix} = \begin{bmatrix} -\frac{c_1}{J_1} & \frac{k}{J_1} & 0 & 0 \\ -1 & 0 & 1 & 0 \\ 0 & -\frac{k}{J_2} & -\frac{c_2}{J_2} & \frac{K_m n}{J_2} \\ 0 & 0 & -\frac{K_m n}{L} & -\frac{R}{L} \end{bmatrix} \begin{bmatrix} \omega \\ \tilde{\phi} \\ \omega_r \\ I \end{bmatrix} + \begin{bmatrix} -\frac{1}{J_1} \\ 0 \\ 0 \\ 0 \end{bmatrix} T + \begin{bmatrix} 0 \\ 0 \\ 0 \\ \frac{1}{L} \end{bmatrix} V. \tag{5.4}$$

The translational dynamics of the drill string are represented by the following differential

equation

$$M\dot{v} = W_0 - W - K_f v, \tag{5.5}$$

where v is the vertical velocity (penetration rate) of the drill bit, $M > 0$ is the combined mass of the drill pipes and the BHA, W_0 is the difference between the submerged weight of the drilling system and the constant upward force supplied by the hoisting system, $K_f > 0$ is the viscous friction coefficient, and W is the weight-on-bit which is the upward reaction force applied to the bit.

The interaction between the drill bit and the rock is described by the so called drilling response model [20], which defines (generally speaking, nonlinear) relationships between the angular ω and the vertical v velocities of the bit, the torque-on-bit (denoted below by T_b to distinguish from an equivalent torque T used in equation (5.1)) and the weight-on-bit W. Specifically, both the torque-on-bit and the weight-on-bit are decomposed into sums of cutting and frictional components:

$$T_b = T^c + T^f, \quad W = W^c + W^f, \tag{5.6}$$

where the superscripts c and f denotes the cutting and the frictional components, respectively. In the case of a bit without hollow areas, the cutting components are defined as follows [20, 19]:

$$T^c := \frac{1}{2}a^2\epsilon d, \quad W^c := a\zeta\epsilon d, \tag{5.7}$$

where $a > 0$ is the radius of the bit, $\epsilon \geq 0$ is the intrinsic specific energy, which is the amount of energy consumed for cutting a unit volume of the material by an ideally sharp bit, ζ represents the ratio of the vertical force to the horizontal force between the rock and the cutter contact surfaces, and $d > 0$ is the depth of cut, *i.e.*, the vertical distance to which the bit moves during one revolution. In the steady state, the depth of cut can be approximated by the following expression [20]:

$$d \approx 2\pi\frac{v}{\omega}. \tag{5.8}$$

The frictional components T^f, W^f depend on the so-called drilling phase. Depending on the

depth of cut, three phases of drilling are defined [20]. In phase 1, which corresponds to small $d > 0$, the frictional components depend on d linearly. In phase 2, which begins as d reaches some critical value d_*, the frictional components remain constant regardless of changes in d. Phase 3, which begins once d reaches another critical value d_b, is characterized by a "lack of uniqueness in the response of the bit" [20, Section 3.3], however, for the sake of simplicity, T^f, W^f can be approximated in phase 3 as linear (more precisely, affine) functions of d with unknown slopes. Overall, the frictional components are described by the following mathematical model:

$$T^f := \begin{cases} (a^2/2) \cdot \mu\gamma\sigma\kappa d, & \text{for } d < d_* \text{ (phase 1)}, \\ (a^2/2) \cdot \mu\gamma\sigma\kappa d_*, & \text{for } d_* \le d \le d_b \text{ (phase 2)}, \\ (a/2) \cdot \mu\gamma(\frac{d-d_b}{\beta} + a\sigma\kappa d_*), & \text{for } d > d_b \text{ (phase 3)}, \end{cases} \tag{5.9}$$

$$W^f := \begin{cases} a\sigma\kappa d, & \text{for } d < d_* \text{ (phase 1)}, \\ a\sigma\kappa d_*, & \text{for } d_* \le d \le d_b \text{ (phase 2)}, \\ \frac{d-d_b}{\beta} + a\sigma\kappa d_*, & \text{for } d > d_b \text{ (phase 3)}, \end{cases} \tag{5.10}$$

where $\mu > 0$ is the friction coefficient, which is a ratio between parallel and normal components of the cutter force which acts along the wear flat, $\gamma > 0$ is the bit constant which reflects the bit design and the distribution of the contact forces, $\sigma > 0$ is the contact strength defined as a bound of the normal stress that can be transmitted by the wear flat, $\kappa > 0$ is the rate of change of contact length with d, $d_* > 0$ is the critical value of d when contact forces are fully mobilized, which depends on the bit bluntness, $d_b > d_*$ is the critical value of d when the contact surface between the bit and the rock increases, and β is a coefficient which characterizes the slopes of T^f, W^f in phase 3. In the following, we will use the specific mathematical structure of the weigh-on-bit W described above. As for torque-on-bit T_b, we will not use its mathematical description explicitly, but instead assume that the equivalent torque applied to the drill bit has a form $T(t) := T_b(t) + T'(t)$, where $T'(t)$ is a sufficiently regular function of time which represents an equivalent of all physical effects not accounted for in the above model.

5.4 Problem formulation and assumptions

In this section, we state the control problem addressed in this work and formulate the corresponding assumptions.

5.4.1 Problem formulations

In this paper, the following problem is addressed.

Problem 1: Regulation of the vertical rate of penetration. Given $v_d > 0$, find a control algorithm that guarantees

$$v(t) \to v_d \quad \text{as } t \to \infty. \tag{5.11}$$

5.4.2 Assumptions

The problem formulated above is addressed in this work under the following two assumptions.

Assumption 5.1 *The following signals/variables are available for measurement: i) vertical penetration rate v; ii) rotary table velocity ω_r; iii) armature current I.* •

It is worth to notice that both velocity of the rotary table ω_r and the armature current I are ground level signals which in practice are readily available for measurement and can be communicated to the (ground level) controller without delays. We also assume that the stiffness of the system in the vertical direction is infinite, so that the vertical penetration rate can also be measured at the ground level. On the other hand, measurement of the downhole level variables (such as equivalent torque T, rotational velocity of the drill bit ω, and the angular displacement of the bit $\tilde{\phi}$) is not assumed. Since measurement of the downhole variables are not used in the control algorithm, no assumptions about the communication process between the downhole and the ground level are necessary.

Assumption 5.2 *The following parameters are known to the designer: i) equivalent moments of inertia $J_1, J_2 > 0$; ii) nominal equivalent viscous damping coefficients $c_1, c_2 \geq 0$; iii) equivalent torsional stiffness $k > 0$; iv) gearbox ratio n.* •

All parameters mentioned in Assumption 5.2 are nominal parameters related to the structural design of the drilling system and therefore can be assumed known with reasonable precision. Dynamic effects due to variation of these parameters, such as additional torques, are considered disturbances and can be accounted for in the equivalent torque signal $T(t)$. On the other hand, parameters of the translational dynamics (5.5) and those of the bit-rock interaction model (5.6), (5.7), (5.9), (5.10) are assumed to be (constant) unknown.

5.5 Control design

The design of control algorithms that solve the problem of regulation of the vertical penetration rate formulated in Section 5.4 is presented below. The control design process consists of four steps. In Step 1, we present design of a family of control algorithms that solve the vertical penetration rate problem under the assumption that the angular velocity of the drill bit ω can be controlled directly. More precisely, we design an auxiliary control signal ω_d such that $\omega \equiv \omega_d$ solves the control problem. In Step 2, we present a trajectory tracking with disturbance rejection control algorithm for the rotational dynamics that guarantees tracking of the reference angular velocity ω_d while simultaneously rejecting the disturbance which physically corresponds to the equivalent torque applied to the drill bit. Implementation of this control algorithm requires knowledge of the equivalent torque as well as its derivatives, as well as derivatives of the reference angular velocity, none of which are immediately available. Therefore, in Step 3 we present design of higher-order sliding mode (HOSM) observers that provide estimates of the required signals and their derivatives. HOSM observers have a unique property of finite-time convergence, and the corresponding estimates are exact in the absence of disturbances and robust in their presence. Finally, in Step 4, all components of the control algorithm are combined, and stability of the overall control system is justified.

5.5.1 Step 1: Design for the reference angular velocity

At this first step, we design control algorithms that solve the problem of regulation of the vertical penetration rate assuming the angular velocity of the drill bit ω can be controlled directly. As described above in Section 5.4, we do this under the assumption that all the parameters entering the equation of the translational dynamics (5.5) as well as the formulas that

describe the rock-bit interaction (5.6)-(5.10) are constant and unknown. Under these assumptions, Problem 1 is solved below using the speed-gradient methodology [49]. We begin with deriving the equations that relate the angular velocity ω to the translational dynamics (5.5). Taking into account (5.6), (5.7), and (5.10), one can write

$$W(d) = a_w d + b_w, \tag{5.12}$$

where $a_w > 0$ and b_w are coefficients that depend on phase of drilling and the parameters of the rock-bit interaction model. Substituting (5.12) into (5.5), one can write

$$\dot{v} = -\left(\frac{K_f}{M} + \frac{2\pi a_w}{M\omega}\right)v + \frac{W_0 - b_w}{M}, \tag{5.13}$$

and using notation $K_1 := \frac{K_f}{M} > 0$, $K_2 := \frac{2\pi a_w}{M} > 0$, $K_3 := \frac{W_0 - b_w}{M} > 0$, equation (5.13) can be written in the form

$$\dot{v} = -(K_1 + K_2\omega^{-1})v + K_3. \tag{5.14}$$

It is clear that for any constant $\omega(t) \equiv \omega_* > 0$, equation (5.14) has a globally exponentially stable equilibrium at

$$v_* = \frac{K_3}{K_1 + K_2\omega_*^{-1}}.$$

Conversely, given $v_* \in (0; \frac{K_3}{K_1})$, the choice $\omega(t) \equiv \omega_*$ where

$$\omega_* = \frac{K_2 v_*}{K_3 - K_1 v_*},$$

makes v_* the globally exponentially stable equilibrium of (5.14).

Let $v_d > 0$ be a desired vertical rate of penetration, and let $\omega_* > 0$ be determined by (5.5.1) by setting $v_* = v_d$. Denote

$$\theta := K_1 + K_2\omega^{-1}, \quad \theta_* := K_1 + K_2\omega_*^{-1}, \quad \tilde{\theta} := \theta - \theta_*. \tag{5.15}$$

From (5.5.1) one can see that $K_3 = \theta_* v_d$. Equation (5.14) becomes

$$\dot{v} = -\theta v + \theta_* v_d.$$

Using notation $\tilde{v} := v - v_*$, one can write

$$\dot{\tilde{v}} = -(\tilde{\theta} + \theta_*)v + \theta_* v_d = -\tilde{\theta}v - \theta_*\tilde{v}. \tag{5.16}$$

Equation (5.16) describes the dynamics of the vertical penetration. For the purposes of control design, let us augment the dynamics (5.16) with the following equation

$$\dot{\tilde{\theta}} \equiv \dot{\theta} = -K_2 \frac{\dot{\omega}}{\omega^2}. \tag{5.17}$$

which can be obtained by differentiating (5.15) with respect to time while taking into account that K_1, K_2 are positive constants. Equation (5.16) together with (5.17) describe the relationship between the vertical rate of penetration and the rotational velocity.

Our goal at this step is to design a control algorithm that guarantees the global asymptotic stability of the system (5.16), (5.17) assuming the rotational velocity ω is directly available for control. The global asymptotic stability (5.16), (5.17) would, in particular, imply that $\tilde{v} \to 0$ as $\to +\infty$, which solves the problem of regulation of the vertical penetration rate. In order to solve this problem, we apply the speed-gradient control design methodology [49]. To this end, consider a family of goal functions

$$Q_{v,q} := \frac{1}{q} \cdot |\tilde{v}|^q, \quad \text{where } q = 2, 3, \ldots \tag{5.18}$$

Calculating the time derivative of $Q_{v,q}$ along the trajectories of (5.16), one obtains

$$\begin{aligned} \dot{Q}_{v,q} &= |\tilde{v}|^{q-1} \operatorname{sign}\{\tilde{v}\}\, \dot{\tilde{v}} = |\tilde{v}|^{q-1} \operatorname{sign}\{\tilde{v}\} \left(-\tilde{\theta}v - \theta_*\tilde{v}\right) \\ &= -\tilde{\theta}v\, |\tilde{v}|^{q-1} \operatorname{sign}\{\tilde{v}\} - q\, Q_{v,q}\theta_*. \end{aligned} \tag{5.19}$$

Taking into account $\tilde{\theta} := \theta - \theta_*$, one can calculate

$$\frac{\partial \dot{Q}_{v,q}}{\partial \theta} = -v \cdot |\tilde{v}|^{q-1} \operatorname{sign}\{\tilde{v}\}, \tag{5.20}$$

and the corresponding family of speed-gradient algorithms [49, Chapter 3] can be obtained as

follows

$$\dot{\tilde{\theta}} \equiv \dot{\theta} = -\gamma_1 \frac{\partial \dot{Q}_{v,q}}{\partial \theta} = \gamma_1 \, v \, |\tilde{v}|^{q-1} \operatorname{sign}\{\tilde{v}\}, \quad q = 2, 3, \ldots \tag{5.21}$$

Taking into account (5.17), we see that (5.21) is equivalent to the following algorithm for the rotational velocity ω:

$$\dot{\omega} = -\gamma_v \, \omega^2 \, v \, |\tilde{v}|^{q-1} \operatorname{sign}\{\tilde{v}\}, \quad q = 2, 3, \ldots \tag{5.22}$$

where $\gamma_v := \gamma_1 / K_2 > 0$.

The following result is valid.

Theorem 5.5.1 *The translational drilling dynamics* (5.16)*,* (5.17) *controlled by algorithm* (5.22) *is globally asymptotically stable. In particular,*

$$v(t) \to v_d \quad \text{as } t \to +\infty. \tag{5.23}$$

Proof. Conditions for asymptotic stability of a nonlinear system controlled by a speed-gradient algorithm can be found in [49, Theorem 3.10]. The statement of Theorem 5.5.1 formulated above can therefore be proven by demonstrating that system (5.16), (5.17), (5.22) satisfies all conditions of [49, Theorem 3.10]. Theorem 3.10 of [49] contains a relatively high number of technical assumptions, however, essential conditions are as follows. First, $Q_{v,q}$ must grow without bound as $|\tilde{v}| \to \infty$, which obviously follows from the definition of $Q_{v,q}$ given by equation (5.18). Second, convexity of $\dot{Q}_{v,q}$ with respect to θ, which in our case trivially follows from the fact that the right-hand side of (5.19) is linear w.r.t. θ. The third essential condition is the existence of a constant θ_* and $\rho > 0$ such that $\dot{Q}_{v,q} \le -\rho \cdot Q_{v,q}$ whenever $\theta = \theta_*$. This is also satisfied in our case for θ_* as defined above (*i.e.*, $\theta_* := K_1 + K_2 \omega_*^{-1}$), and $\rho := q \cdot \theta_*$, which can be shown by combining (5.16), (5.18), and (5.19). Finally, the vertical penetration velocity v must be a persistently exciting signal [49, Definition 3.1], which is trivially satisfied due to the fact that in normal mode of drilling operation $v(t) \ge \epsilon_v$ for some $\epsilon_v > 0$. The rest of conditions imposed by [49, Theorem 3.10] are related to regularity of different functions that comprise the system's description, all of which are immediately satisfied for the system in question. Thus all conditions of [49, Theorem 3.10] are satisfied, and the statement of Theorem 5.5.1 follows.

•

Theorem 5.5.1 implies that any algorithm of the form (5.21) solves the problem of regulation of the rate of penetration (Problem 1).

5.5.2 Step 2: Tracking of the reference angular velocity

At this step, our goal is to design a control algorithm for rotational dynamics (5.4) which guarantees tracking of the reference velocity signal ω_d while simultaneously rejecting the disturbances represented by an equivalent torque $T(t)$. The algorithm is designed here under the assumption that all state variables of the rotational dynamics (5.4) as well as the reference velocity signal ω_d and the torque $T(t)$ together with required number of their derivatives are available for controller. This assumption will be fundamentally relaxed in the subsequent part of the paper. Let us rewrite the system (5.4) in the state-space form

$$\begin{aligned} \dot{x} &= Ax + Bu + DT, \\ y &= Cx, \end{aligned} \tag{5.24}$$

where

$$A = \begin{bmatrix} -\frac{c_1}{J_1} & \frac{k}{J_1} & 0 & 0 \\ -1 & 0 & 1 & 0 \\ 0 & -\frac{k}{J_2} & -\frac{c_2}{J_2} & \frac{K_m n}{J_2} \\ 0 & 0 & -\frac{K_m n}{L} & -\frac{R}{L} \end{bmatrix}, \quad B = \begin{bmatrix} 0 \\ 0 \\ 0 \\ \frac{1}{L} \end{bmatrix}, D = \begin{bmatrix} -\frac{1}{J_1} \\ 0 \\ 0 \\ 0 \end{bmatrix}, \quad C = \begin{bmatrix} 1 \\ 0 \\ 0 \\ 0 \end{bmatrix}^T, \tag{5.25}$$

$$x = \begin{bmatrix} \omega & \tilde{\phi} & \omega_r & I \end{bmatrix}^T, \quad u = V. \tag{5.26}$$

In the above model, $u = V$ is the control input signal, and T is the disturbance which is to be rejected. The control algorithm has the following form

$$u = -Kx + u_d + u_T, \tag{5.27}$$

where $K := \begin{bmatrix} k_1 & k_2 & k_3 & k_4 \end{bmatrix}$ is the feedback gain matrix chosen such that the closed-loop system has desired dynamical properties, defined by a matrix $A - BK$, u_d is the component

which is responsible for tracking of the desired value of the output, and u_T is the component which ensures disturbance rejection. In order to define these components, one can represent the system (5.24)-(5.27) in the input-output form:

$$\Omega(s) = \begin{bmatrix} W_u(s) & W_T(s) \end{bmatrix} \begin{bmatrix} U_d(s) + U_T(s) \\ T(s) \end{bmatrix}, \tag{5.28}$$

where $\Omega(s)$ is the Laplace transform of the output $y = \omega$, and $W_u(s) := C\left[s\mathbb{I} - A + BK\right]^{-1} B$, $W_T(s) := C\left[s\mathbb{I} - A + BK\right]^{-1} D$ are transfer functions that correspond to a part of the control input $u_d + u_T$ and the disturbance input T, respectively. Let $\Omega_d(s)$ denote the Laplace transform of $\omega_d(t)$. From (5.28), one concludes that the following control inputs

$$U_T(s) = -\frac{W_T(s)}{W_u(s)} T(s), \quad U_d(s) = \frac{1}{W_u(s)} \Omega_d(s), \tag{5.29}$$

result in $\Omega(s) = \Omega_d(s)$.

Assuming that the system parameters are known, it is possible to calculate the transfer functions in (5.29) directly. In this case, they can be represented as polynomials:

$$-\frac{W_T(s)}{W_u(s)} = \beta(s) = \beta_3 s^3 + \beta_2 s^2 + \beta_1 s + \beta_0, \tag{5.30}$$

$$\frac{1}{W_u(s)} = \alpha(s) = \alpha_4 s^4 + \alpha_3 s^3 + \alpha_2 s^2 + \alpha_1 s + \alpha_0, \tag{5.31}$$

where the coefficients $\beta_0, \ldots, \beta_3, \alpha_0, \ldots, \alpha_4$ are functions of the system's parameters that enter equations (5.24)-(5.27). Explicit formulas for $\beta_0, \ldots, \beta_3, \alpha_0, \ldots, \alpha_4$ are given in Appendix A.

5.5.3 Step 3: HOSM observers design

Direct implementation of the control strategy (5.27) is not possible under the assumptions formulated in Section 5.4 because a number of variables and/or signals are not available for measurement. Specifically, among the four state variables (5.26) of the rotational dynamics equations, only ω_r and I are available for measurement. In addition, the implementation of control algorithm (5.29), (5.30) for u_T requires knowledge of the equivalent torque T as well as its time derivatives up to the third order, none of which are available. Finally, algorithm (5.29),

(5.31) for u_d requires knowledge of derivatives of ω_d up to the order four. In order to obtain estimates of all these variables/signals, we use approach which is based on hybrid high-order sliding mode (HOSM) homogeneous observers. These observers have unique properties in that they provide theoretically exact estimates of state variables as well as derivatives of signals [111], which makes them perfectly suitable for various control tasks, in particular those that require precise compensation of signals.

In order to design an observer, consider the equations of rotational dynamics (5.4). Assuming the armature current I is an independent measurable variable, one can augment the system (5.4) with a state-like equations for equivalent torque T and its derivatives to arrive at the following system:

$$\begin{aligned} \dot{\bar{x}} &= \bar{A}\bar{x} + \bar{B}I + \bar{D}T_4 \\ \omega_r &= \bar{C}\bar{x} \end{aligned} \tag{5.32}$$

where

$$\bar{x} = \begin{bmatrix} \omega_r \\ \tilde{\phi} \\ \omega \\ T \\ T_1 \\ T_2 \\ T_3 \end{bmatrix}, \bar{A} = \begin{bmatrix} -\frac{c_2}{J_2} & -\frac{k}{J_2} & 0 & 0 & 0 & 0 & 0 \\ 1 & 0 & -1 & 0 & 0 & 0 & 0 \\ 0 & \frac{k}{J_1} & -\frac{c_1}{J_1} & -\frac{1}{J_1} & 0 & 0 & 0 \\ 0 & 0 & 0 & 0 & 1 & 0 & 0 \\ 0 & 0 & 0 & 0 & 0 & 1 & 0 \\ 0 & 0 & 0 & 0 & 0 & 0 & 1 \\ 0 & 0 & 0 & 0 & 0 & 0 & 0 \end{bmatrix}, \bar{B} = \begin{bmatrix} \frac{K_m n}{J_2} \\ 0 \\ 0 \\ 0 \\ 0 \\ 0 \\ 0 \end{bmatrix}, \bar{C} = \begin{bmatrix} 1 \\ 0 \\ 0 \\ 0 \\ 0 \\ 0 \\ 0 \end{bmatrix}^T, \bar{D} = \begin{bmatrix} 0 \\ 0 \\ 0 \\ 0 \\ 0 \\ 0 \\ 1 \end{bmatrix}, \tag{5.33}$$

and $T_i := T^{(i)}$, $i = 1, 2, 3, 4$, are i-th derivatives of T. In the above system (5.32), the rotational velocity of the rotary table ω_r plays the role of the measurable output, the armature current I is known (measurable) input, while $T_4 := T^{(4)}$ is an unknown input.

Our task is to design a state observer for the system (5.32). For this purpose, we design a hybrid HOSM homogeneous observer [111, Section 7.2.3] which provides exact estimates of the state variables in the presence of an unknown bounded disturbance input (in our case, T_4). The hybrid HOSM observer consists of linear and HOSM parts. The linear part is of the form

$$\dot{\hat{z}} = \bar{A}\hat{z} + \bar{B}I + \bar{L}\left(\omega_r - \hat{z}_1\right), \tag{5.34}$$

where $\hat{z} \in \mathbb{R}^7$, and $\bar{L} \in \mathbb{R}^7$ is such that $\bar{A} - \bar{L}\bar{C}$ is stable. The HOSM component has a form

$$\begin{aligned}
\dot{v}_1 &= -\lambda_{11} M_1^{1/7} \cdot |v_1 - \omega_r + \hat{z}_1|^{6/7} \cdot \operatorname{sign}\{v_1 - \omega_r + \hat{z}_1\} + v_2, \\
\dot{v}_2 &= -\lambda_{12} M_1^{1/6} \cdot |v_2 - \dot{v}_1|^{5/6} \cdot \operatorname{sign}\{v_2 - \dot{v}_1\} + v_3, \\
\dot{v}_3 &= -\lambda_{13} M_1^{1/5} \cdot |v_3 - \dot{v}_2|^{4/5} \cdot \operatorname{sign}\{v_3 - \dot{v}_2\} + v_4, \\
\dot{v}_4 &= -\lambda_{14} M_1^{1/4} \cdot |v_4 - \dot{v}_3|^{3/4} \cdot \operatorname{sign}\{v_4 - \dot{v}_3\} + v_5, \\
\dot{v}_5 &= -\lambda_{15} M_1^{1/3} \cdot |v_5 - \dot{v}_4|^{2/3} \cdot \operatorname{sign}\{v_5 - \dot{v}_4\} + v_6, \\
\dot{v}_6 &= -\lambda_{16} M_1^{1/2} \cdot |v_6 - \dot{v}_5|^{1/2} \cdot \operatorname{sign}\{v_6 - \dot{v}_5\} + v_7, \\
\dot{v}_7 &= -\lambda_{17} M_1 \cdot \operatorname{sign}\{v_7 - \dot{v}_6\}
\end{aligned} \tag{5.35}$$

where $M_1 > 0$ is a sufficiently large constant, and $\lambda_{11}, \ldots, \lambda_{17}$ are to be chosen recursively [79]. The overall estimate $\hat{\bar{x}} \in \mathbb{R}^7$ of the state $\bar{x}$ can be found according to the formula

$$\hat{\bar{x}} = \hat{z} + P^{-1} v, \tag{5.36}$$

where

$$v = \begin{bmatrix} v_1 \\ v_2 \\ v_3 \\ v_4 \\ v_5 \\ v_6 \\ v_7 \end{bmatrix}, \quad P = \begin{bmatrix} \bar{C} \\ \bar{C}(\bar{A} - \bar{L}\bar{C}) \\ \bar{C}(\bar{A} - \bar{L}\bar{C})^2 \\ \bar{C}(\bar{A} - \bar{L}\bar{C})^3 \\ \bar{C}(\bar{A} - \bar{L}\bar{C})^4 \\ \bar{C}(\bar{A} - \bar{L}\bar{C})^5 \\ \bar{C}(\bar{A} - \bar{L}\bar{C})^6 \end{bmatrix}. \tag{5.37}$$

It is straightforward to check that the relative degree of system (5.32), (5.33) with respect to unknown input T_4 is equal to the system's order (both are equal to 7), and therefore the system is strongly observable [111, Definition 7.2 and Theorem 7.2]. Applying Theorem 7.3 from [111], one concludes that if T_4 is bounded then for sufficiently large $M > 0$ the hybrid

HOSM observer (5.34)-(5.37) guarantees that, in the absence of measurement noise, the estimate $\hat{\bar{x}}$ converges to the actual state $\bar{x}$ in finite time, *i.e.*, $\hat{\bar{x}}(t) \equiv \bar{x}(t)$ for all $t \geq t_0 + T$ with some $T > 0$, where t_0 is the initial instant of the estimation process.

For implementation of the algorithm (5.29), (5.31) it is also necessary to estimate the time derivatives of ω_d. For this purpose we use a hybrid differentiator proposed in [78], which combines a HOSM differentiator and a classical high-gain differentiator; the latter component improves the speed of convergence. Based on the reference signal $\dot{\omega}_d$ generated by the algorithm (5.22), the following observer is designed:

$$\begin{aligned}
\dot{f}_1 &= -\lambda_{21} M_2^{1/4} |f_1 - \dot{\omega}_d|^{3/4} \operatorname{sign}\{f_1 - \dot{\omega}_d\} - \mu_4 \sigma_2 (f_1 - \dot{\omega}_d) + f_2, \\
\dot{f}_2 &= -\lambda_{22} M_2^{1/3} |f_2 - \dot{f}_1|^{2/3} \operatorname{sign}\{f_2 - \dot{f}_1\} - \mu_3 \sigma_2 (f_2 - \dot{f}_1) + f_3, \\
\dot{f}_3 &= -\lambda_{23} M_2^{1/2} |f_3 - \dot{f}_2|^{1/2} \operatorname{sign}\{f_3 - \dot{f}_2\} - \mu_2 \sigma_2 (f_3 - \dot{f}_2) + f_4, \\
\dot{f}_4 &= -\lambda_{24} M_2 \operatorname{sign}\{f_4 - \dot{f}_3\} - \mu_1 \sigma_2 (f_4 - \dot{f}_3),
\end{aligned} \tag{5.38}$$

where $f_i(t)$, $i = 1, 2, 3, 4$ is an estimate of i-th derivative of $\omega_d(t)$, $M_2 > 0$ is a sufficiently large number, $\lambda_{2i} > 1$ are HOSM differentiators parameters to be chosen recursively [79], $\mu_i > 0$ are coefficients chosen such that the polynomial $r(s) = s^4 + \mu_4 s^3 + \mu_4\mu_3 s^2 + \mu_4\mu_3\mu_2 s + \mu_4\mu_3\mu_2\mu_1$ is Hurwitz, and $\sigma_2 > 0$ is an adjustable gain. The observer state variables f_2, f_3, f_4 provide estimates for $\ddot{\omega}_d$, $\dddot{\omega}_d$, and $\omega_d^{(4)}$, respectively.

5.5.4 Step 4: Overall control algorithm

The block diagram of the drilling control system is shown in Figure 5.2. The overall control algorithm combines algorithms described in Sections 5.5.1, 5.5.2, where the unmeasurable variables are replaced with their corresponding estimates obtained using observers from Section 5.5.3. Specifically, the reference (desired) rotational velocity signal ω_d is generated using the algorithm identical to (5.22), as follows

$$\dot{\omega}_d = -\gamma_v \, \omega_d^2 \, v \, |\tilde{v}|^{q-1} \operatorname{sign}\{\tilde{v}\}, \tag{5.39}$$

where $\gamma_v > 0$ and $q \in \{2, 3, \ldots\}$. The reference signal $\omega_d(t)$ is then fed into the tracking control algorithm described in Section 5.5.2, where the necessary higher derivatives of ω_d are restored using hybrid differentiator (5.38). Similarly, the tracking control algorithm uses estimates of

the equivalent torque T and its derivatives generated by hybrid HOSM observer (5.34)-(5.37). Overall, the control law for armature voltage V is obtained from (5.27) by replacing ω and $\tilde{\phi}$ with their estimates $\hat{\tilde{x}}_3$ and $\hat{\tilde{x}}_2$, respectively, *i.e.*,

$$V = -K\begin{bmatrix}\hat{\omega} & \hat{\tilde{\phi}} & \omega_r & I\end{bmatrix}^T + \hat{u}_d + \hat{u}_T, \tag{5.40}$$

where

$$\hat{u}_T = \begin{bmatrix}\beta_3 & \beta_2 & \beta_1 & \beta_0\end{bmatrix}\begin{bmatrix}\hat{T}_3 & \hat{T}_2 & \hat{T}_2 & \hat{T}\end{bmatrix}^T, \tag{5.41}$$

$$\hat{u}_d = \begin{bmatrix}\alpha_4 & \alpha_3 & \alpha_2 & \alpha_1 & \alpha_0\end{bmatrix}\begin{bmatrix}f_4 & f_3 & f_2 & \dot{\omega}_d & \omega_d\end{bmatrix}^T, \tag{5.42}$$

are obtained from (5.29), (5.30), and (5.29), (5.31), respectively, by replacing T and its derivatives with their estimates produced by hybrid HOSM observer (5.34)-(5.37) and derivatives of ω_d with their estimates produced by (5.38).

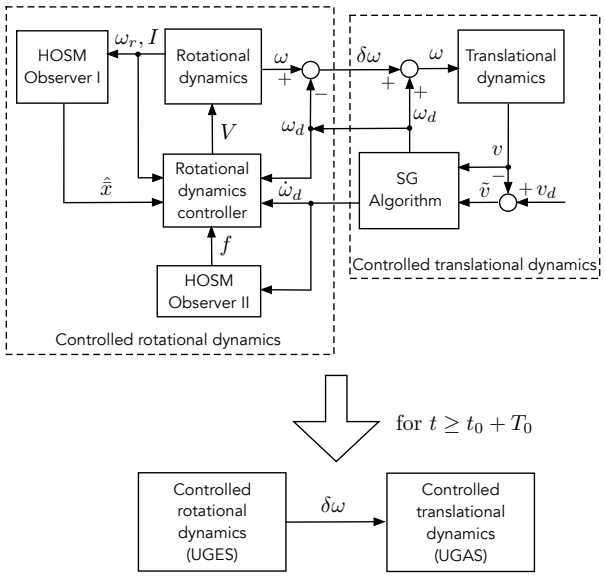

Figure 5.2: Structure of the control system

Now consider the overall interconnected system which consists of the translational dynamics (5.16), (5.17), the rotational dynamics (5.24)-(5.26) with control algorithm (5.39)-(5.42), and the HOSM observers (5.34)-(5.37) and (5.38). The state of this interconnection comprises the states of the individual subsystems. The stability of the overall system can be justified as

follows. First, given an arbitrary compact set of initial conditions $\mathcal{I}$ and a constant $T_0 > 0$, it can be shown that if the overall system's state at a time instant t_0 belongs to $\mathcal{I}$, and if $\gamma_v > 0$ in (5.39) is sufficiently small, then the trajectories of the interconnected system are uniformly bounded on the interval $[t_0, t_0 + T_0]$. On the other hand, uniform boundedness of system's trajectories on $[t_0, t_0 + T_0]$ implies that, if coefficients (gains) of the HOSM observers (5.34)-(5.37) and (5.38) are chosen appropriately, then the states of these observers converge to the actual estimated variables in finite time before the instant $t_0 + T_0$. Therefore, starting from instant $t_0 + T_0$ at the latest, the disturbance input T to (5.24) is rejected, and the controlled rotational dynamics (denoted by the dashed rectangle on the left of Figure 5.2, top) is uniformly globally exponentially stable with $\delta\omega(t) := \omega(t) - \omega_d(t) \to 0$ exponentially as $t \to +\infty$. On the other hand, Theorem 5.5.1 implies that the controlled translational dynamics (denoted by the dashed rectangle on the right of Figure 5.2, top) is uniformly globally asymptotically stable. Therefore, starting from the instant $t_0 + T_0$, the overall system can be represented as a cascade interconnection of two subsystems (see Figure 5.2, bottom), where the driving system is time varying and uniformly globally exponentially stable, while the driven system is uniformly globally asymptotically stable. The uniform global asymptotic stability of such a cascade system follows from the existing results (see for example [95, Corollary 1]).

5.6 Simulation results

In this section, we present several examples of simulation results of the closed-loop drilling system. We simulate the process of drilling through several rock layers of different hardness using the control algorithms described in the previous section. Numerical values of the parameters used in the simulations are given in Tables 5.1, 5.2.

5.6.1 Calculation of parameters

In order to calculate some of the drilling system parameters, we apply approximate formulas given in [16]:

$$J_1 = \rho I_c L_c + \frac{\rho I_p L_p}{3}, \quad I_c = \frac{\pi}{32}(D_c^4 - d_c^4), \quad I_p = \frac{\pi}{32}(D_p^4 - d_p^4), \tag{5.43}$$

Table 5.1: Numerical values of the drilling system and environment parameters (Chapter 5)

Parameter, Units	Description	Value	Parameter, Units	Description	Value
Given drilling system parameters					
L_p, m	Length of drill pipes	1100	L_c, m	Length of drill collars	250
D_p, m	Outer diameter of drill pipes	0.127 (5.0 in)	D_c, m	Outer diameter of drill collars	0.178 (7.0 in)
d_p, m	Inner diameter of drill pipes	0.109 (4.28 in)	d_c, m	Inner diameter of drill collars	0.057 (2.25 in)
m_p, kg/m	Unit mass of drill pipes	29.02	m_c, kg/m	Unit mass of drill collars	175.58
ρ, kg/m^3	Density of steel	7900	G, N/m^2	Shear modulus of steel	$79.6 \cdot 10^9$
c_1, Nms/rad	Damping of top-drive system	25.7	$\tilde{c}$, Ns/rad	Damping per unit length	0.027
J_r, kgm^2	Mass moment of inertia of the rotary table	1000	J_m, kgm^2	Mass moment of inertia of the motor's rotor	35
K_m, Vs	Motor torque constant	6.5	n, $-$	Gearbox ratio	2
R, Ω	Motor armature resistance	0.015	L, H	Motor armature inductance	0.0025
a, m	Drill bit radius	0.11	$\mu\gamma$, $-$	Coefficient of friction at the wear flat – rock interface multiplied by bit constant	1.1
ζ, $-$	Ratio of the vertical force to the horizontal force between the rock and the cutter contact surfaces	0.75	d_*, mm	Critical value of depth of cut between phase 1 and phase 2	0.5
W_0, N	Difference between submerged weight of drilling system and constant upward force	7000	K_f, Nm/rad	Viscous friction coefficient	25
Calculated drilling system parameters					
J_1, kgm^2	Mass moment of inertia of drill collars and drill pipes	226.11	J_2, kgm^2	Mass moment of inertia of top-drive system	1140
c_2, Nms/rad	Equivalent viscous damping coefficient	10	k, Nm	Equivalent torsional stiffness of drill pipes	859.57
M, kg	Mass of drill string	75813			
Parameters of the environment					
ϵ, MPa	Intrinsic specific energy	$\{30, 35, 31, 25\}$	σ, MPa	Contact strength	2ϵ
κ, $-$	Rate of change of contact length with depth of cut	1.5			

$$c_2 = \frac{L_p \tilde{c}}{3}, \quad k = \frac{G I_p}{L_p}, \quad J_2 = J_r + n^2 J_m, \quad M = m_p L_p + m_c L_c, \tag{5.44}$$

Table 5.2: Numerical values of the drilling controller parameters (Chapter 5)

Parameter	Description	Value
Parameters set by operator		
v_d, mm/s	Desired penetration rate	$\{4, 6\}$
γ_v	Coefficient that defines speed of $\omega \to \omega_d$ convergence	$\{1500, 700\}$
Given controller parameters		
$\sigma\{A - BK\}$	Spectrum of the state matrix of the closed-loop system	$\begin{bmatrix}-2.5 & -2 & -1.5 & -1\end{bmatrix}$
$\sigma\{\bar{A} - \bar{L}\bar{C}\}$	Spectrum of the state observer matrix (5.34)	$\begin{bmatrix}-0.5 & -0.35 \pm 0.35j & -0.43 \pm 0.25j & -0.48 \pm 0.13j\end{bmatrix}$
$\mu_1 \dots \mu_4$	Coefficients of the HOSM observer (5.38)	$\begin{bmatrix}0.48 & 1.43 & 3.5 & 10\end{bmatrix}$
$\lambda_{24} \dots \lambda_{21}$	Coefficients of the HOSM observer (5.38)	$\begin{bmatrix}1.1 & 1.5 & 2 & 3\end{bmatrix}$
$\lambda_{17} \dots \lambda_{11}$	Coefficients of the HOSM part of the state observer (5.35)	$\begin{bmatrix}1.1 & 1.5 & 2 & 3 & 5 & 8 & 10\end{bmatrix}$
$\{M_1, M_2, \sigma_2\}$	Gains of HOSM observers (5.35), (5.38)	$\{1, 10, 10\}$
q	Exponent number in the control law for the angular velocity (5.22)	2
Calculated controller parameters		
K	Vector of proportional control gains (5.40)	$\begin{bmatrix}-2.2336 & -2.9836 & -10.292 & 0.0022\end{bmatrix}$
$\bar{L}$	Vector of gains of the state observer's linear part (5.34)	$\begin{bmatrix}2.92 & 0.98 & -10.37 & -495.1 & -155.6 & -28.48 & -2.34\end{bmatrix}^T$
$\beta_0 \dots \beta_3$	Coefficients of the disturbance rejection part of the overall controller (5.41)	$\begin{bmatrix}-2.1484 & 3.3581 & 1.7564 & 0.255\end{bmatrix} \cdot 10^{-3}$
$\alpha_0 \dots \alpha_4$	Coefficients of the tracking part of the overall controller (5.42)	$\begin{bmatrix}0.4325 & 1.1101 & 1.0236 & 0.4037 & 0.0577\end{bmatrix}$

where subscripts c and p denote parameters of drill collars and drill pipes, respectively, L means length, I is a polar moment of inertia, D and d are outer and inner diameters, $\tilde{c}$ is a damping coefficient per unit length, m is mass per unit length, G and ρ are sheer modulus and density of the pipes' material, and J_m, J_r mean mass moment of inertia of the motor and the rotary table.

In order to define parameters of the environment properly, we take into account the follow-

ing relations that are usually met in practice [20]:

$$\zeta \in [0.5; 0.8], \quad \mu\gamma\zeta < 1, \quad \frac{\sigma}{\epsilon} \in [1; 10], \quad \kappa \in [1; 10]. \tag{5.45}$$

The parameters of the drilling controller are calculated based on the open-loop system parameters and desired location of the poles of the closed-loop system and the observer denoted by $\sigma\{A - BK\}$, $\sigma\{\bar{A} - \bar{L}\bar{C}\}$, respectively. Their values are presented in Table 5.2.

5.6.2 Simulation results for piecewise constant parameters of the environment

First, we simulate drilling through uniform rock layers with constant intrinsic specific energy, a situation which corresponds to our theoretical assumptions. In every simulation presented below, the initialization process is performed as follows. During the first 15 seconds of each simulation, a constant voltage $V = 390$ V is applied to the system's input while the control algorithm is turned off. This is done to allow the estimation processes converge before the corresponding estimates are used in the control algorithm. At $t = 15$ s, the control algorithm is turned on and remain active until the end of each simulation process.

Examples of simulation results of the closed-loop system for the vertical penetration rate regulation are presented in Figures 5.3 - 5.6. In these simulations, the reference vertical velocity is set $v_d = 4$ mm/s until approximately $t = 175$ s, and is subsequently increased to $v_d = 6$ mm/s. The control law consists of the algorithm (5.22) that generates reference rotational velocity ω_d, and algorithms (5.40)-(5.42) where all estimates are obtained using the corresponding observers from Section 5.5.3. A dashed red line on all plots shows the time ($t = 15$ s) when the controller is turned on. Most of the time the drilling process happens in phase 2, going into phase 1 in the second layer only (see dashed green line in Figure 5.5). One can observe that the estimates $\hat{\tilde{\phi}}$, $\hat{\omega}$, $\hat{T}$ converge to the actual values of the signals $\tilde{\phi}$, ω, and T, respectively, and the reference angular velocity ω_r is tracked almost perfectly. It also confirms the efficiency of the proposed tracking and disturbance rejection scheme, as the vertical velocity converges to its desired value in every rock layer.

Remark 5.1 *It is important to note that the results presented in the above simulations are feasible in practice. Indeed, maximum armature voltage and current for modern commercially*

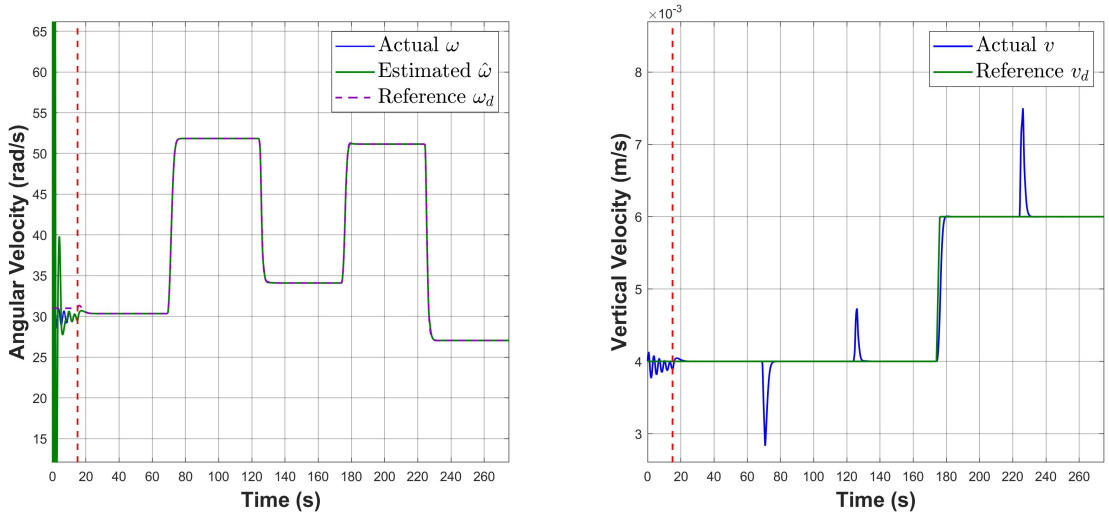

Figure 5.3: Piecewise constant parameters: actual and estimated output angular velocity of the drill bit $\omega(t)$, $\hat{\omega}(t)$ vs. reference angular velocity $\omega_d(t)$ (left plot); rate of penetration $v(t)$ (right plot).

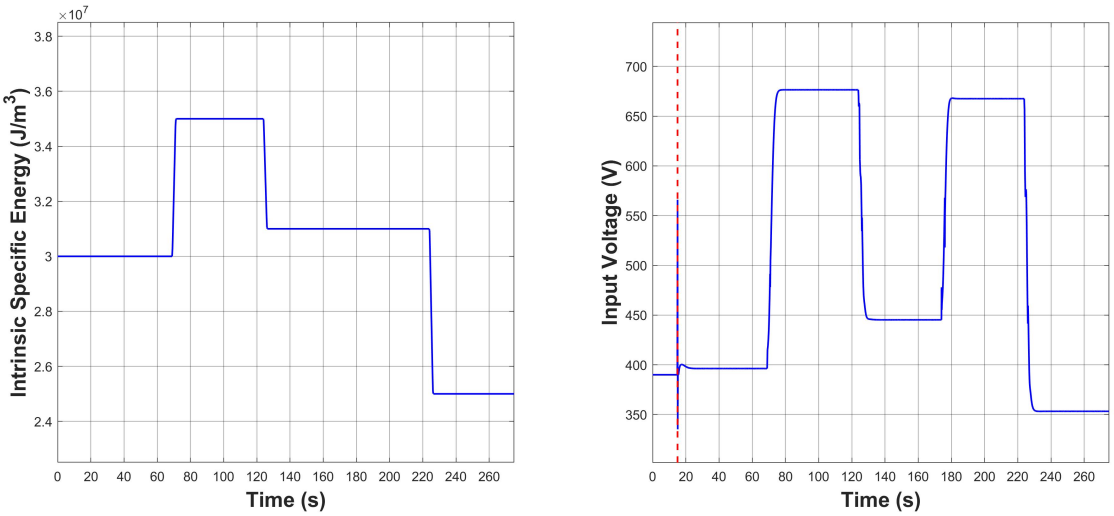

Figure 5.4: Piecewise constant parameters: intrinsic specific energy $\epsilon(t)$ (left plot); input control signal $V(t)$ (right plot).

available DC motors are around 810 V and 2100 A, respectively (see, for example, Siemens specifications [112]). In general, maximum achievable penetration rate in steady state depends on the motor's power. An example for a drilling system with parameters from Table 5.1 is shown in Figure 5.7. It can be seen that with reduction of applied force and increase of rock hardness, maximum velocity drops drastically, especially when it is not possible to achieve phase 2 of the drilling process.

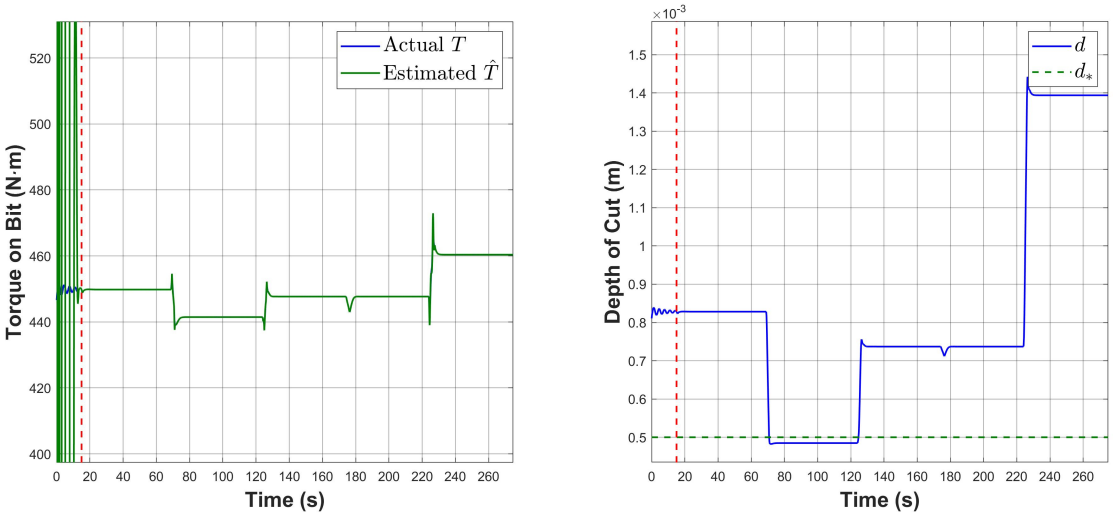

Figure 5.5: Piecewise constant parameters: actual torque on bit $T(t)$ vs. estimated torque-on-bit $\hat{T}(t)$ (left plot);
depth of cut $d(t)$ (right plot).

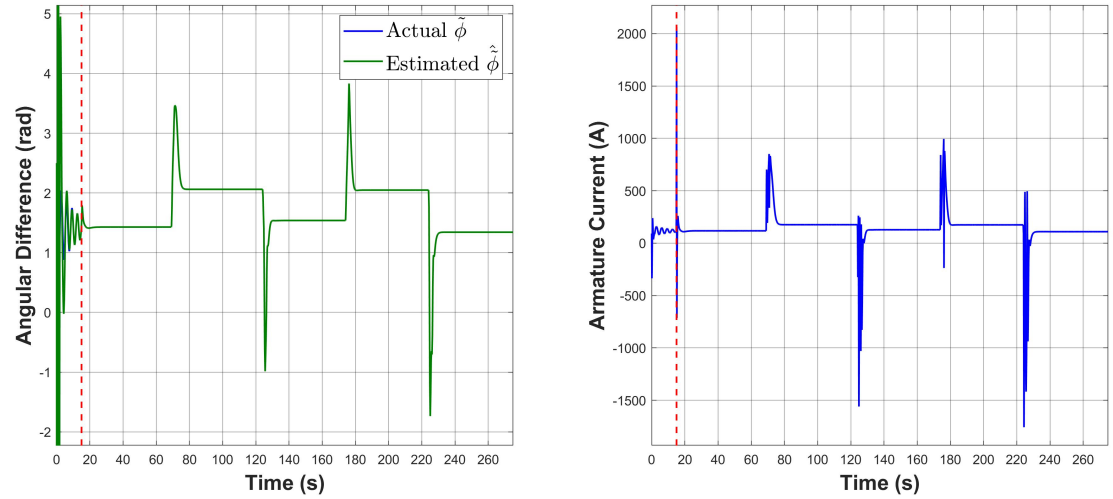

Figure 5.6: Piecewise constant parameters: actual angular difference $\tilde{\phi}(t)$ vs. estimated angular difference $\hat{\tilde{\phi}}(t)$ (left plot);
armature current $I(t)$ (right plot).

5.6.3 Simulation results in the case of random variations of intrinsic specific energy

In practice, rock layers may not be perfectly uniform, and the hardness of the drilled material may slightly vary. As long as the overall control algorithm provides global asymptotic stability, one can expect the closed-loop system to have robustness property. In the following

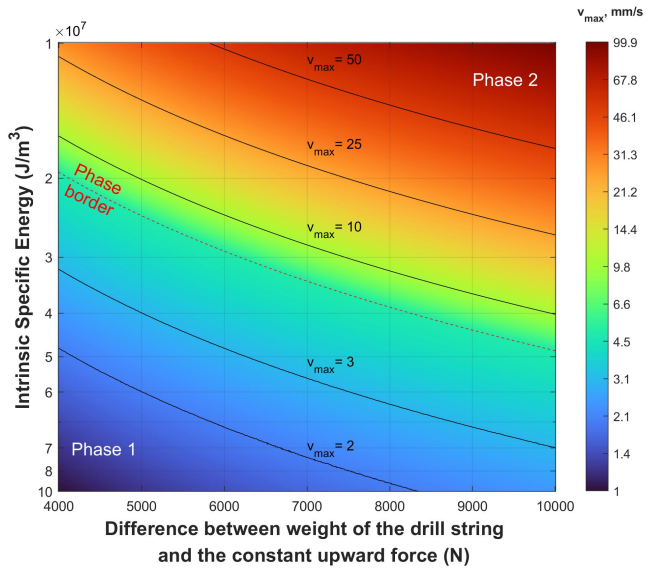

Figure 5.7: Maximum achievable penetration rate in steady state for a drilling system with parameters from Table 5.1 and maximum armature voltage 810 V.

simulation, we examine robustness of stability of the closed-loop system with respect to small variations in the rock structure.

We introduce random variations by adding a white noise of small magnitude to the parameter $\epsilon(t)$. The discrete-time white noise signal is generated, such that its sample time approximately corresponds to a new sample every 2 mm of the bit's vertical displacement. This signal then comes through a low-pass filter and is added to the nominal value of intrinsic specific energy. All other parameters remain the same as in Section 5.6.2.

Simulation results are shown in Figures 5.8 - 5.11. It can be seen that, even though penetration rate is not constant, it converges to some small neighborhood of the reference vertical velocity, which means that the stability is preserved. Another important observation is the following: the reference rotational velocity ω_d is tracked perfectly, despite the fact that it is subject to random changes.

5.6.4 Simulation results for a distributed parameter model of the drilling system

In the simulation results presented above, the underlying assumption is that the finite dimensional lumped parameter model (5.4) used for the purpose of control design accurately describes the actual rotational dynamics of the system. In practice, the dynamics of the drilling

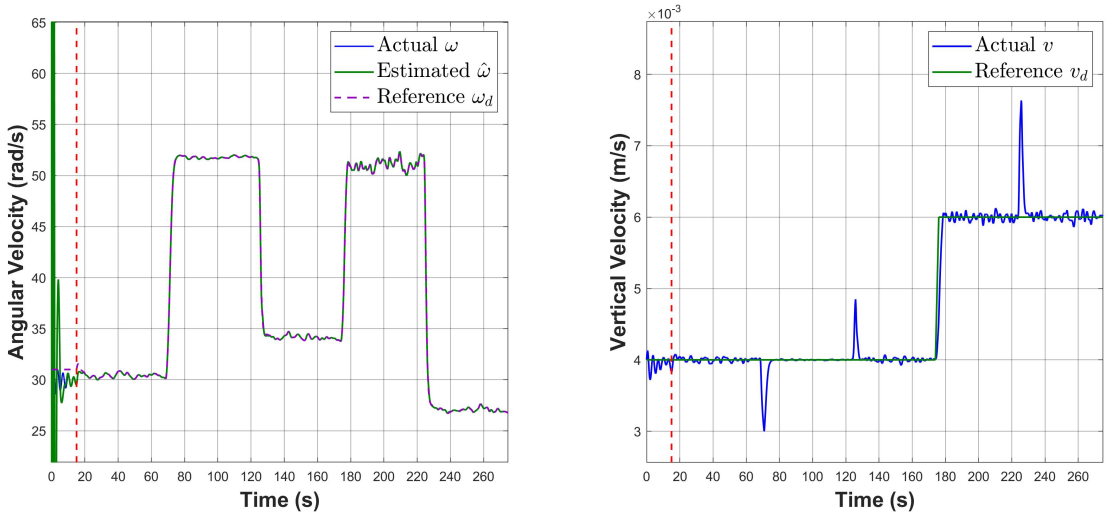

Figure 5.8: The case of small random variations of the intrinsic specific energy: actual and estimated output angular velocity of the drill bit $\omega(t)$, $\hat{\omega}(t)$ vs. reference angular velocity $\omega_d(t)$ (left plot); rate of penetration $v(t)$ (right plot).

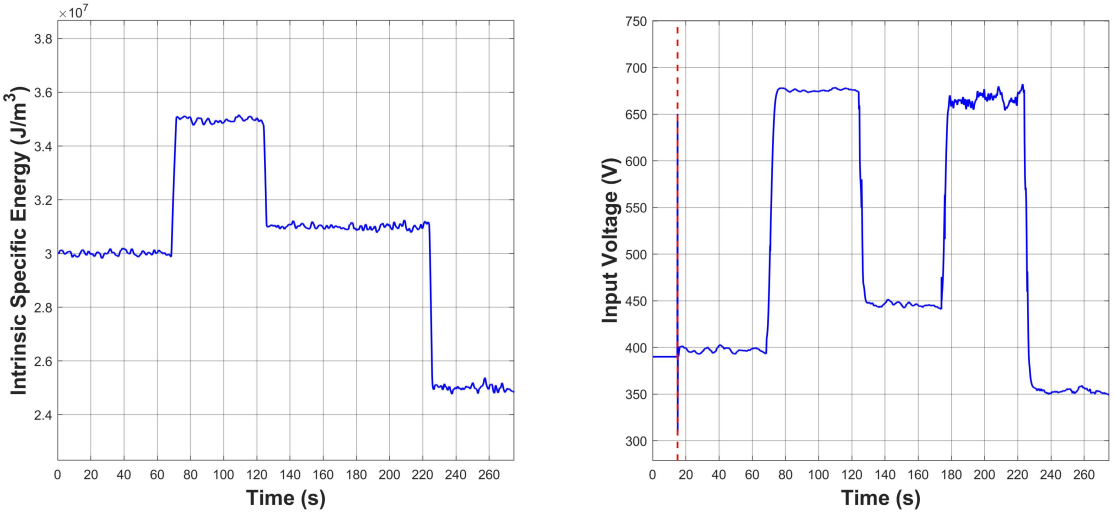

Figure 5.9: The case of small random variations of the intrinsic specific energy: intrinsic specific energy $\epsilon(t)$ (left plot); input control signal $V(t)$ (right plot).

systems can be extremely complex [102] and generally speaking are more adequately described by infinite-dimensional distributed parameter models (see for example [106]). In this section, we test the robustness of our control design approach by simulating the designed control/observation algorithms in conjunction with a distributed parameter model of the drilling system. Specifically, we simulate the situation where the rotational dynamics of the drilling

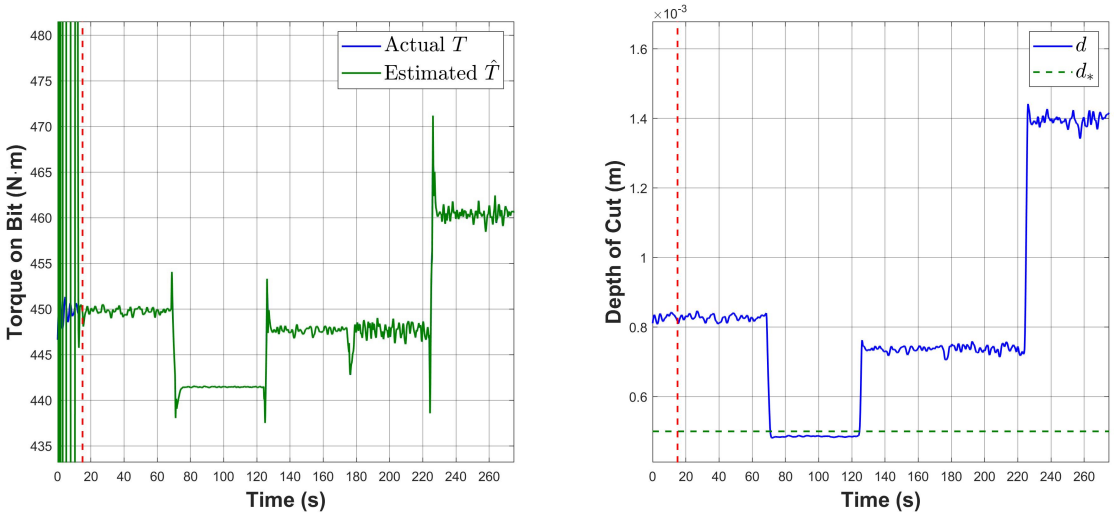

Figure 5.10: The case of small random variations of the intrinsic specific energy: actual torque on bit $T(t)$ vs. estimated torque-on-bit $\hat{T}(t)$ (left plot); depth of cut $d(t)$ (right plot).

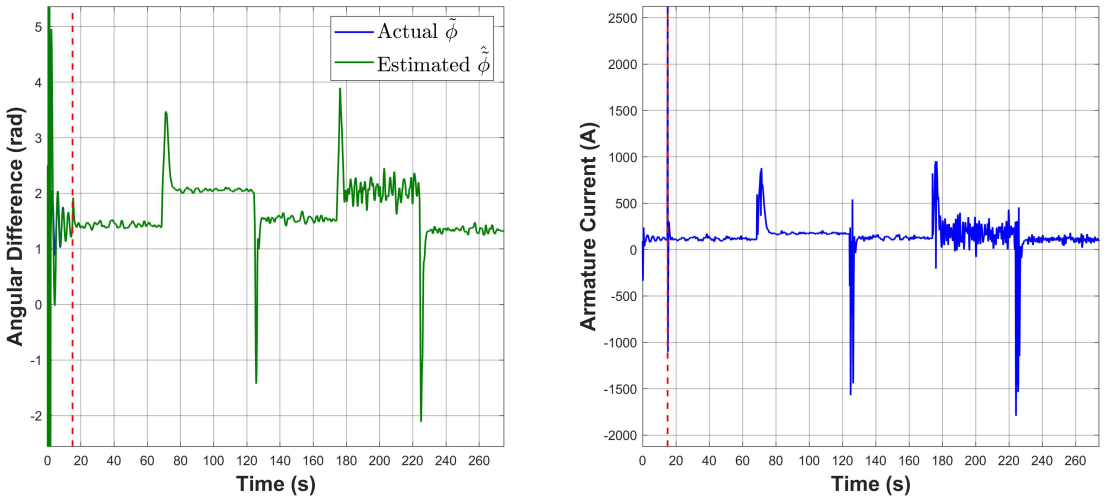

Figure 5.11: The case of small random variations of the intrinsic specific energy: actual angular difference $\tilde{\phi}(t)$ vs. estimated angular difference $\hat{\tilde{\phi}}(t)$ (left plot); armature current $I(t)$ (right plot).

system are described by partial differential equations of the following form [15]:

$$\rho I_p \phi^p_{tt}(x,t) = \frac{GI_p}{L_p^2}\phi^p_{xx}(x,t) - \frac{c_1}{L_p}\phi^p_t(x,t) \tag{5.46}$$

$$\rho I_c \phi^c_{tt}(x,t) = \frac{GI_c}{L_c^2}\phi^c_{xx}(x,t) - \frac{c_1}{L_c}\phi^c_t(x,t) \tag{5.47}$$

with the following boundary conditions:

$$\frac{GI_p}{L_p}\phi^p_x(0,t) = J_1\phi^p_{tt}(0,t) + c_2\phi^p_t(0,t) - K_m n I(t), \tag{5.48}$$

$$\frac{GI_c}{L_c}\phi^c_x(1,t) = -J_B\phi^c_{tt}(1,t) - T(t), \tag{5.49}$$

$$\phi^p_t(1,t) = \phi^c_t(0,t), \tag{5.50}$$

$$\phi^p_x(1,t) = \frac{I_c L_p}{I_p L_c}\phi^c_x(0,t), \tag{5.51}$$

where $\phi^p(x,t)$, $\phi^c(x,t)$ are the angles of rotation along the drill pipes and the BHA, respectively, as functions of normalized distance $0 \le x \le 1$ and time t. In the above equations, subscripts denote partial derivatives, for example, $\phi^p_t(x,t) := \partial\phi^p(x,t)/\partial t$, $\phi^p_x(x,t) := \partial\phi^p(x,t)/\partial x$, $\phi^p_{tt}(x,t) := \partial^2\phi^p(x,t)/\partial t^2$, *etc*. Parameters ρ, G, L_p, L_c, I_p, I_c, c_1, c_2, K_m, n, J_1 are the same as those used in the lumped parameter model (see Table 5.1), and $J_B := \rho I_c L_c$. The control signal $I(t)$ is calculated as follows:

$$\dot{I} = -\frac{K_m n}{L}\phi^p_t(0,t) - \frac{R}{L}I + \frac{1}{L}V, \tag{5.52}$$

where V is a control voltage obtained in Section 5.5.4. The following signals are used in the control algorithm:

$$\omega_r = \phi^p_t(0,t), \quad \omega = \phi^c_t(1,t), \quad \tilde{\phi} = \phi^p(0,t) - \phi^c(1,t). \tag{5.53}$$

Numerical simulation scheme for the model (5.46) - (5.51) is described in Appendix B. Our preliminary simulations demonstrate that the distributed parameter model (5.46) - (5.53) exhibits somewhat more oscillatory response as compared to the lumped parameter model (5.4). In order to cope with this, we adjust the coefficients of the HOSM observer (5.34)-(5.37) with

the goal of slowing down its dynamics. Specifically, we choose $M_1 = 0.01$ and

$$\sigma\{\bar{A} - \bar{L}\bar{C}\} = \Big[-0.01 \quad -0.0071 \pm 0.0071\,j \quad -0.0087 \pm 0.005\,j \quad -0.0097 \pm 0.0026\,j\Big].$$

Coefficient γ_v is also reduced to $\{750, 350\}$. Simulation results for the case of distributed parameter model (5.46) - (5.53) are presented in Figures 5.12 - 5.13. It can be seen from these figures that mismatch between the lumped and the distributed parameter models leads to noticeable discrepancies between the estimated $\hat{T}(t)$ and the actual $T(t)$ torques-on-bit as well as between the the estimated $\hat{\tilde{\phi}}(t)$ and the actual $\tilde{\phi}(t)$ differences in angular positions. These estimation errors however do not appear to affect the process of regulation of the vertical penetration rate, as it can be seen that the vertical penetration rate $v(t)$ converges to its desired value(s) v_d, and the transient response around the times when either the reference value v_d or the intrinsic specific energy ϵ changed is very similar to that in the case of the lumped parameter model. Also, the angular velocity $\omega(t)$ tracks its reference trajectory $\omega_d(t)$ very closely.

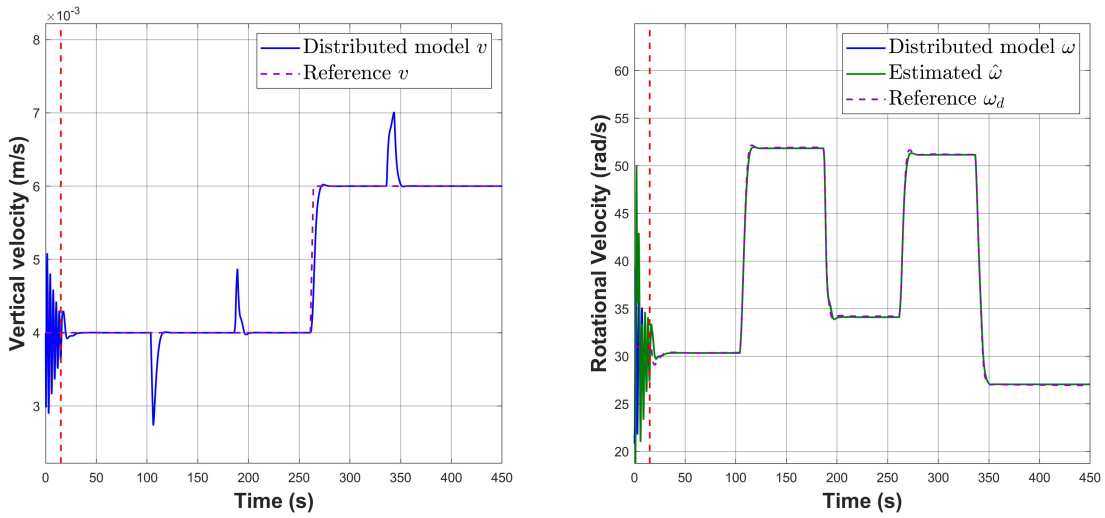

Figure 5.12: Distributed parameter model: actual and reference vertical rate of penetration $v(t)$, $v_d(t)$ (left plot); actual, estimated and reference angular velocity of the drill bit $\omega(t)$, $\hat{\omega}(t)$, $\omega_d(t)$ (right plot).

In the next and final example of simulations, we illustrate the situation where the drilling system recovers from sudden application of a strong torque-on-bit disturbance which results in both angular velocity of the drill bit and the vertical rate of penetration dropped to near zero values. Such strong disturbances that momentarily stall the rotation of the drill bit is the primary cause of the so-called stick-slip oscillations, which have multiple negative effects on

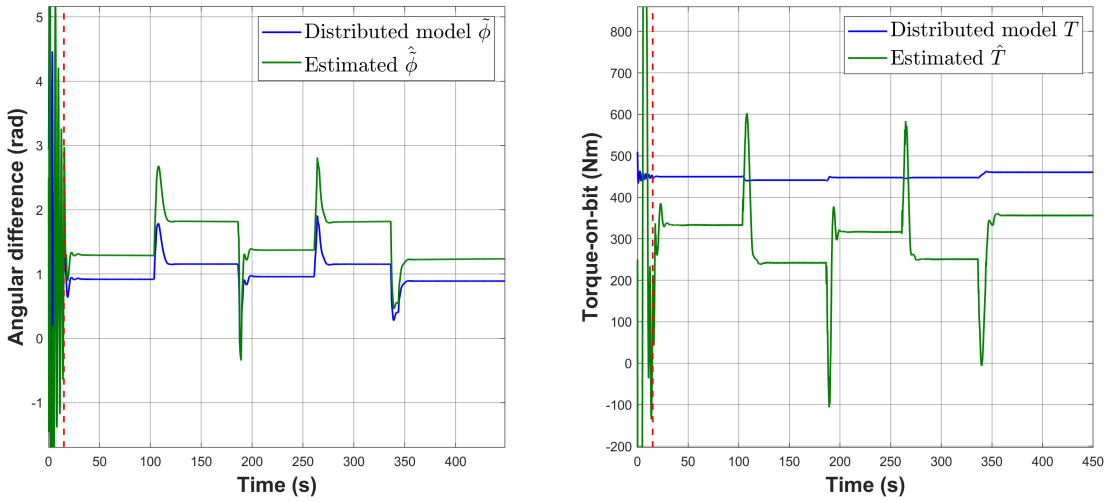

Figure 5.13: Distributed parameter model: actual and estimated angular difference $\tilde{\phi}(t)$, $\hat{\tilde{\phi}}(t)$ (left plot); actual and estimated torque-on-bit $T(t)$, $\hat{T}(t)$(right plot).

the performance of drilling systems and should be avoided [16, 106]. The simulated scenario consists of the following steps:

1. Phase I, 0 s - 15 s: similarly to the previous sets of simulations, a constant voltage V = 390 V is applied to the system's input while the control algorithm is turned off.

2. Phase II, 15 s - 50 s: the control algorithm is on. By the end of this phase the vertical penetration rate is approximately in the steady-state.

3. Phase III, 50 s - 60 s: the control algorithm is turned off, while the motor torque T_m (essentially, the armature current I) is kept constant. An additional counter-torque T_{add} is applied at the lower end of the drill string, such that rotational and vertical velocities are driven to near-zero.

4. Phase IV, 60 s - 120 s: the disturbance T_{add} is switched off, and the control algorithm is turned on again.

The results of simulations are shown in Figures 5.14, 5.15. It can be seen that, after the disturbance T_{add} is removed, the system returns to the steady state with little to no oscillations.

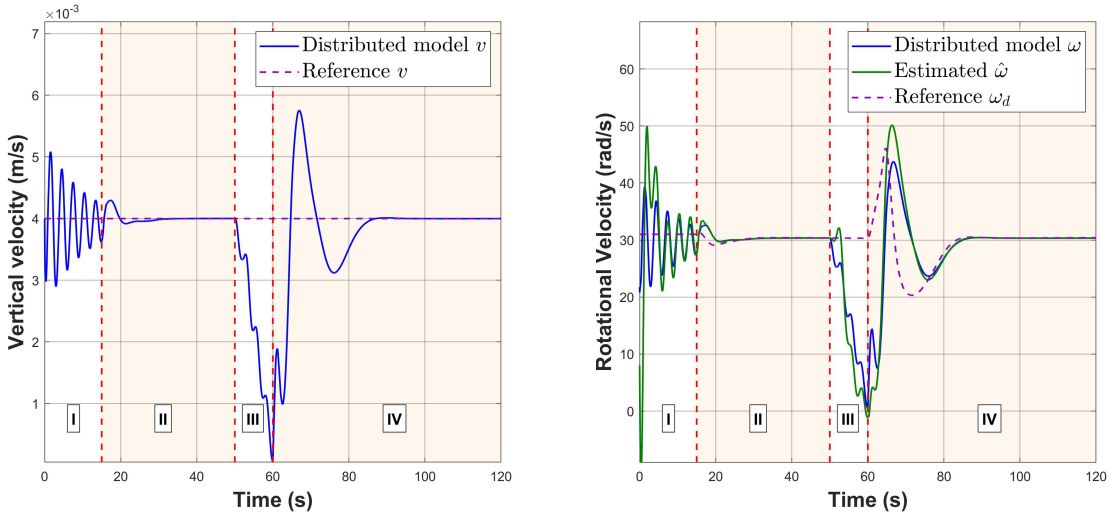

Figure 5.14: Transient processes in the distriputed parameter model: Actual and reference rate of penetration $v(t)$, $v_d(t)$ (left plot); actual, estimated and reference angular velocity of the drill bit $\omega(t)$, $\hat{\omega}(t)$, $\omega_d(t)$(right plot).

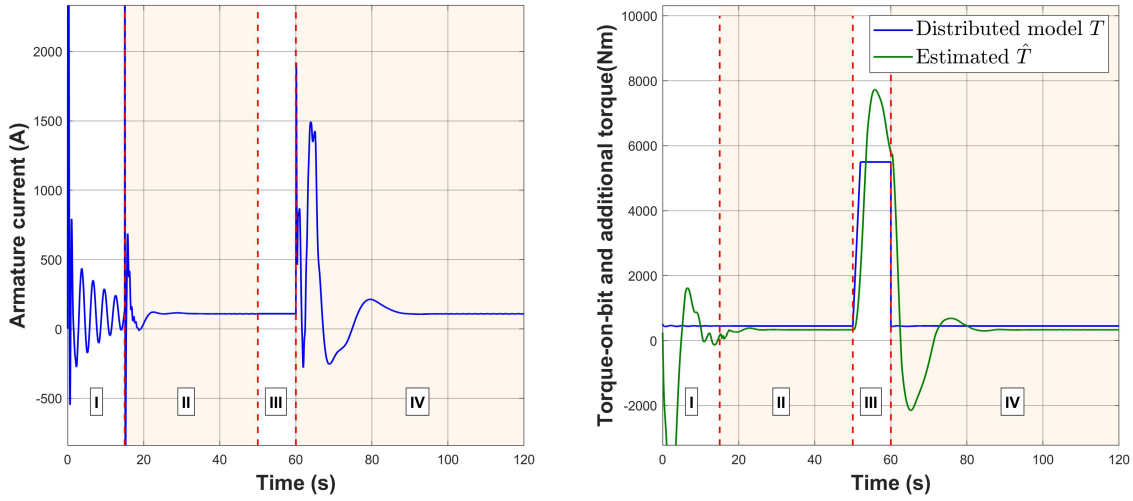

Figure 5.15: Transient processes in the distriputed parameter model: Armature current $I(t)$ (left plot); actual and estimated torque-on-bit and additional torque $T(t)$, $\hat{T}(t)$(right plot).

5.7 Conclusions

In this paper, the problem of the vertical penetration rate regulation in rotary drilling systems is addressed. A control algorithm that guarantees global asymptotic stability of the closed-loop system is developed. The proposed solution does not require real-time measurement of the downhole variables and their communication to the ground level. This is a practically im-

portant improvement upon existing results as the measurements of the downhole variables are noisy and the communication channel between the downhole and the ground level is characterized by latency and low bandwidth thus creating a bottleneck in the control design process for drilling systems. In this type of systems, the measurements of the downhole variables can be used for process monitoring; in particular, substantial discrepancy between the results of measurement and the estimates obtained using observers can serve as an indication that the model used in the control design may require an update. Simulation results demonstrate validity and efficiency of the proposed solutions. Extension of the control design approach from the finite-dimensional approximate models of the drilling systems used in this paper to more realistic infinite dimensional models while addressing the corresponding spectrum of complex dynamical phenomena is a topic for future research.

Appendix 1. Coefficients of the transfer functions (5.30), (5.31)

The coefficients $\beta_0 \dots \beta_3$, $\alpha_0 \dots \alpha_4$ of the transfer functions (5.30), (5.31) can be expressed in terms of parameters of the rotational dynamics (5.1)-(5.3) as follows [86]:

$$\begin{aligned}
\beta_3 &= \frac{J_2 L}{k K_m n}, \\
\beta_2 &= \frac{J_2(k_4 + R) + c_2 L}{k K_m n}, \\
\beta_1 &= \frac{c_2(k_4 + R) + K_m n(k_3 + K_m n) + kL}{k K_m n}, \\
\beta_0 &= \frac{k(k_4 + R) + k_2 K_m n}{k K_m n},
\end{aligned}$$

$$\begin{aligned}
\alpha_4 &= \frac{J_1 J_2 L}{k K_m n}, \\
\alpha_3 &= \frac{L(c_2 J_1 + c_1 J_2) + J_1 J_2(k_4 + R)}{k K_m n}, \\
\alpha_2 &= \frac{1}{k K_m n}(J_1 K_m n(k_3 + K_m n) + kL(J_1 + J_2) + c_1 c_2 L + (c_1 J_2 + c_2 J_1)(k_4 + R)), \\
\alpha_1 &= \frac{1}{k K_m n}(K_m n(c_1 k_3 + c_1 K_m n + J_1 k_2) + kL(c_1 + c_2) + (c_1 c_2 + k J_1 + k J_2)(k_4 + R)), \\
\alpha_0 &= \frac{k(c_1 + c_2)(k_4 + R) + c_1 k_2 K_m n}{k K_m n} + k_1 + k_3 + K_m n.
\end{aligned}$$

Appendix 2. Numerical simulation scheme for the distributed parameter model (5.46) - (5.51)

For simulation of the system (5.46) - (5.51) we use a simple implicit finite difference method. The drill string is divided into $n = \frac{1}{\Delta x} + 1$ intervals with step size equal to Δx. Similarly, there are $m = \frac{t_{sim}}{\Delta t} + 1$ time intervals, where t_{sim} is a total simulation time, and Δt is a time step size. Let i, j be space and time step numbers, respectively. We calculate time and space derivatives in each node (i, j) according to the following formulas:

$$\frac{d}{dt}(\cdot)_{i,j} = \frac{(\cdot)_{i,j} - (\cdot)_{i,j-1}}{\Delta t}, \quad \frac{d^2}{dt^2}(\cdot)_{i,j} = \frac{(\cdot)_{i,j-2} - 2(\cdot)_{i,j-1} + (\cdot)_{i,j}}{\Delta t^2}, \tag{5.54}$$

$$\frac{d}{dx}(\cdot)_{i,j} = \frac{(\cdot)_{i,j} - (\cdot)_{i-1,j}}{\Delta x}, \quad \frac{d^2}{dx^2}(\cdot)_{i,j} = \frac{(\cdot)_{i+1,j} - 2(\cdot)_{i,j} + (\cdot)_{i-1,j}}{\Delta x^2}, \tag{5.55}$$

where $(\cdot)$ is a corresponding function (ϕ^p or ϕ^c). Substituting these formulas into the equations (5.46) - (5.51), one can rearrange them in the following way:

$$a_1\phi^p_{1,j} + a_2\phi^p_{2,j} = b_1, \tag{5.56}$$

$$a_3\phi^p_{i-1,j} + a_4\phi^p_{i,j} + a_5\phi^p_{i+1,j} = b_{i_p}, \quad i_p \in \{2, .., n_p - 1\} \tag{5.57}$$

$$a_6\phi^p_{n_p-1,j} + a_7\phi^p_{n_p,j} + \phi^c_{n_p+1,j} - \phi^c_{n_p+2,j} = 0, \tag{5.58}$$

$$\phi^c_{n_p+1,j} - \phi^c_{n_p+2,j} = b_{n_p+1}, \tag{5.59}$$

$$a_8\phi^c_{i-1,j} + a_9\phi^c_{i,j} + a_{10}\phi^c_{i+1,j} = b_{i_c}, \quad i_c \in \{n_p + 2, .., n - 1\} \tag{5.60}$$

$$a_{11}\phi^c_{n-1,j} + a_{12}\phi^c_{n,j} = b_n, \tag{5.61}$$

where $n_p = \text{round}\left\{\frac{L_p}{L_p+L_c}\right\} + 1$, $a_1 = -\frac{1}{\Delta x} - \frac{J_1 L_p}{GI_p\Delta t^2} - \frac{c_2 L_p}{GI_p\Delta t}$, $a_2 = \frac{1}{\Delta x}$, $a_3 = a_5 = -\frac{G}{\rho L_p^2 \Delta x^2}$, $a_4 = \frac{1}{\Delta t^2} + \frac{2G}{\rho L_p^2\Delta x^2} + \frac{c_1}{L_p\rho I_p\Delta t}$, $a_6 = -\frac{I_p L_c}{I_c L_p}$, $a_7 = \frac{I_p L_c}{I_c L_p}$, $a_8 = a_{10} = -\frac{G}{\rho L_c^2\Delta x^2}$, $a_9 = \frac{1}{\Delta t^2} + \frac{2G}{\rho L_c^2\Delta x^2} + \frac{c_1}{L_c\rho I_c\Delta t}$, $a_{11} = -\frac{1}{\Delta x}$, $a_{12} = \frac{1}{\Delta x} + \frac{J_B L_c}{GI_c\Delta t^2}$, $b_1 = \frac{J_1 L_p}{GI_p\Delta t^2}\phi^p_{1,j-2} - \frac{L_p}{GI_p\Delta t}\left(\frac{2J_1}{\Delta t} + c_2\right)\phi^p_{1,j-1} - \frac{K_m n L_p}{GI_p} I_{j-1}$, $b_{i_p} = -\frac{1}{\Delta t^2}\phi^p_{1,j-2} + \left(\frac{2}{\Delta t^2} + \frac{c_1}{\rho L_p I_p \Delta t}\right)\phi^p_{1,j-1}$, $b_{n_p+1} = \phi^p_{n_p,j-1} - \phi^c_{n_p+1,j-1}$, $b_{i_c} = -\frac{1}{\Delta t^2}\phi^c_{1,j-2} + \left(\frac{2}{\Delta t^2} + \frac{c_1}{\rho L_c I_c \Delta t}\right)\phi^c_{1,j-1}$, $b_n = -\frac{J_B L_c}{GI_c\Delta t^2}\left(\phi^c_{n,j-2} - 2\phi^c_{n,j-1}\right) - \frac{L_c}{GI_c}T_{j-1}$.

The equations (5.56) - (5.61) can be solved in the matrix form with respect to angular positions in every node at every moment of time:

$$\begin{bmatrix} \phi^p_{1,j} \\ \phi^p_{2,j} \\ \vdots \\ \phi^p_{n_p-1,j} \\ \phi^p_{n_p,j} \\ \phi^c_{n_p+1,j} \\ \phi^c_{n_p+2,j} \\ \vdots \\ \phi^c_{n-1,j} \\ \phi^c_{n,j} \end{bmatrix} = \begin{bmatrix} a_1 & a_2 & 0 & 0 & \dots & 0 & 0 & 0 & \dots & 0 \\ a_3 & a_4 & a_5 & 0 & \dots & 0 & 0 & 0 & \dots & 0 \\ \vdots & & \ddots & & & & & & & \vdots \\ 0 & \dots & a_3 & a_4 & a_5 & 0 & 0 & 0 & \dots & 0 \\ 0 & \dots & 0 & a_6 & a_7 & 1 & -1 & 0 & \dots & 0 \\ 0 & \dots & 0 & 0 & 1 & -1 & 0 & 0 & \dots & 0 \\ 0 & \dots & 0 & 0 & 0 & a_8 & a_9 & a_{10} & \dots & 0 \\ \vdots & & & & & \vdots & & \ddots & & \vdots \\ 0 & \dots & 0 & 0 & 0 & 0 & \dots & a_8 & a_9 & a_{10} \\ 0 & \dots & 0 & 0 & 0 & 0 & \dots & 0 & a_{11} & a_{12} \end{bmatrix}^{-1} \begin{bmatrix} b_1 & b_2 & \dots & b_{n_p-1} & 0 & b_{n_p+1} & b_{n_p+2} & \dots & b_{n-1} & b_n \end{bmatrix}^T \tag{5.62}$$

In the simulation, we use the following step sizes: $\Delta x = 0.05$, $\Delta t = 0.01$.

Chapter 6

Sliding Mode Control of Rotary Drilling Systems with Full Parametric Uncertainty

This chapter is based on the following article:

Maksim V. Faronov and Ilia G. Polushin. Control of rotary drilling systems with uncertain parameters. In *2023 IEEE Conference on Control Technology and Applications (CCTA)*, Bridgetown, Barbados, August 2023 (accepted).

6.1 Abstract

We propose an algorithm for regulation of vertical penetration rate in rotary drilling systems for the case where parameters of the environment are unknown, and only nominal (approximate) values of the drillstring parameters are available. The algorithm is implemented in two phases: identification and control. First, we identify the values of drilling system's parameters, and subsequently use these parameters in the control scheme. The controller is based on a super-twisting high-order sliding mode control algorithm, as well as several high-order sliding mode observers. The proposed approach utilizes two measurements at the drill bit level during the identification phase only; however, in contrast with the existing results, it does not require knowledge of any parameters except for the motor characteristics. Feasibility of the proposed algorithm is confirmed by simulation results.

6.2 Introduction

Drilling automation in an important engineering field which has attracted substantial attention from control researchers over the recent years [5]. Automatic control solutions not only provide valuable assistance to drilling operators, but also allow to address some challenges associated with the drilling process, such as mitigation of vibrations [15], pressure regulation [36], and others. A number of control strategies for drilling systems was developed, such as sliding mode control with uncertainties [113], $\mathcal{H}_\infty$-based method [103], adaptive backstepping [89], to name a few. Nevertheless, the area of drilling automation remains relatively underdeveloped, and improvements can be made in terms of relaxation of simplifying assumptions and finding an appropriate balance between complexity of the control law and precise modeling of the real physical processes.

In this work, we extend the results presented in earlier papers [114, 110], where we developed a control algorithm for regulation of the vertical penetration rate in rotary drilling systems using only ground level measurements. It was assumed that parameters of the environment and of the drill bit are unknown; however, knowledge of parameters of the rotational dynamics was required. Here, we relax this assumption and design the control algorithm under full parametric uncertainty of the drillstring. We propose a multi-step approach, where at first we estimate unknown parameters, using two downhole measurements. After that, in the control phase, only the ground-level measurements are required. The control algorithm for regulation of the rate of vertical penetration is designed under the assumption that the angular velocity of the bit is controlled directly. The reference angular velocity is then tracked using estimates of non-measured signals as well as their derivatives. Even though we require some underground measurements for parameters identification, it may be conducted offline, or in the systems where wired pipe telemetry is used [115].

The rest of the paper is organized as follows. Description and the mathematical model of the drilling system is presented in Section 6.3. In Section 6.4, the control problem is formulated, and the assumptions are stated. We describe identification of unknown parameters in Section 6.5, and estimation of non-measured signals in Section 6.6. Control design is discussed in details in Section 6.7. Simulation results are given in Section 6.8. Finally, in Section 6.9, conclusions are made, and future research topics are outlined.

6.3 Model of the drilling system

6.3.1 Components of the system

A rotary drilling system drills the layers of rock by rotating a drillstring and applying certain weight and torque to its lower end. A rigid body on that bottom end of the drillstring is called a drill bit. When rotated, the bit performs actual rock cutting by means of its blades. Bottom Hole Assembly (BHA) consists of heavy collars; it applies additional pressure to the bit and carries important equipment. BHA is connected to the ground level through the drill pipes - hollow tubes, joined together in a single string. On the ground, a drilling rig contains, among other components, an electric drive that generates torque and rotates the drillstring, and a hoisting system which can regulate weight-on-bit. A basic structure of the drilling system is shown in Figure 6.1.

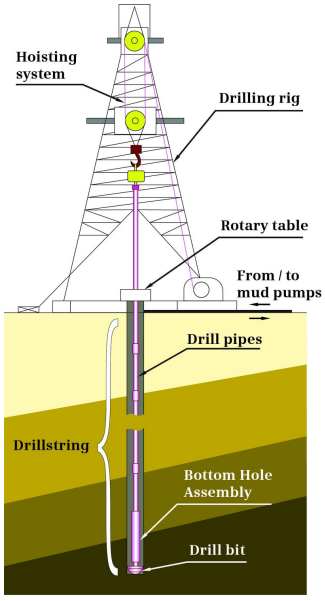

Figure 6.1: The structure of the drilling system

6.3.2 Model of rotational dynamics

The rotational dynamics can be represented by the following equations [16]:

$$J_1\ddot{\phi} + c_1\dot{\phi} + k(\phi - \phi_r) + T = 0, \tag{6.1}$$

$$J_2\ddot{\phi}_r + c_2\dot{\phi}_r - k(\phi - \phi_r) - nT_m = 0, \tag{6.2}$$

where (6.1) describes the dynamics of BHA and the drill pipes while (6.2) those of the rotary table and the drive. In these equations, ϕ denotes the angular position of the drill bit, ϕ_r is the angular position of the rotary table, $J_1 > 0$ is the equivalent combined moment of inertia of the BHA and the drill pipes while $J_2 > 0$ is that of the rotary table and the drive, $c_1, c_2 \geq 0$ are the equivalent nominal viscous damping coefficients, $k > 0$ is the equivalent torsional stiffness of the drill pipes, T_m is the torque generated by the motor, n is the gearbox ratio, and T is an equivalent torque applied to the drill bit which includes the torque-on-bit [20] (*i.e.*, the reaction torque generated due to rock cutting process) as well as an equivalent sum of all other torques due to different effects not accounted for in the model (6.1).

The dynamics of the electric drive (a DC motor with a separated excitation circuit) are described by standard equations

$$L\dot{I} + RI - V_b - V = 0, \quad V_b = K_m n\dot{\phi}_r, \quad T_m = K_m I, \tag{6.3}$$

where I is the armature current, L is an equivalent armature inductance, R is an equivalent armature resistance, V_b is the back EMF, V is the armature voltage, and $K_m > 0$ is a motor constant which depends on its characteristics. Using notation $\tilde{\phi} := \phi_r - \phi$, $\omega := \dot{\phi}$, $\omega_r := \dot{\phi}_r$, the rotational dynamics (6.1)-(6.3) can be represented in the state-space form [50, 83, 86], as follows

$$\begin{aligned} \dot{x} &= Ax + Bu + DT, \\ y &= Cx, \end{aligned} \tag{6.4}$$

$$A = \begin{bmatrix} a_1 & a_2 & 0 & 0 \\ -1 & 0 & 1 & 0 \\ 0 & a_3 & a_4 & a_5 \\ 0 & 0 & a_6 & a_7 \end{bmatrix}, B = \begin{bmatrix} 0 \\ 0 \\ 0 \\ b_4 \end{bmatrix}, D = \begin{bmatrix} d_1 \\ 0 \\ 0 \\ 0 \end{bmatrix}, C = \begin{bmatrix} 1 \\ 0 \\ 0 \\ 0 \end{bmatrix}^T, x = \begin{bmatrix} \omega \\ \tilde{\phi} \\ \omega_r \\ I \end{bmatrix}, u = V, \tag{6.5}$$

where, for convenience, we denote

$$a_1 = -\frac{c_1}{J_1}, \quad a_2 = \frac{k}{J_1}, \quad a_3 = -\frac{k}{J_2}, \quad a_4 = -\frac{c_2}{J_2}, \quad a_5 = \frac{K_m n}{J_2},$$
$$a_6 = -\frac{K_m n}{L}, \quad a_7 = -\frac{R}{L}, \quad d_1 = -\frac{1}{J_1}, \quad b_4 = \frac{1}{L}. \quad (6.6)$$

6.3.3 Model of translational dynamics

A model of the translational dynamics is defined by the following equation:

$$M\dot{v} = W_0 - W - K_f v, \quad (6.7)$$

where v is the vertical penetration rate of the drill bit, $M > 0$ is the total mass of the drillstring, W_0 is the difference between the submerged weight of the drilling system and the constant upward force supplied by the hoisting system, $K_f > 0$ is the viscous friction coefficient, and W is the weight-on-bit which is the upward reaction force applied to the bit.

6.3.4 Model of bit-rock interaction

The interaction between the drill bit and the rock is defined by relationships between the rotational ω and the vertical v velocities of the bit, the torque-on-bit (denoted by T_b to distinguish from an equivalent torque T used in equation (6.1)), and the weight-on-bit W. These relationships constitute so called drilling response model [20], which is briefly described below.

The torque-on-bit and the weight-on-bit are decomposed into sums of cutting and frictional components:

$$T_b = T^c + T^f, \quad W = W^c + W^f, \quad (6.8)$$

where the superscripts c and f denotes the cutting and the frictional components, respectively. In the simplest case, where a bit does not contain hollow areas, the cutting components are defined as follows [20, 19]:

$$T^c := \frac{1}{2}a^2 \epsilon d, \quad W^c := a\zeta\epsilon d, \quad (6.9)$$

where $a > 0$ is the radius of the bit, $\epsilon \geq 0$ is the intrinsic specific energy, which is the amount of energy consumed for cutting a unit volume of the material by an ideally sharp bit, ζ represents the ratio of the vertical force to the horizontal force between the rock and the cutter contact surfaces, and $d > 0$ is the depth of cut, *i.e.*, the vertical distance to which the bit moves during one revolution. In the steady state, the depth of cut can be approximated by the following expression [20]:

$$d \approx 2\pi \frac{v}{\omega}. \tag{6.10}$$

The frictional components T^f, W^f are defined depending on the drilling phase. In total, there are three phases of drilling [20]. In phase 1, which corresponds to small $d > 0$, the frictional components are linear functions of d. In phase 2, which begins as d reaches some critical value d_*, the frictional components remain constant regardless of d. Phase 3 starts once d reaches another critical value d_b and can also be approximated as linear with respect to d with unknown slopes. Overall, the following mathematical model describes the frictional components:

$$T^f := \begin{cases} (a^2/2) \cdot \mu\gamma\sigma\kappa d, & \text{for } d < d_* \text{ (phase 1)}, \\ (a^2/2) \cdot \mu\gamma\sigma\kappa d_*, & \text{for } d_* \leq d \leq d_b \text{ (phase 2)}, \\ (a/2) \cdot \mu\gamma(\frac{d-d_b}{\beta} + a\sigma\kappa d_*), & \text{for } d > d_b \text{ (phase 3)}, \end{cases} \tag{6.11}$$

$$W^f := \begin{cases} a\sigma\kappa d, & \text{for } d < d_* \text{ (phase 1)}, \\ a\sigma\kappa d_*, & \text{for } d_* \leq d \leq d_b \text{ (phase 2)}, \\ \frac{d-d_b}{\beta} + a\sigma\kappa d_*, & \text{for } d > d_b \text{ (phase 3)}, \end{cases} \tag{6.12}$$

where $\mu > 0$ is the friction coefficient, which is a ratio between parallel and normal components of the cutter force which acts along the wear flat, $\gamma > 0$ is the bit constant which reflects the bit design and the distribution of the contact forces, $\sigma > 0$ is the contact strength defined as a bound of the normal stress that can be transmitted by the wear flat, $\kappa > 0$ is the rate of change of contact length with d, $d_* > 0$ is the critical value of d when contact forces are fully mobilized, which depends on the bit bluntness, $d_b > d_*$ is the critical value of d when the contact surface between the bit and the rock increases, and β is a coefficient which characterizes the slopes of

T^f, W^f in phase 3.

6.4 Control goal and assumptions

The problem that we are solving in this paper can be formulated as follows. Given $v_d > 0$, find a control algorithm that guarantees

$$v(t) \to v_d \quad \text{as } t \to \infty. \tag{6.13}$$

We solve this problem in two phases: identification phase, where unknown parameters of the drilling system are identified using a number of downhole measurements, and control phase, where we design a control algorithm using estimated parameters. The following three assumptions are used:

Assumption 6.1 *The following signals/variables are available for measurement at all times: i) vertical penetration rate v; ii) rotary table velocity ω_r; iii) armature current I.* •

Assumption 6.2 *The following signals/variables are available for measurement during identification phase only: i) angular difference between the top and the bottom of the drillstring $\tilde{\phi}$; ii) torque-on-bit T.* •

Assumption 6.3 *In the matrices* (6.5)*, constant parameters of the drillstring c_1, J_1, k, c_2, J_2 are unknown, while parameters of the motor K_m, n, R, L are known exactly.* •

Remark 6.1 *Parameters of the motor are assumed to be known because they can be easily obtained from specifications or simple tests.*

6.5 Identification of drillstring parameters

Due to the fact that I is measurable, and its equation does not contain any uncertainties, we can consider the following reduced third-order model with current as an input:

$$\dot{x}_k = A_k x_k + B_k I + D_k T, \tag{6.14}$$

$$y_k = C_k x_k, \tag{6.15}$$

where $x_k = \left[\omega_r \ \tilde{\phi} \ \omega\right]^T$. Further, we represent all its parameters as a sum of nominal values and parametric errors:

$$A_k = \bar{A}_k + \Delta A_k, \quad D_k = \bar{D}_k + \Delta D_k, \tag{6.16}$$

$$\bar{A}_k = \begin{bmatrix} \bar{a}_4 & \bar{a}_3 & 0 \\ 1 & 0 & -1 \\ 0 & \bar{a}_2 & \bar{a}_1 \end{bmatrix}, \quad \Delta A_k = \begin{bmatrix} \Delta a_4 & \Delta a_3 & 0 \\ 1 & 0 & -1 \\ 0 & \Delta a_2 & \Delta a_1 \end{bmatrix}, \quad \bar{D}_k = \begin{bmatrix} 0 \\ 0 \\ \bar{d}_1 \end{bmatrix}, \quad \Delta D_k = \begin{bmatrix} 0 \\ 0 \\ \Delta d_1 \end{bmatrix}, \tag{6.17}$$

$$B_k = \bar{B}_k + \Delta B_k, \quad C_k = \begin{bmatrix} 1 & 0 & 0 \\ 0 & 1 & 0 \end{bmatrix}, \quad \bar{B}_k = \begin{bmatrix} \bar{a}_5 \\ 0 \\ 0 \end{bmatrix}, \quad \Delta B_k = \begin{bmatrix} \Delta a_5 \\ 0 \\ 0 \end{bmatrix}, \tag{6.18}$$

where bar notation means nominal value of the corresponding parameter (6.6), and Δ is the difference between actual and nominal values.

We define a generalized input and its matrix as

$$u_g = [I \ T]^T, \quad B_g = [B_k \ D_k]. \tag{6.19}$$

The model (6.14), (6.15) becomes

$$\dot{x}_k = \bar{A}_k x_k + \bar{B}_g u_g + E\Theta, \tag{6.20}$$

$$y_k = C_k x_k, \tag{6.21}$$

where $x_k \in R^n$, $u_g \in R^m$, $\Theta \in R^m$, $y_k \in R^m$, $m = 2$, $n = 3$. An uncertain part can be reformulated as follows

$$E\Theta = \Delta A x + \Delta B_g u_g, \tag{6.22}$$

$$E = \begin{bmatrix} 1 & 0 \\ 0 & 0 \\ 0 & 1 \end{bmatrix}, \quad \Theta = \begin{bmatrix} \theta_1 \phi_1 \\ \theta_2 \phi_2 \end{bmatrix}, \tag{6.23}$$

and $\theta_1 = \begin{bmatrix} \Delta a_4 & \Delta a_3 & \Delta a_5 \end{bmatrix}$, $\theta_2 = \begin{bmatrix} \Delta a_2 & \Delta a_1 & \Delta d_1 \end{bmatrix}$, $\phi_1 = \begin{bmatrix} \omega_r & \tilde{\phi} & I \end{bmatrix}^T$, $\phi_2 = \begin{bmatrix} \tilde{\phi} & \omega & T \end{bmatrix}^T$. In this model, uncertainties that have to be estimated are θ_1, θ_2.

Definition 6.1 *The system* (6.20), (6.21) *has a vector relative degree* $(r_1, ..., r_m)$ *with respect to the inputs* Θ *if the following conditions are met [116]:*

$$c_i A_k^s E = 0_{1\times m}, \quad i = 1, .., m, \quad s = 0, 1, .., r_i - 2, \tag{6.24}$$

where c_i *are i-th rows of the matrix* C_k*, and*

$$\det Q \neq 0, \quad Q = \begin{bmatrix} c_1 \bar{A}_k^{r_1 - 1} E \\ \vdots \\ c_m A_k^{r_m - 1} E \end{bmatrix}. \tag{6.25}$$

If there are no numbers r_i*, such that both conditions* (6.24), (6.25) *are met, the system does not have a vector relative degree.* •

Direct calculation shows that the system (6.20), (6.21) has a vector relative degree $r = \begin{pmatrix} r_1 & r_2 \end{pmatrix} = \begin{pmatrix} 1 & 2 \end{pmatrix}$.

Following [117], we define the hybrid high order sliding mode (HOSM) observer as follows:

$$\dot{z} = \bar{A}_k z + \bar{B}_g u_g \tag{6.26}$$

$$y_z = C_k z \tag{6.27}$$

$$\hat{x}_k = z + T_k^{-1} v_k, \tag{6.28}$$

where

$$T_k = \begin{bmatrix} c_1 & c_2 & c_2\bar{A}_k \end{bmatrix}^T, \tag{6.29}$$

and HOSM component of the order $m \cdot (\max\{r_1, r_2\} + 1) = 6$ has the form:

$$\begin{aligned} \dot{v}_{i,1} &= -\lambda_{i,3} M_i^{1/3} \cdot \left| v_{i,1} - y_i + y_{zi} \right|^{2/3} \operatorname{sign}\{v_{i,1} - y_i + y_{z,i}\} + v_{i,2}, \\ \dot{v}_{i,2} &= -\lambda_{i,2} M_i^{1/2} \cdot \left| v_{i,2} - \dot{v}_{i,1} \right|^{1/2} \operatorname{sign}\{v_{i,2} - \dot{v}_{i,1}\} + v_{i,3}, \\ \dot{v}_{i,3} &= -\lambda_{i,1} M_i \cdot \operatorname{sign}\{v_{i,3} - \dot{v}_{i,2}\} \end{aligned} \tag{6.30}$$

where $i = 1, 2$, $M_i > 0$ are sufficiently large numbers, $\lambda_{ij} > 1$, $j = 1, 2, 3$ are HOSM differentiators parameters to be chosen recursively [79]. In our case,

$$v_k = \begin{bmatrix} v_{11} & \dots & v_{1,r_1} & v_{21} & \dots & v_{2,r_2} \end{bmatrix}^T = \begin{bmatrix} v_{11} & v_{21} & v_{22} \end{bmatrix}^T. \tag{6.31}$$

It is proven [117] that the observer (6.26)-(6.31) exactly converges in finite time if matrix $\bar{A}_k$ is Hurwitz, the triple $\{\bar{A}_k, E, C_k\}$ has no invariant zeros, the system (6.20), (6.21) has full vector relative degree, and the input u_g and its derivative $\dot{u}_g$ are bounded by amplitude. Direct calculations reveal that these conditions are satisfied.

The following expression is defined as an equivalent output injection:

$$z_{eq} = \begin{bmatrix} v_{1,r_1+1} \\ \vdots \\ v_{m,r_m+1} \end{bmatrix} - \begin{bmatrix} c_1\bar{A}_k^{r_1} \\ \vdots \\ c_m\bar{A}_k^{r_m} \end{bmatrix} T_k^{-1} v_k = \begin{bmatrix} v_{12} \\ v_{23} \end{bmatrix} - \begin{bmatrix} c_1\bar{A}_k \\ c_2\bar{A}_k^2 \end{bmatrix} T_k^{-1} v_k. \tag{6.32}$$

Assuming that the observer (6.26)-(6.31) exactly converges at time T_0, it can be shown that for $t > T_0$

$$z_{eq} = Q\Theta, \quad Q = \begin{bmatrix} c_1\bar{A}_k^{r_1-1}E \\ \vdots \\ c_m\bar{A}_k^{r_m-1}E \end{bmatrix} = \begin{bmatrix} c_1E \\ c_2\bar{A}_kE \end{bmatrix}. \tag{6.33}$$

Therefore,

$$\Theta = \bar{z}_{eq}, \quad \bar{z}_{eq} = z_{eq} Q^{-1}, \tag{6.34}$$

or, using the definition of Θ,

$$\theta_i \phi_i = \bar{z}_{eq_i}. \tag{6.35}$$

Multiplying both sides of (6.35) by ϕ_i^T and taking integral, the following equality that holds for $T_0 < t_0 < t_1$ can be obtained:

$$\int_{t_0}^{t_1} \bar{z}_{eq_i} \phi_i^T d\tau = \int_{t_0}^{t_1} \theta_i \phi_i \phi_i^T d\tau \tag{6.36}$$

We define the following matrix:

$$\Gamma_i = \left(\int_{t_0}^{t_1} \phi_i \phi_i^T d\tau \right)^{-1}. \tag{6.37}$$

Now, using (6.36), estimates of the errors can be written in terms of measured and calculated values:

$$\hat{\theta}_i = \left(\int_{t_0}^{t_1} \bar{z}_{eq_i} \phi_i^T d\tau \right) \Gamma_i. \tag{6.38}$$

For simulation convenience, one can set $t_1 = t$, $t_0 = t - \Delta t_i$, where Δt_i is an adjustable time delay. Finally, estimated coefficients of the rotational dynamics model are

$$\hat{a}_1 = \bar{a}_1 + \hat{\theta}_{22}, \quad \hat{a}_2 = \bar{a}_2 + \hat{\theta}_{21}, \quad \hat{a}_3 = \bar{a}_3 + \hat{\theta}_{12},$$
$$\hat{a}_4 = \bar{a}_4 + \hat{\theta}_{11}, \quad \hat{a}_5 = \bar{a}_5 + \hat{\theta}_{13}, \quad \hat{d}_1 = \bar{d}_1 + \hat{\theta}_{23}, \tag{6.39}$$

where $\hat{\theta}_{1j}$, $\hat{\theta}_{2j}$ are j-th elements of vectors $\hat{\theta}_1$, $\hat{\theta}_2$.

6.6 Estimation of non-measured variables

With identified parameters of the rotational dynamics, we can now estimate additional variables that will be used in the control design. Specifically, we need to design an observer for

$\tilde{\phi}$ and T, which are not measured outside of identification phase, as well as ω and derivatives $\dot{T}$, $\ddot{T}$. For this purpose, we use a HOSM observer which provides estimates of the state variables and unknown input(s). It is based on the technique [111] and discussed in details in our previous works [114], [110]. In short, we extend the rotational dynamics model to include derivatives of T:

$$\begin{aligned} \dot{x}_e &= A_e x_e + B_e I + D_e T_3 \\ \omega_r &= C_e x_e, \end{aligned} \tag{6.40}$$

where

$$x_e = \begin{bmatrix} \omega_r \\ \tilde{\phi} \\ \omega \\ T \\ T_1 \\ T_2 \end{bmatrix}, A_e = \begin{bmatrix} \hat{a}_4 & \hat{a}_3 & 0 & 0 & 0 & 0 \\ 1 & 0 & -1 & 0 & 0 & 0 \\ 0 & \hat{a}_2 & \hat{a}_1 & \hat{d}_1 & 0 & 0 \\ 0 & 0 & 0 & 0 & 1 & 0 \\ 0 & 0 & 0 & 0 & 0 & 1 \\ 0 & 0 & 0 & 0 & 0 & 0 \end{bmatrix}, B_e = \begin{bmatrix} \hat{a}_5 \\ 0 \\ 0 \\ 0 \\ 0 \\ 0 \end{bmatrix}, C_e = \begin{bmatrix} 1 \\ 0 \\ 0 \\ 0 \\ 0 \\ 0 \end{bmatrix}^T, D_e = \begin{bmatrix} 0 \\ 0 \\ 0 \\ 0 \\ 0 \\ 1 \end{bmatrix}, \tag{6.41}$$

and $T_i := T^{(i)}$, $i = 1, 2, 3$, are i-th derivatives of T. For the system (6.40), (6.41), the following observer is used:

$$\dot{\hat{z}} = A_e \hat{z} + B_e I + L_e \left(\omega_r - \hat{z}_1\right), \tag{6.42}$$

where L_e is such that $A_e - L_e C_e$ is stable,

$$\dot{\nu}_i = -\lambda_{1i} M_1^{1/(7-i)} \cdot |\nu_i - \dot{\nu}_{i-1}|^{(6-i)/(7-i)} \operatorname{sign}\{\nu_i - \dot{\nu}_{i-1}\} + \nu_{i+1}, \tag{6.43}$$

where $i = 1, 2, .., 6$, $\dot{\nu}_0 = \omega_r + \hat{z}_1$, $\nu_7 = 0$, $M_1 > 0$ is a sufficiently large number, and λ_{1i} are to be chosen recursively [79], and

$$\hat{x}_e = \hat{z} + P^{-1} \nu, \tag{6.44}$$

where

$$v = \begin{bmatrix} v_1 \\ v_2 \\ v_3 \\ v_4 \\ v_5 \\ v_6 \end{bmatrix}, \quad P = \begin{bmatrix} C_e \\ C_e(A_e - L_eC_e) \\ C_e(A_e - L_eC_e)^2 \\ C_e(A_e - L_eC_e)^3 \\ C_e(A_e - L_eC_e)^4 \\ C_e(A_e - L_eC_e)^5 \end{bmatrix}. \tag{6.45}$$

6.7 Control design

In order to achieve the control goal outlined in Section 6.4, we first assume that we can control rotational velocity of the bit directly. In the first step, we design an algorithm for reference angular velocity, such that rate of penetration is converged to the desired value. After that, we ensure tracking of that reference signal by employing sliding mode techniques and using estimated variables and identified parameters.

6.7.1 Algorithm for reference angular velocity

The reference angular velocity signal ω_d is generated by an algorithm based on the speed-gradient methodology [49]. It is fully described in our paper [86], which is why we only give its equation here:

$$\dot{\omega}_d = -\gamma\, \omega_d^2\, v\, |\tilde{v}|^{q-1}\, \mathrm{sign}\{\tilde{v}\}, \tag{6.46}$$

where $q \in \{1, 2, \ldots\}$, $\tilde{v} := v - v_d$, $v_d > 0$ is a constant desired vertical penetration rate, and $\gamma > 0$ is an adjustable parameter chosen by a designer.

6.7.2 Tracking of the reference velocity

Our goal is to ensure tracking of the reference rotational velocity of the bit $\omega \to \omega_d$ in finite time. Let us define the following sliding variable:

$$\sigma = \dddot{e} + k_1\ddot{e} + k_2\dot{e} + k_3 e, \tag{6.47}$$

where $e = \omega_d - \omega$, and k_1, k_2, k_3 are coefficients chosen such that polynomial $s^3 + k_1 s^2 + k_2 s + k_3$ is Hurwitz. It can be shown that the derivative of σ can be expressed in the following way:

$$\dot{\sigma} = e^{(4)} + k_1 e^{(3)} + k_2\ddot{e} + k_3\dot{e} = f(x, T, \dot{T}, \ddot{T}, T^{(3)}, \dot{\omega}_d, \ddot{\omega}_d, \omega_d^{(3)}, \omega_d^{(4)}) - ru, \tag{6.48}$$

where function f is assumed to be bounded, i.e. $|f| \leq M$ for some $M > 0$, and $r > 0$ is a constant that depends on the parameters of the system.

The fact that control signal u appears explicitly in (6.48) allows us to apply a super-twisting control algorithm [111]

$$u = c_{sm}|\sigma|^{1/2}\,\mathrm{sign}\{\sigma\} + w, \tag{6.49}$$

$$\dot{w} = b_{sm}\,\mathrm{sign}\{\sigma\}, \tag{6.50}$$

where $c_{sm} > 0$, $b_{sm} > 0$. It is possible to show that the closed-loop compensated σ dynamics is converged to zero in finite time (see [111, sections 1.8 and 4.3]).

In order to implement the control law (6.49), (6.50), it is necessary to estimate σ (6.47). One way to do it is to estimate the derivatives of e, using HOSM observers. However, simulations show that practical implementation is quite difficult in this case due to significant chattering. The following method demonstrates better results: using the definition of tracking error $e = \omega_d - \omega$, we express $\dot{\omega}$, $\ddot{\omega}$, $\omega^{(3)}$ through other measured and estimated state variables, using the model (6.4), and substitute it into the equation (6.47):

$$\sigma = \omega_d^{(3)} + k_1\ddot{\omega}_d + k_2\dot{\omega}_d + k_3\omega_d - \left(m_1\omega + m_2\tilde{\phi} + m_3\omega_r + m_4 I + m_5 T + m_6\dot{T} + m_7\ddot{T}\right), \tag{6.51}$$

where

$$m_1 = a_1^3 - 2a_1a_2 + a_1^2k_1 - a_2k_1 + a_1k_2 + k_3, \tag{6.52}$$

$$m_2 = a_1^2a_2 - a_2^2 + a_2a_3 + a_1a_2k_1 + a_2k_2, \tag{6.53}$$

$$m_3 = a_1a_2 + a_2a_4 + a_2k_1, \tag{6.54}$$

$$m_4 = a_2a_5, \tag{6.55}$$

$$m_5 = d_1(a_1^2 - a_2 + a_1k_1 + k_2), \tag{6.56}$$

$$m_6 = d_1(a_1 + k_1), \tag{6.57}$$

$$m_7 = d_1. \tag{6.58}$$

It is clear that we need to estimate the derivatives $\ddot{\omega}_d$, $\omega_d^{(3)}$, which is done by means of HOSM observer:

$$\begin{aligned}
\dot{f}_1 &= -\lambda_{11}M_\omega^{1/3}|f_1 - \dot{\omega}_d|^{2/3}\,\mathrm{sign}\{f_1 - \dot{\omega}_d\} - \mu_{13}\sigma_\omega(f_1 - \dot{\omega}_d) + f_2,\\
\dot{f}_2 &= -\lambda_{12}M_\omega^{1/2}|f_2 - \dot{f}_1|^{1/2}\,\mathrm{sign}\{f_2 - \dot{f}_1\} - \mu_{12}\sigma_\omega(f_2 - \dot{f}_1) + f_3,\\
\dot{f}_3 &= -\lambda_{13}M_\omega\,\mathrm{sign}\{f_3 - \dot{f}_2\} - \mu_{11}\sigma_\omega(f_3 - \dot{f}_2),
\end{aligned} \tag{6.59}$$

where $f_i(t)$, $i = 1, 2, 3$ are estimates of $\omega_d^{(i)}$, $M_\omega > 0$ is a sufficiently large number, $\lambda_{1i} > 1$ are HOSM differentiators parameters to be chosen recursively [79], $\mu_{1i} > 0$ are coefficients chosen such that the polynomial $s^3 + \mu_{13}s^2 + \mu_{13}\mu_{12}s + \mu_{13}\mu_{12}\mu_{11}$ is Hurwitz, and $\sigma_\omega > 0$ is an adjustable gain.

Taking into account all estimates of parameters and signals, the overall expression for estimated sliding variable σ is

$$\hat{\sigma} = f_3 + k_1f_2 + k_2\dot{\omega}_d + k_3\omega_d - \left(\hat{m}_1\hat{\omega} + \hat{m}_2\hat{\dot{\phi}} + \hat{m}_3\omega_r + \hat{m}_4I + \hat{m}_5\hat{T} + \hat{m}_6\hat{\dot{T}} + \hat{m}_7\hat{\ddot{T}}\right), \tag{6.60}$$

where f_2, f_3 are defined in (6.59), estimates $\hat{\omega}$, $\hat{\dot{\phi}}$, $\hat{T}$, $\hat{\dot{T}}$, $\hat{\ddot{T}}$ are taken from $\hat{x}_e$ described in Section 6.6, and $\hat{m}_1, ..., \hat{m}_7$ are coefficients (6.52) - (6.58) with estimated parameters from Section 6.5.

The estimate $\hat{\sigma}$ is then used in the super-twisting control algorithm (6.49), (6.50).

6.8 Simulation results

Simulation results of the estimation and control algorithms designed in Sections 6.5, 6.6, 6.7 are presented here. We simulate drilling process through several rock layers with different stiffness. Moreover, because in real world rotational dynamics are described by even more complex infinite-dimensional models, we use one of them [15] to demonstrate that our approach works well in real applications. The model is described by the following partial differential equations:

$$\rho I_p \phi^p_{tt}(x,t) = \frac{GI_p}{L_p^2}\phi^p_{xx}(x,t) - \frac{c_1}{L_p}\phi^p_t(x,t) \tag{6.61}$$

$$\rho I_c \phi^c_{tt}(x,t) = \frac{GI_c}{L_c^2}\phi^c_{xx}(x,t) - \frac{c_1}{L_c}\phi^c_t(x,t) \tag{6.62}$$

with the following boundary conditions:

$$\frac{GI_p}{L_p}\phi^p_x(0,t) = J_1\phi^p_{tt}(0,t) + c_2\phi^p_t(0,t) - K_m n I(t), \tag{6.63}$$

$$\frac{GI_c}{L_c}\phi^c_x(1,t) = -J_B\phi^c_{tt}(1,t) - T(t), \tag{6.64}$$

$$\phi^p_t(1,t) = \phi^c_t(0,t), \tag{6.65}$$

$$\phi^p_x(1,t) = \frac{I_c L_p}{I_p L_c}\phi^c_x(0,t), \tag{6.66}$$

where $\phi^p(x,t)$, $\phi^c(x,t)$ are the angles of rotation along the drill pipes and the BHA, respectively, as functions of normalized distance $0 \le x \le 1$ and time t. In the above equations, subscripts denote partial derivatives, for example, $\phi^p_t(x,t) := \partial\phi^p(x,t)/\partial t$, $\phi^p_x(x,t) := \partial\phi^p(x,t)/\partial x$, $\phi^p_{tt}(x,t) := \partial^2\phi^p(x,t)/\partial t^2$, *etc*. Parameters ρ, G, L_p, L_c, I_p, I_c are physical characteristics of the drill pipes and BHA (density, sheer modulus, length and polar moment of inertia, respectively),

and $J_B := \rho I_c L_c$. The control current $I(t)$ is calculated as follows:

$$\dot{I} = -\frac{K_m n}{L}\phi_t^p(0,t) - \frac{R}{L}I + \frac{1}{L}V, \tag{6.67}$$

where V is a control voltage generated by the algorithm from Section 6.7. The following variables are used in the control algorithm:

$$\omega_r = \phi_t^p(0,t), \quad \omega = \phi_t^c(1,t), \quad \tilde{\phi} = \phi^p(0,t) - \phi^c(1,t). \tag{6.68}$$

We simulate two modes of operation: identification and tracking. During identification mode (the first 30 seconds) we keep the loop open and set a multiharmonic input voltage $u = 390 + 10\sin(0.4t) + 8\sin(0.6t)$ to ensure persistence of excitation, and perform identification of the parameters (we use lumped parameters model (6.4) in this phase). At the same time, we turn on the observer (6.42) - (6.45) to let its outputs approximately converge to the actual values. After that, we switch control voltage to super-twisting control algorithm (6.49), (6.50), using parametric estimates at $t = 30s$ to estimate, in turn, non-measured variables and calculate $\hat{\sigma}$ in real time.

Numerical values of the drilling system parameters and parameters of the environment are presented in Table 6.1

We simulate the system with some parametric errors, specifically,

$$\begin{bmatrix} \Delta J_1 \\ \Delta c_1 \\ \Delta k \\ \Delta J_2 \\ \Delta c_2 \end{bmatrix} = \begin{bmatrix} 50 \\ -10 \\ -100 \\ 260 \\ -5 \end{bmatrix}. \tag{6.69}$$

In terms of distributed parameter model, it also corresponds to $\Delta L_c = 59.3m$, $\Delta L_p = 145.6m$. Estimates of the coefficients a_1 - a_5, d_1 are presented in Figure 6.2. The whole amplitude in the beginning is not shown; however, large overshoots do not affect the work of the system, because these variables are purely computational for $t < 30s$. Nominal and real values correspond to black and red dashed lines, respectively. It can be seen that the estimates

Table 6.1: Numerical values of the parameters used in simulations (Chapter 6)

Parameter	Value	Parameter	Value
Parameters set by operator			
v_d, mm/s	{3,2}	γ_v	{1000, 3000}
Drilling system parameters			
$\bar{L}_p$, m	1100	$\bar{L}_c$, m	250
I_p, m^4	$1.19{\cdot}10^{-5}$	I_c, m^4	$9.71{\cdot}10^{-5}$
$\bar{J}_1$, kgm^2	226.1	n	2
$\bar{J}_2$, kgm^2	1140	W_0, N	7000
$\bar{c}_1$, Nms	25.7	M, kg	75813
$\bar{c}_2$,Nms	10	K_f, Nm	25
$\bar{k}$, Nm	859.6	a, m	0.11
R, Ω	0.1	ζ	0.75
L, H	0.025	d_*, mm	0.5
K_m, Vs	6.5	$\mu\gamma$	1.1
Drilling controller parameters			
$\lambda_{i3} \dots \lambda_{i1}$	$\begin{bmatrix}1.1 & 1.5 & 2\end{bmatrix}$	σ_ω	5
M_1	0.0005	M_ω	3
Δt_1, s	3	Δt_2, s	7
c_{sm}	0.95	b_{sm}	0.44
$\sigma\{A_e - L_e C_e\}$	$[-0.5 \quad -0.35 \pm 0.35j \quad -0.43 \pm 0.25j$ $-0.48 \pm 0.13j]$		
k_1, k_2, k_3	$\begin{bmatrix}6 & 11 & 6\end{bmatrix}$		
$\mu_{13} \dots \mu_{11}$	$\begin{bmatrix}12 & 3.92 & 1.28\end{bmatrix}$		
Parameters of the environment			
ϵ, MPA	{30,35,31,25}		
$\sigma\kappa$, N/m^2	3ϵ		

converge to either actual values or very small neighborhood of actual parameters.

Simulation results for state variables, torque-on-bit, depth of cut, control signal, and sliding variable are shown in Figures 6.3 - 6.6. Red dashed line separates identification and tracking modes. One can see that stability is ensured, and all variables converge to their desired values in reasonable time. There is a small mismatch between real and estimated torque due to imperfect parameters identification and different models, but the error does not affect the result in terms of velocity regulation.

6.9 Conclusions

In this paper, a problem of vertical velocity regulation in rotary drilling systems with parametric uncertainties is addressed, and an observer-based control algorithm is designed for this task. In contrast with previous results, the proposed algorithm is robust with respect to parametric errors, which means that only approximate nominal values of the drilling system's mechanical parameters can be used. Additionally, parameters of the environment are also considered unknown, and underground measurements are only required in the identification phase. The proposed approach was tested by simulations; the results showed that it is feasible and efficient.

In the future, it could be possible to extend these results to the case of directional drilling systems, where the tasks of velocity regulation and trajectory tracking should be solved simultaneously.

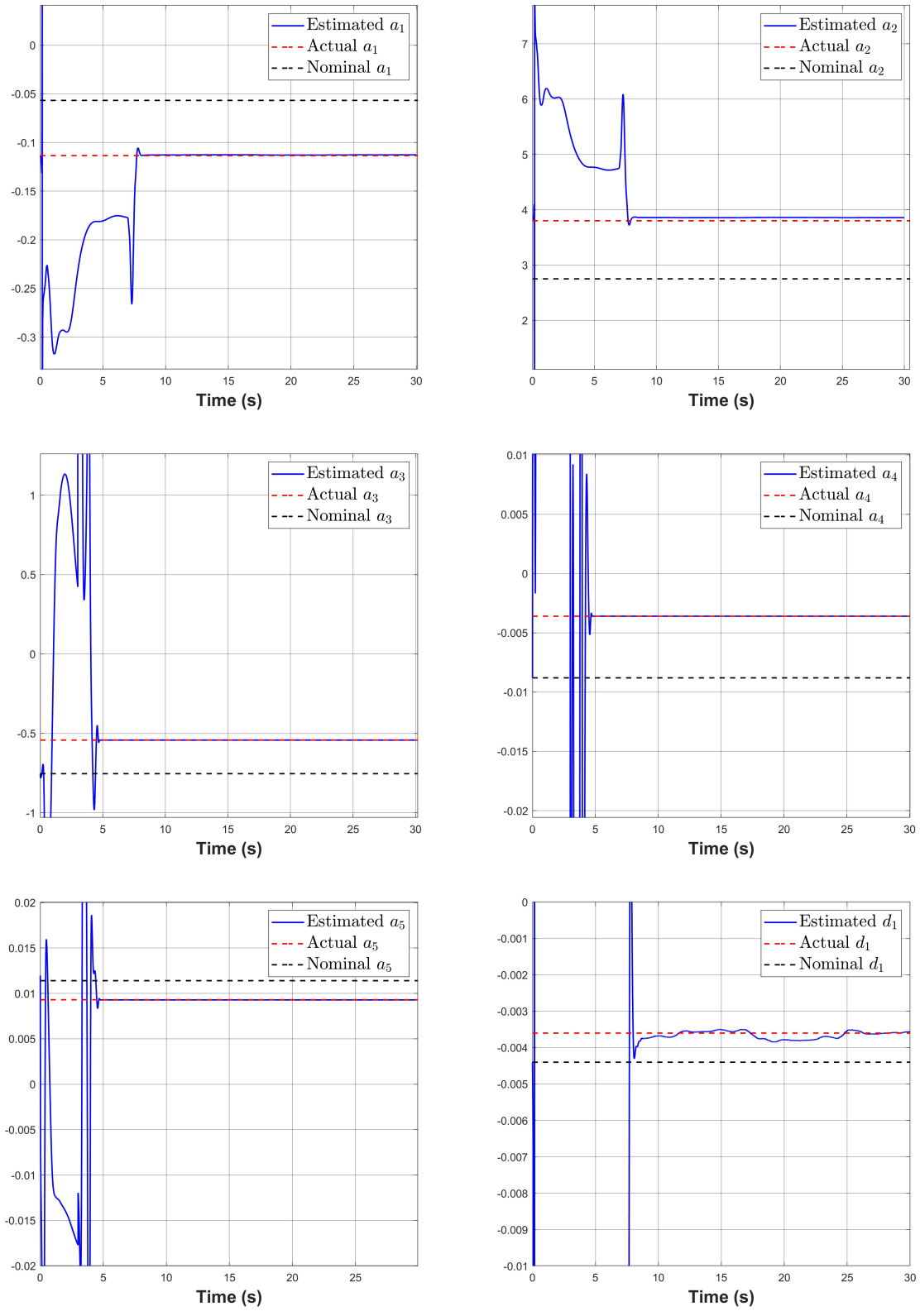

Figure 6.2: Actual, nominal, and estimated coefficients of the rotational dynamics model a_1, a_2, a_3, a_4, a_5, d_1

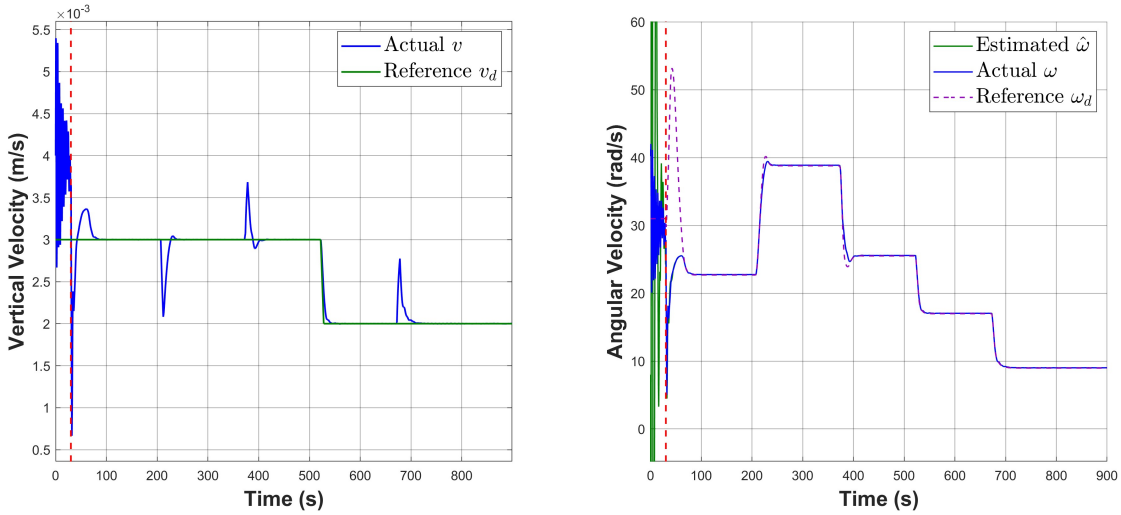

Figure 6.3: Rate of penetration v (left plot); actual, estimated, and reference rotational velocity of the drill bit ω, $\hat{\omega}$, ω_d (right plot)

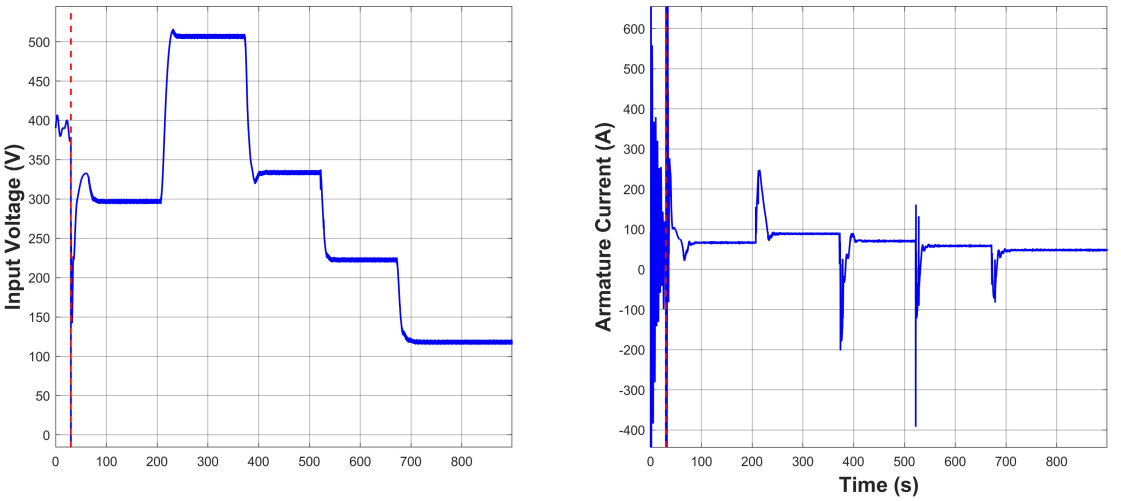

Figure 6.4: Control voltage V (left plot); armature current I (right plot)

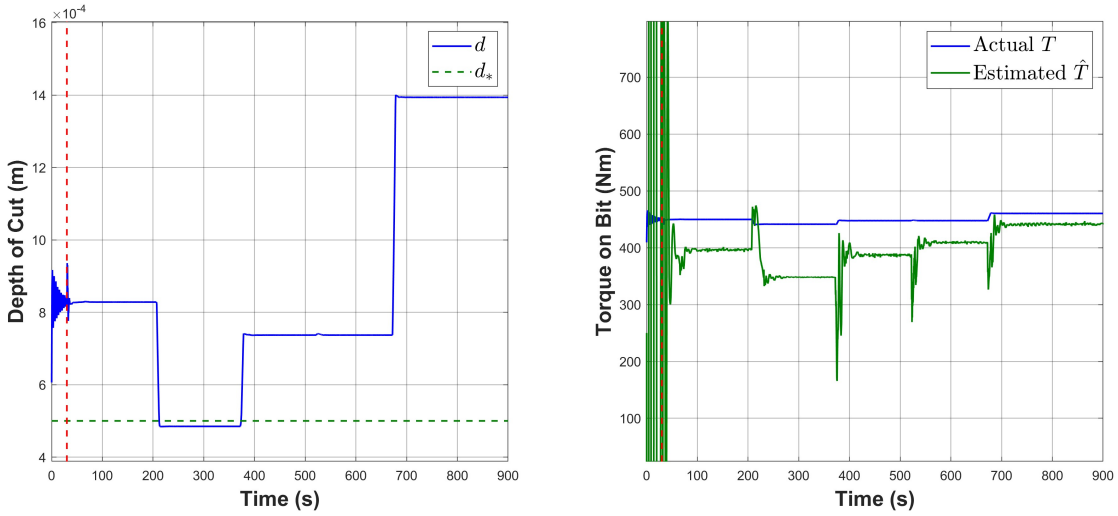

Figure 6.5: Depth of cut d (left plot); actual and estimated torque-on-bit T, $\hat{T}$ (right plot)

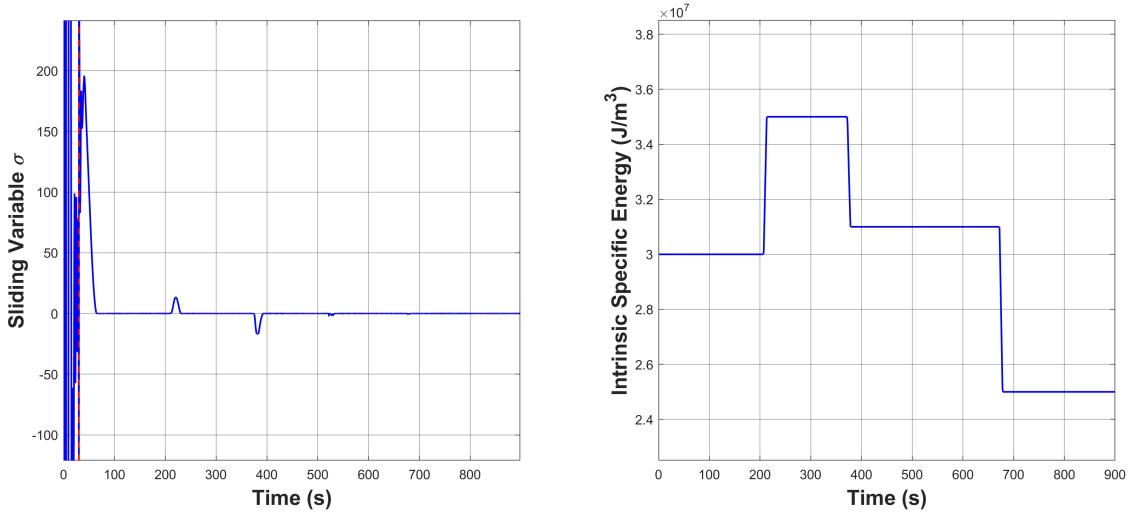

Figure 6.6: Sliding variable σ (left plot); intrinsic specific energy of the rock ϵ (right plot)

Chapter 7

Conclusions

7.1 Summary

In this thesis, we presented new control algorithms for conventional rotary drilling systems. These algorithms ensure safe and stable automated drilling operations according to the desired values set by a human operator. It translates into two problems that we considered: regulation of vertical penetration rate and regulation of drilling power. Solution of the second problem has an advantage in a way that it better protects the drill bit from wearout and is generally safer; however, control laws that we obtained for drilling power regulation can only be proved theoretically if parameters of the environment are known beforehand; otherwise, it works in the first phase of drilling only. For this reason, the research is mainly focused on vertical velocity regulation.

In Chapters 2 to 6, different cases were considered, and several control strategies were proposed depending on the amount of available information and required precision of the drilling model. In all of them, we had a multi-step approach: first, a reference rotational velocity of the drill bit is generated, such that the control goal is achieved, as if the angular velocity was controlled directly. After that, it is ensured that the actual signal tracks the reference one with good precision.

First, in Chapter 2, we defined the drilling power and designed a control law to regulate it, assuming that all parameters are known, and downhole measurements are available continuously without delays. Reference rotational velocity was calculated and then tracked using high-order sliding mode observers, while disturbance introduced by torque-on-bit was also re-

jected. In the next chapter, we relaxed the assumption that parameters of the environment are available. We generated reference angular velocity by use of speed gradient method, taking advantage of the fact that torque-on-bit and weight-on-bit are linear functions with respect to depth of cut. In Chapter 4, we used an infinite-dimensional model of the rotational dynamics, which describes the real-world drilling system more precisely. With the same algorithm for reference rotational velocity, we introduced a method for its tracking that guarantees exponential convergence. The algorithm uses a distributed-parameter reference model and a disturbance observer. Next, in Chapter 5, we eliminated the necessity of downhole measurements (and, therefore, any and all communication requirements) by using a HOSM observer for estimation of all downhole signals that utilizes only two ground-level measurements - angular velocity of the rotary table and armature current of the motor. We tested this controller against small disturbances in the rock structure, as well as with infinite-dimensional model of the rotational dynamics. Finally, in Chapter 6, we investigated the case of uncertain parameters of the drilling system itself (i.e. mechanical characteristics and damping coefficients), proposed a strategy to identify them, and then used the estimates in a new tracking scheme based on a super-twisting sliding mode controller.

All results were tested in simulations, where we simulated a drilling process through several (homogeneous in most cases) rock layers with different stiffness. We defined one or two desired levels of penetration rate or drilling power, and showed that in every layer the proposed control algorithms successfully converge all variables to their desired values in reasonable time.

7.2 Future Work

In the future, our approach may be enhanced in the areas of directional drilling and adaptive control. In the former problem, most efforts are focused on a precise trajectory tracking; however, it would be useful to investigate how tracking of both spacial trajectory and desired velocity can be achieved together. Another improvement may include identification of all drilling parameters within a single mode of operation.

There exist many other challenges in drilling automation, including pressure control during MPD in a closed annulus, trajectory control in directional drilling, detection of undesirable events in the wellbore, automatic well control by means of managing dangerous influxes of fluids or gases into the well, precise modeling of the wellbore in real time, and other problems.

Novel automatic control solutions in these areas would improve quality and safety of drilling and greatly benefit the industry.

Bibliography

[1] E. I. Epelle and D. I. Gerogiorgis, "A review of technological advances and open challenges for oil and gas drilling systems engineering," *AIChE Journal*, vol. 66, no. 4, 2020.

[2] F. Poletto and F. Miranda, *Seismic While Drilling: Fundamentals of Drill-bit Seismic for Exploration*. Elsevier, 2nd ed., 2022.

[3] A. Depouhon and E. Detournay, "Instability regimes and self-excited vibrations in deep drilling systems," *Journal of Sound and Vibration*, vol. 333, pp. 2019–2039, 2014.

[4] V. Smil, *Oil: A Beginner's Guide*. Oneworld Publications, 2008.

[5] J.-M. Godhavn, A. Pavlov, G.-O. Kaasa, and N. L. Rolland, "Drilling seeking automatic control solutions," *IFAC Proceedings Volumes*, vol. 44, pp. 10842–10850, Jan. 2011.

[6] Q. Gu, A. Fallah, A. Ambrus, Z. Ma, D. Chen, P. Ashok, and E. van Oort, "A switching MPD controller for mitigating riser gas unloading events in offshore drilling," *SPE Drilling and Completion*, vol. 35, no. 2, pp. 201–217, 2020.

[7] A. S. Cohen *et al.*, "Reconstructing the environmental context of human origins in Eastern Africa through scientific drilling," *Annual Review of Earth and Planetary Sciences*, vol. 50, pp. 451–476, 2022.

[8] C. Chongbin, Q. Qiquan, S. Xiaomeng, D. Zongquan, T. Dewei, and J. Shengyuan, "Multi-state autonomous drilling for lunar exploration," *Chinese Journal of Aeronautics*, vol. 29, no. 5, pp. 1397–1404, 2016.

[9] D. G. G. Rosa, J. F. S. Feiteira, A. M. Lopes, and P. A. F. de Abreu, "Analysis and implementation of a force control strategy for drilling operations with an industrial robot,"

Journal of the Brazilian Society of Mechanical Sciences and Engineering, vol. 39, pp. 4749–4756, 2017.

[10] E. H. Voormolen *et al.*, "Benchmarking distance control and virtual drilling for lateral skull base surgery," *World Neurosurgery*, vol. 109, pp. e217–e228, 2018.

[11] Y. Bar-Cohen and K. Zacny, eds., *Drilling in extreme environments: penetration and sampling on Earth and other planets*. Wiley-VCH, 2009.

[12] S. Goldman, H. Flashner, and B. Yang, "An approach to modeling percussive drilling systems," *Journal of Vibration and Acoustics*, vol. 144, May 2022.

[13] C. Zha, G. Liu, J. Li, Y. Li, Y. Xi, and B. Guo, "Combined percussive-rotary drilling to increase rate of penetration and life of drill bit in drilling hard rock formation," *Chemistry and Technology of Fuels and Oils*, vol. 53, pp. 254–262, 2017.

[14] M. E. Hossain and A. A. Al-Majed, *Fundamentals of Sustainable Drilling Engineering*. Scrivener Publishing, 2015.

[15] M. B. S. Marquez, I. Boussaada, H. Mounier, and S.-I. Niculescu, *Analysis and Control of Oilwell Drilling Vibrations: A Time-Delay Systems Approach*. Advances in Industrial Control, Springer, 2015.

[16] J. Jansen and L. Steen, "Active damping of self excited torsional vibrations in oil well drillstrings," *Journal of Sound and Vibration*, vol. 179, no. 4, pp. 647–668, 1995.

[17] M. Fazaelizadeh, *Real Time Torque and Drag Analysis during Directional Drilling*. PhD thesis, University of Calgary, 2013.

[18] U. J. F. Aarsnes and O. M. Aamo, "Linear stability analysis of self-excited vibrations in drilling using an infinite dimensional model," *Journal of Sound and Vibration*, vol. 360, pp. 239–259, 2016.

[19] E. Detournay and P. Defourny, "A phenomenological model for the drilling action of drag bits," *International Journal of Rock Mechanics and Mining Sciences and Geomechanics Abstracts*, vol. 29, no. 1, pp. 13–23, 1992.

[20] E. Detournay, T. Richard, and M. Shepherd, "Drilling response of drag bits: Theory and experiment," *International Journal of Rock Mechanics and Mining Sciences*, vol. 45, pp. 1347–1360, 2008.

[21] L. Perneder, E. Detournay, and G. Downton, "Bit/rock interface laws in directional drilling," *International Journal of Rock Mechanics and Mining Sciences*, vol. 51, pp. 81–90, 2012.

[22] N. A. H. Kremers, E. Detournay, and N. van de Wouw, "Model-based robust control of directional drilling systems," *IEEE Transactions on Control System Technologies*, vol. 24, no. 1, pp. 226–239, 2016.

[23] Z. Li and K. Itakura, "An analytical drilling model of drag bits for evaluation of rock strength," *Soils and Foundations*, vol. 52, no. 2, pp. 216–227, 2012.

[24] Y. Nishimatsu, "The mechanics of rock cutting," *International Journal of Rock Mechanics and Mining Sciences*, vol. 9, pp. 261–270, 1972.

[25] A. F. A. Serrarens, M. J. G. van de Molengraft, J. J. Kok, and L. van den Steen, "H_∞ control for suppressing stick-slip in oil well drillstrings," *IEEE Control Systems Magazine*, vol. 18, no. 2, pp. 19–30, 1998.

[26] D. Karnopp, "Computer simulation of stick-slip friction in mechanical dynamic systems," *Journal of Dynamic Systems Measurement and Control*, vol. 107, no. 1, pp. 100–103, 1985.

[27] E. M. Navarro-Lopez and D. Cortes, "Sliding-mode control of a multi-DOF oilwell drillstring with stick-slip oscillations," in *2007 American Control Conference*, pp. 3837–3842, 2007.

[28] W. C. Chin, Y. Su, L. Sheng, L. Ti, H. Bian, and R. Shi, *Measurement While Drilling: Signal Analysis, Optimization and Design*. Hoboken, New Jersey: Scrivener Publishing, 2014.

[29] S. M. Mwachaka, A. Wu, and Q. Fu, "A review of mud pulse telemetry signal impairments modeling and suppression methods," *Journal of Petroleum Exploration and Production Technology*, vol. 9, pp. 779–792, 2019.

[30] J. Shaoa, Z. Yanb, *et al.*, "Differential signal extraction for continuous wave mud pulse telemetry," *Journal of Petroleum Science and Engineering*, vol. 148, pp. 127–130, 2017.

[31] G. C. Downton, "Challenges of modeling drilling systems for the purposes of automation and control," *IFAC Proceedings Volumes*, vol. 45, pp. 201–210, Jan. 2012.

[32] Halliburton, "JetPulse High-Speed Telemetry Service." https://www.halliburton.com/en-US/ps/sperry/drilling/telemetry/jetpulse-telemetry-service.html?node-id=hfyjrqux, 2019.

[33] Halliburton, "QuickPulse Automated Directional Gamma Service." https://www.halliburton.com/content/dam/ps/public/ss/contents/Data_Sheets/web/quickpulse-automated-directional-gamma-service.pdf?node-id=hfyjrqux&nav=en-US_sperry_public, 2019.

[34] Y. Lin, X. Kong, Y. Qui, and Q. Yuan, "Calculation analysis of pressure wave velocity in gas and drilling mud two-phase fluid in annulus during drilling operations," *Mathematical Problems in Engineering*, pp. 1–17, 2013.

[35] H. Li, Y. Meng, G. Li, L. Zhu, Y. Li, and Y. Chen, "Effects of suspended solid particles on the propagation and attenuation of mud pressure pulses inside drill string," *Journal of Natural Gas Science and Engineering*, vol. 22, pp. 340–347, 2015.

[36] H. Mahdianfan and A. Pavlov, "Adaptive output regulation for offshore managed pressure drilling," *International Journal of Adaptive Control and Signal Processing*, vol. 31, pp. 652–673, 2017.

[37] M. A. Namuq, M. Reich, and S. Bernstein, "Continuous wavelet transformation: A novel approach for better detection of mud pulses," *Journal of Petroleum Science and Engineering*, vol. 110, pp. 232–242, 2013.

[38] Y. Zheng, X. Sun, J. Chen, and J. Yue, "Extracting pulse signals in measurement while drilling using optimum denoising methods based on the ensemble empirical mode decomposition," *Petroleum Exploration and Development*, vol. 39, no. 6, pp. 798–801, 2012.

[39] X. Zhong, L. Cen, Y. Zhao, T. Huang, and J. Shi, "Measurement While Drilling Mud Pulse Signal Denoising and Extraction Approach Based on Particle-Swarm-Optimized Time-Varying Filtering Empirical Mode Decomposition," *SPE Drilling and Completion*, vol. 36, no. 03, pp. 483–493, 2021.

[40] X. Zhang, H. Zhang, J. Guo, L. Zhu, and S. Lv, "Research on mud pulse signal detection based on adaptive stochastic resonance," *Journal of Petroleum Science and Engineering*, vol. 157, pp. 643–650, 2017.

[41] F. Qu, Z. Zhang, J. Hu, J. Xu, S. Wang, and Y. Wu, "Adaptive dual-sensor noise cancellation method for continuous wave mud pulse telemetry," *Journal of Petroleum Science and Engineering*, vol. 162, pp. 386–393, 2018.

[42] X. Zhang, H. Zhang, J. Guo, and L. Zhu, "Auto measurement while drilling mud pulse signal recognition based on deep neural network," *Journal of Petroleum Science and Engineering*, vol. 167, pp. 37–43, 2018.

[43] J. Chen, S. Li, C. MacMillan, G. Cortes, and D. Wood, "Long range electromagnetic telemetry using an innovative casing antenna system," in *SPE Annual Technical Conference and Exhibition*, Sept. 2015.

[44] J. Pagtalunan, K. Parmar, S. Kim, B. Moon, and S. S. Park, "Experimental study on repeater-free acoustic telemetry for downhole operations," *Journal of Petroleum Science and Engineering*, vol. 202, 2021.

[45] I. N. de Almeida Jr., P. D. Antunes, F. O. C. Gonzalez, R. A. Yamachita, A. Nascimento, and J. L. Goncalves, "A review of telemetry data transmission in unconventional petroleum environments focused on information density and reliability," *Journal of Software Engineering and Applications*, vol. 8, pp. 455–462, 2015.

[46] S. T. Edwards, C. J. Coley, N. A. Whitley, R. G. Keck, V. Ramnath, T. Foster, K. Coghill, and M. Honey, "A summary of wired drill pipe field trials and deployments in BP," Mar. 2013.

[47] M. Andersen, S. Zainoune, and E. Vandvi, "Capturing real-time data during drilling and tripping operations improves efficiency and well placement," *World Oil*, pp. 25–28, Mar. 2021.

[48] P. Ioannou and J. Sun, *Robust Adaptive Control*. PTR Prentice Hall, 1996.

[49] A. L. Fradkov, I. V. Miroshnik, and V. O. Nikiforov, *Nonlinear and Adaptive Control of Complex Systems*. Kluwer Academic Publishers, 1999.

[50] F. Shah and I. Polushin, "Design of telerobotic drilling control system with haptic feedback," *Journal of Control Science and Engineering*, pp. 1–15, 2013.

[51] S. Belokobylskii and V. Prokopov, "Friction-induced self-excited vibrations of drill rig with exponential drag law," *Sov. Applied Mechanics*, vol. 18, no. 12, pp. 1134–1138, 1982.

[52] W. R. Tucker and C. Wang, "An integrated model for drill-string dynamics," *Journal of Sound and Vibration*, vol. 224, no. 1, pp. 123–165, 1999.

[53] C. Germay, N. V. de Wouw, H. Nijmeijer, and R. Sepulchre, "Nonlinear drillstring dynamics analysis," *SIAM Journal on Applied Dynamical Systems*, vol. 8, no. 2, pp. 527–553, 2009.

[54] C. Germay, V. Denoel, and E. Detournay, "Multiple mode analysis of the self-excited vibrations of rotary drilling systems," *Journal of Sound and Vibration*, vol. 325, no. 1, pp. 362–381, 2009.

[55] B. Saldivar, S. Mondie, J. J. Loiseau, and V. Rasvan, "Suppressing axial-torsional coupled vibrations in drillstrings," *Journal of Control Engineering and Applied Informatics*, vol. 15, no. 1, pp. 3–10, 2013.

[56] B. Saldivar, S. Mondie, and A. V. J. Carlos, "The control of drilling vibrations: A coupled PDE-ODE modeling approach," *International Journal of Applied Mathematics and Computer Science*, vol. 26, no. 2, pp. 335–349, 2016.

[57] D. J. Runia, S. Dwars, and I. P. Stulemeijer, "A brief history of the shell "Soft Torque Rotary System" and some recent case studies," in *SPE/IADC Drilling Conference and Exhibition*, pp. 1–10, Mar. 2013.

[58] S. Dwars, "Recent Advances in Soft Torque Rotary Systems," in *SPE/IADC Drilling Conference and Exhibition*, pp. 1–12, Mar. 2015.

[59] S. Fubin, S. Linxiu, L. Lin, and Z. Qizhi, "Adaptive pid control of rotary drilling system with stick slip oscillation," in *2nd International Conference on Signal Processing Systems (ICSPS)*, pp. V2–289–V2–292, 2010.

[60] R. Riane, M. Z. Doghmane, M. Kidouche, and S. Djezzar, "Observer-based h-infinity controller design for high frequency stick-slip vibrations mitigation in drill-string of rotary drilling systems," *Vibration*, vol. 5, no. 2, pp. 264–289, 2022.

[61] R. Hernandez-Suarez, H. Puebla, R. Aguilar-Lopez, and E. Hernandez-Martinez, "An integral high-order sliding mode control approach for stick-slip suppression in oil drill-strings," *Petroleum Science and Technology*, vol. 27, no. 8, pp. 788–800, 2009.

[62] M. Zribi, M. Karkoub, and C. C. Huang, "Control of stick-slip oscillations in oil well drill strings using the back-stepping technique," *International Journal of Acoustics and Vibrati*, vol. 16, no. 3, pp. 134–143, 2011.

[63] E. M. Navarro-Lopez and R. Suarez, "Practical approach to modelling and controlling stick-slip oscillations in oilwell drillstrings," in *Proceedings of the 2004 IEEE International Conference on Control Application*, pp. 1454–1460, Sept. 2004.

[64] B. Saldivar, T. Knüppel, F. Woittennek, I. Boussaada, H. Mounier, and S. Niculescu, "Flatness-based control of torsional-axial coupled drilling vibrations," *IFAC Proceedings Volumes*, vol. 47, no. 3, pp. 7324–7329, 2014. 19th IFAC World Congress.

[65] R. Tucker and C. Wang, "On the effective control of torsional vibrations in drilling systems," *Journal of Sound and Vibration*, vol. 224, no. 1, pp. 101–122, 1999.

[66] E. M. Navarro-Lopez, "An alternative characterization of bit-sticking phenomena in a multi-degree-of-freedom controlled drillstring," *Nonlinear Analysis: Real World Applications*, vol. 10, no. 5, pp. 3162–3174, 2009.

[67] F. Abdulgalil and H. Siguerdidjane, "Nonlinear control design for suppressing stick-slip oscillations in oil well drillstrings," in *2004 5th Asian Control Conference (IEEE Cat. No.04EX904)*, vol. 2, pp. 1276–1281 Vol.2, 2004.

[68] J. Rudat and D. Dashevskiy, "Development of an innovative model-based stick/slip control system," in *SPE/IADC Drilling Conference and Exhibition*, (Amsterdam, The Netherlands), pp. 1–12, Mar. 2011.

[69] D. Ba, G. Chen, P. Li, K. An, and X. Liu, "Fuzzy Smith predictor–based active disturbance rejection controller for time-delay systems with application to drilling stick–slip vibration control," *Proceedings of the Institution of Mechanical Engineers, Part I: Journal of Systems and Control Engineering*, pp. 1–14, 2022.

[70] T. Vromen, C.-H. Dai, N. van de Wouw, T. Oomen, P. Astrid, A. Doris, and H. Nijmeijer, "Mitigation of torsional vibrations in drilling systems: A robust control approach," *IEEE Transactions on Control Systems Technomogy*, vol. 27, no. 1, pp. 249–265, 2019.

[71] H. Ibrahim Basturk, "Observer-Based Boundary Control Design for the Suppression of Stick–Slip Oscillations in Drilling Systems With Only Surface Measurements," *Journal of Dynamic Systems, Measurement, and Control*, vol. 139, June 2017.

[72] C. Fairhurst and W. Lacabanne, "Hard rock drilling techniques," *Mine and Quarry Engineering*, pp. 157–161, 194–197, 1957.

[73] J. Zhou and G. Nygaard, "Automatic model-based control scheme for stabilizing pressure during dual-gradient drilling," *Journal of Process Control*, vol. 21, pp. 1138–1147, Sept. 2011.

[74] A. Albert, O. M. Aamo, J.-M. Godhavn, and A. Pavlov, "Suppressing pressure oscillations in offshore drilling: Control design and experimental results," *IEEE Transactions on Control Systems Technology*, vol. 23, pp. 813–819, Mar. 2015.

[75] B. Glass, H. Cannon, M. Branson, S. Hanagud, and G. Paulsen, "Dame: Planetary-prototype drilling automation," *Astrobiology*, vol. 8, no. 3, pp. 653–664, 2008.

[76] K. Zacny, Y. Bar-Cohen, *et al.*, "Extraterrestrial drilling and excavation," in *Drilling in Extreme Environments*, ch. 6, pp. 347–557, Wiley-Blackwell, 2009.

[77] H. K. Khalil, *Nonlinear Systems*. Upper Saddle River, NJ: Prentice Hall, 3rd ed., 2002.

[78] A. Levant and M. Livne, "Globally convergent differentiators with variable gains," *International Journal of Control*, vol. 91, no. 9, pp. 1994–2008, 2018.

[79] A. Levant, "Higher-order sliding modes, differentiation and output-feedback control," *International Journal of Control*, vol. 76, no. 9-10, pp. 924–941, 2003.

[80] J. Thorogood, W. Aldred, F. Florence, and F. Iversen, "Drilling automation: Technologies, terminology, and parallels with other industries," *SPE Drilling and Completion*, vol. 25, no. 4, pp. 419–425, 2010.

[81] A. W. Eustes, "The evolution of automation in drilling," *SPE Annual Technical Conference and Exhibition*, 2007.

[82] B. A. Kennedy, ed., *Surface mining*. Society for mining, metallurgy, and exploration, 2nd ed., 1990.

[83] M. V. Faronov and I. G. Polushin, "Algorithm for power stabilization in rotary drilling systems," in *Proceedings of the 2019 IEEE 15th International Conference on Automation Science and Engineering (CASE)*, (Vancouver, Canada), pp. 867–872, Aug. 2019.

[84] H. Lee and V. I. Utkin, "Chattering suppression methods in sliding mode control systems," *Annual Reviews in Control*, vol. 31, pp. 179–188, 2007.

[85] J. Tang, Q. Quan, S. Jiang, J. Liang, and Z. Deng, "Intelligent drilling and coring technologies for unmanned interplanetary exploration," in *Drilling* (A. Samsuri, ed.), ch. 2, pp. 17–35, IntechOpen, 2018.

[86] M. V. Faronov and I. G. Polushin, "Regulation of penetration rate and drilling power in rotary drilling systems," in *IEEE 16th International Workshop on Advanced Motion Control (AMC 2020)*, (Kristiansand, Norway), pp. 97–104, Sept. 2020.

[87] M. Krstic and A. Smyshlyaev, *Boundary Control of PDEs: A Course on Backstepping Designs*. Systems and Control: Foundations and Applications, Society for Industrial and Applied Mathematics, Philadelphia, 2007.

[88] A. Smyshlyaev and M. Krstic, "Boundary control of an anti-stable wave equation with anti-damping on the uncontrolled boundary," *Systems and Control Letters*, vol. 58, pp. 617–623, 2009.

[89] D. Bresch-Pietri and M. Krstic, "Adaptive output feedback for oil drilling stick-slip instability modeled by wave PDE with anti-damped dynamic boundary," in *2014 American Control Conference*, (Portland, Oregon, USA), pp. 386–391, June 2014.

[90] J.-J. Liu and J.-M. Wang, "Active disturbance rejection control and sliding mode control of one-dimensional unstable heat equation with boundary uncertainties," *IMA Journal of Mathematical Control and Information*, vol. 32, pp. 97–117, 2015.

[91] B.-Z. Guo and F.-F. Jin, "Sliding mode and active disturbance rejection control to stabilization of one-dimensional anti-stable wave equations subject to disturbance in boundary input," *IEEE Transactions on Automatic Control*, vol. 58, no. 5, pp. 1269–1274, 2013.

[92] W. Guo and B.-Z. Guo, "Performance output tracking for a wave equation subject to unmatched general boundary harmonic disturbance," *Automatica*, vol. 68, pp. 194–202, 2016.

[93] M. Zamanian, S. Khadem, and M. Ghazavi, "Stick-slip oscillations of drag bits by considering damping of drilling mud and active damping system," *Journal of Petroleum Science and Engineering*, vol. 59, pp. 289–299, 2007.

[94] X. Zhang, H. Feng, and S. Chai, "Performance output exponential tracking for a wave equation with a general boundary disturbance," *Systems and Control Letters*, vol. 98, pp. 79–85, 2016.

[95] A. Loría, E. Panteley, D. Popović, and A. R. Teel, "A nested Matrosov theorem and persistency of excitation for uniform convergence in stable nonautonomous systems," *IEEE Transactions on Automatic Control*, vol. 50, no. 2, pp. 183–198, 2005.

[96] N. Kazantzis and C. Kravaris, "Time-discretization of nonlinear control systems via Taylor methods," *Computers and Chemical Engineering*, vol. 23, pp. 763–784, 1999.

[97] J. D. Macpherson, J. P. de Wardt, F. Florence, C. Chapman, M. Zamora, M. Laing, and F. Iversen, "Drilling-systems automation: Current states, initiatives, and potential impact," *SPE Drilling and Completion*, vol. 28, no. 4, pp. 296–308, 2013.

[98] M. Ghasemi and X. Song, "Trajectory tracking and rate of penetration control of downhole vertical drilling system," *Journal of Dynamic Systems, Measurement, and Control*, vol. 140, no. 9, 2018.

[99] H. Sun, Z. Li, N. Hovakimyan, T. Basar, and G. Downton, "$\mathcal{L}_1$ adaptive control for directional drilling systems," *IFAC Proceedings Volumes*, vol. 45, no. 8, pp. 72–77, 2012.

[100] A. Georgiou, S. A. Evangelou, I. M. Jaimoukha, and G. Downton, "Tracking control for directional drilling systems using robust feedback model predictive control," *IFAC-PapersOnLine*, vol. 53, no. 2, pp. 11974–11981, 2020. 21th IFAC World Congress.

[101] H. Zhang and X. Yuan, "An improved particle swarm algorithm to optimize PID neural network for pressure control strategy of managed pressure drilling," *Neural Computing and Applications*, vol. 32, pp. 1581–1592, 2020.

[102] P. Pastusek, G. Payette, R. Shor, E. Cayeux, U. J. Aarsnes, J. Hedengren, S. Menand, J. Macpherson, R. Gandikota, M. Behounek, R. Harmer, E. Detournay, R. Illerhaus, and Y. Liu, "Creating open source models, test cases, and data for oilfield drilling challenges," in *SPE/IADC International Drilling Conference and Exhibition*, (The Hague, The Netherlands), pp. 1–38, Mar. 2019.

[103] M. Yilmaz, S. Mujeeb, and N. R. Dhansri, "A H-infinity control approach for oil drilling processes," *Procedia Computer Science*, vol. 20, pp. 134–139, 2013. Complex Adaptive Systems.

[104] U. J. F. Aarsnes and N. van de Wouw, "Axial and torsional self-excited vibrations of a distributed drill-string," *Journal of Sound and Vibration*, vol. 444, pp. 127–151, 2019.

[105] X. Liu, N. Vlajic, X. Long, G. Meng, and B. Balachandran, "Nonlinear motions of a flexible rotor with a drill bit: stick-slip and delay effects," *Nonlinear Dynamics*, vol. 72, pp. 61–77, 2013.

[106] U. J. F. Aarsnes and N. van de Wouw, "Dynamics of a distributed drill string system: Characteristic parameters and stability maps," *Journal of Sound and Vibration*, vol. 417, pp. 376–412, 2018.

[107] U. J. F. Aarsnes, F. Di Meglio, and R. J. Shor, "Avoiding stick slip vibrations in drilling through startup trajectory design," *Journal of Process Control*, vol. 70, pp. 24–35, 2018.

[108] F. Di Meglio, P.-O. Lamare, and U. J. F. Aarsnes, "Robust output feedback stabilization of an ODE–PDE–ODE interconnection," *Automatica*, vol. 119, p. 109059, 2020.

[109] J. Auriol, U. J. F. Aarsnes, and R. Shor, "Self-tuning torsional drilling model for real-time applications," in *2020 American Control Conference (ACC)*, pp. 3091–3096, 2020.

[110] M. V. Faronov and I. G. Polushin, "Observer-based control of drilling mode in rotary drilling systems," in *2021 American Control Conference*, (New Orleans, USA), pp. 97–104, May 2021.

[111] Y. Shtessel, C. Edwards, L. Fridman, and A. Levant, *Sliding Mode Control and Observation*. Birkhäuser, 2014.

[112] DC motors information, Siemens. `https://new.siemens.com/global/en/products/drives/electric-motors/dc-motors.html`. accessed: 12 December 2020.

[113] Y. Liu, "Suppressing stick-slip oscillations in underactuated multibody drill-strings with parametric uncertainties using sliding-mode control," *IET Control Theory and Applications*, vol. 9, no. 1, pp. 91–102, 2015.

[114] M. V. Faronov and I. G. Polushin, "Observer-based control of vertical penetration rate in rotary drilling systems," *Journal of Process Control*, vol. 106, pp. 29–43, 2021.

[115] R. Foster and R. Macmillan, "High speed telemetry on wired drill pipe, history, and impact on drilling process," OTC Offshore Technology Conference, May 2018.

[116] M. Mueller, "Normal form for linear systems with respect to its vector relative degree," *Linear Algebra and its Applications*, vol. 430, p. 1292–1312, 2009.

[117] J. A. Dávila, M. Basin, and L. Fridman, "Finite-time parameter identification via high-order sliding mode observer," in *Proceedings of the 2010 American Control Conference*, pp. 2960–2964, 2010.

Appendix A. Reprint Permissions

This thesis is based on papers published in Journal of Process Control and IEEE conference proceedings. It is allowed to reprint them as part of a thesis. Permissions are shown in Figures 7.1, 7.2, respectively.

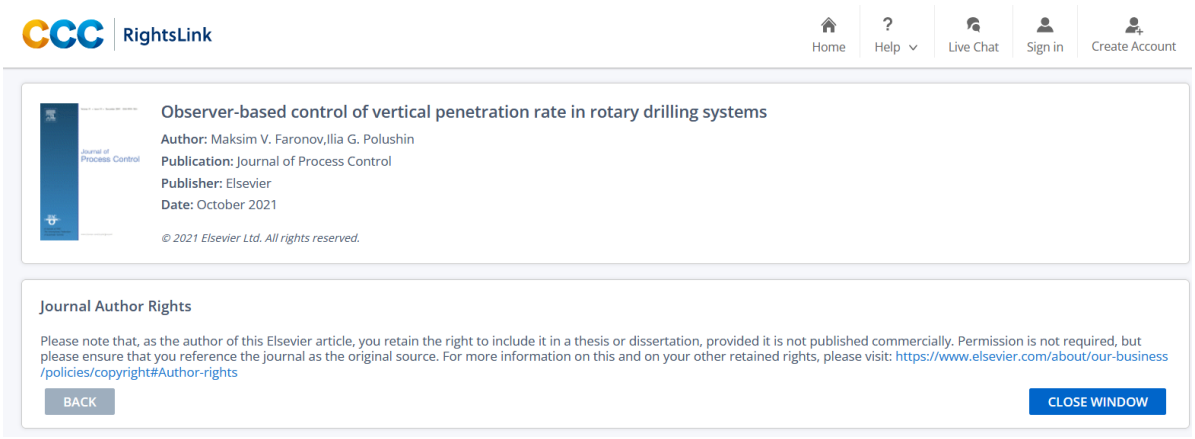

Figure 7.1: Reprint permission from Journal of Process Control

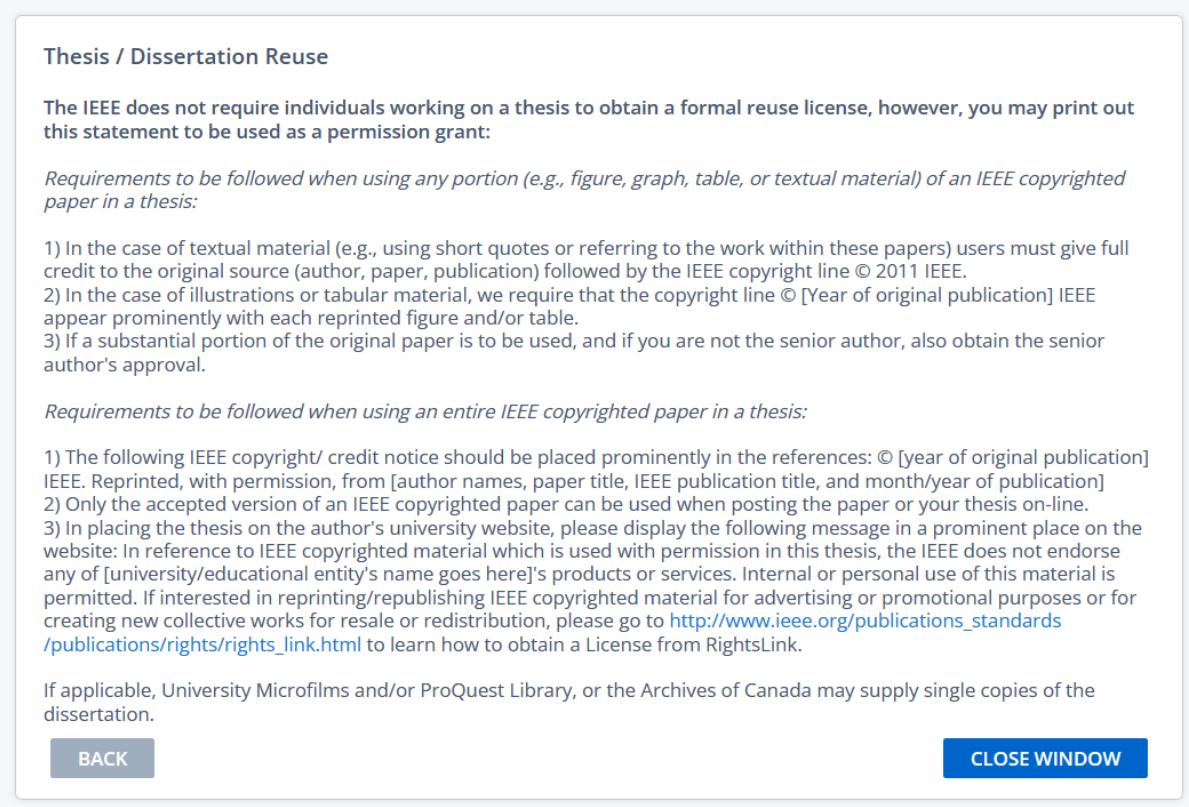

Thesis / Dissertation Reuse

The IEEE does not require individuals working on a thesis to obtain a formal reuse license, however, you may print out this statement to be used as a permission grant:

Requirements to be followed when using any portion (e.g., figure, graph, table, or textual material) of an IEEE copyrighted paper in a thesis:

1) In the case of textual material (e.g., using short quotes or referring to the work within these papers) users must give full credit to the original source (author, paper, publication) followed by the IEEE copyright line © 2011 IEEE.
2) In the case of illustrations or tabular material, we require that the copyright line © [Year of original publication] IEEE appear prominently with each reprinted figure and/or table.
3) If a substantial portion of the original paper is to be used, and if you are not the senior author, also obtain the senior author's approval.

Requirements to be followed when using an entire IEEE copyrighted paper in a thesis:

1) The following IEEE copyright/ credit notice should be placed prominently in the references: © [year of original publication] IEEE. Reprinted, with permission, from [author names, paper title, IEEE publication title, and month/year of publication]
2) Only the accepted version of an IEEE copyrighted paper can be used when posting the paper or your thesis on-line.
3) In placing the thesis on the author's university website, please display the following message in a prominent place on the website: In reference to IEEE copyrighted material which is used with permission in this thesis, the IEEE does not endorse any of [university/educational entity's name goes here]'s products or services. Internal or personal use of this material is permitted. If interested in reprinting/republishing IEEE copyrighted material for advertising or promotional purposes or for creating new collective works for resale or redistribution, please go to http://www.ieee.org/publications_standards /publications/rights/rights_link.html to learn how to obtain a License from RightsLink.

If applicable, University Microfilms and/or ProQuest Library, or the Archives of Canada may supply single copies of the dissertation.

BACK CLOSE WINDOW

Figure 7.2: Reprint permission from IEEE conference proceedings

Curriculum Vitae

Name:	Maksim Faronov
Post-Secondary Education and Degrees:	ITMO University Saint Petersburg, Russia 2006 - 2010 B.Eng.
	ITMO University Saint Petersburg, Russia 2010 - 2012 M.Eng.
	ITMO University Saint Petersburg, Russia 2012 - 2015 Candidate of Eng. Sciences
	University of Western Ontario London, ON 2017 - 2023 Ph.D.
Honours and Awards:	Queen Elizabeth II Scholarship 2020 - 2021
	Ontario Graduate Scholarship 2019 - 2020

Related Work Experience: Teaching Assistant
University of Western Ontario
2018 - 2023

Avionics Engineer
Kontur-NIIRS Ltd., Saint Petersbrug, Russia
2012 - 2017

Publications:

1. Maksim V. Faronov and Ilia G. Polushin. Observer-based control of vertical penetration rate in rotary drilling systems. Journal of Process Control, Volume 106, pp. 29–43, 2021.

2. Maksim V. Faronov and Ilia G. Polushin. Algorithm for power stabilization in rotary drilling systems. In 2019 *IEEE 15th International Conference on Automation Science and Engineering (CASE)*, pp. 867–872, Vancouver, Canada, August 2019.

3. Maksim V. Faronov and Ilia G. Polushin. Regulation of penetration rate and drilling power in rotary drilling systems. In *IEEE 16th International Workshop on Advanced Motion Control (AMC 2020)*, pp. 97–104, Kristiansand, Norway, September 2020.

4. Maksim V. Faronov and Ilia G. Polushin. Observer-based control of drilling mode in rotary drilling systems. In *2021 American Control Conference*, pp. 97–104, New Orleans, USA, May 2021.

5. Maksim V. Faronov and Ilia G. Polushin. Control of penetration rate in distributed parameter rotary drilling systems. In *2021 IEEE Conference on Control Technology and Applications (CCTA)*, pp. 1095–1102, San Diego, USA, August 2021.

6. Maksim V. Faronov and Ilia G. Polushin. Control of rotary drilling systems with uncertain parameters. In *2023 IEEE Conference on Control Technology and Applications (CCTA)*, Bridgetown, Barbados, August 2023 (accepted).